Electronic Supplementary Material (ESI) for Sensors & Diagnostics.

Development of multi-analyte responsive sensors: Optical discrimination of arsenite and arsenate ions, ratiometric detection of arsenite, and application in food and water samples

Nagaraj K[a,b], A. Nityananda Shetty[a], Darshak R. Trivedi[b]*

a= Material Science Laboratory, Department of Chemistry, National Institute of Technology Karnataka (NITK) Surathkal, Srinivasnagar - 575 025, Karnataka, India

b=Supramolecular Chemistry Laboratory, Department of Chemistry, National Institute of Technology Karnataka (NITK) Surathkal, Srinivasnagar - 575 025, Karnataka, India

*Email: darshak_rtrivedi@yahoo.co.in, darshakrtrivedi@nitk.edu.in, Phone No: +91-824-2473205, fax: +91 824 2474033 (Darshak R Trivedi)

SUPPLEMENTARY INFORMATION

Table of contents

Fig. S9 FT- IR spectrum of the receptor N4R3

Fig. S10 ^{1}H- NMR spectrum of receptor N4R3

Fig. S11 ^{13}C- NMR spectrum of receptor N4R3

Fig. S12 LC- MS spectrum of receptor N4R3

Fig. S13 UV- Vis absorption spectrum of receptor N4R1 in the presence of 2 equivalence of different anions in 30% aq. MeCN (MeCN- H_2O, 7:3, v/v)

Fig. S14 Change in color observed for receptor N4R1 (2×10^{-5} M, MeCN: H_2O, 7:3, v/v) with an addition of 2 equivalent NaF, NaCl, NaBr, NaI, NaAcO, $NaNO_3$, $NaHSO_4$, Na_3PO_4, NaH_2PO_4, $NaAsO_2$, Na_3AsO_4, SCN^-, $P_2O_7^{4-}$, S^{2-}, and N_3^- (1×10^{-2} M, H_2O)

Fig. S15 Change in color observed for receptor N4R1 (2×10^{-5} M, MeCN: H_2O, 7:3, v/v) with an addition of 2 equivalent metal ions as its nitrates Cu^{2+}, Hg^{2+}, Zn^{2+}, Ni^{2+}, Co^{2+}, Fe^{3+}, Pb^{2+}, Cd^{2+}, and Cr^{3+} (1×10^{-2} M, H_2O)

Fig. S16 Ratiometric color change of receptor N4R1 (2×10^{-5} M, 30% aq. MeCN) on addition of (i) 0.5 equivalent, (ii) 1 equivalent and (iii) 1.5 equivalent and (iv) 2 equivalent of $NaAsO_2$ (a) 1×10^{-3} M, (b) 1×10^{-4} M, (c) 1×10^{-5} M in H_2O

Fig. S17 UV- Vis spectral response of (a) N4R2 and N4R2+ AsO_2^-/ AsO_4^{3-}/ PO_4^{3-} and (b) N4R3 and N4R3+ AsO_2^-/ AsO_4^{3-}/ PO_4^{3-} in various percentage of water content in Me_2SO

Fig. S18 Color change of receptors (2×10^{-5} M, 30% aq. Me_2SO) (a) N4R1, (b) N4R2 and (c) N4R3 on adding 2 equivalence of Na salts of anions (1×10^{-2} M, in water)

Fig. S19 Color change of receptors (2×10^{-5} M, 30% aq. Me_2SO) (a) N4R1, (b) N4R2 and (c) N4R3 on adding 2 equivalence of metal ions (1×10^{-2} M, in water)

Fig. S20 The absorption variations of the receptor N4R1 (2×10^{-5} M in 30% aq. Me_2SO solution) with stepwise addition of $NaAsO_2$ (1×10^{-2} M in H_2O). Inset plots represent absorption variation with anion addition

Fig. S21 The absorption variations of the receptor N4R1 (2×10^{-5} M in 30% aq. Me_2SO solution) with sequential addition of Na_3AsO_4 (1×10^{-2} M in H_2O). Inset plots represent absorption variation with anion addition

Fig. S22 The absorption variations of the receptor N4R1 (2×10^{-5} M in 30% aq. Me_2SO solution) with sequential addition of Na_3PO_4 (1×10^{-2} M in H_2O). Inset plots represent absorption variation with anion addition

Fig. S23 The absorption variations of the receptor N4R2 (2×10^{-5} M in 30% aq. Me_2SO solution) with sequential addition of $NaAsO_2$ (1×10^{-2} M in H_2O). Inset plots represent absorption variation with anion addition

Fig. S24 The absorption variations of the receptor N4R2 (2×10^{-5} M in 30% aq. Me_2SO solution) with sequential addition of Na_3AsO_4. Inset plots represent absorption variation with anion addition

Fig. S25 The absorption variations of the receptor N4R2 (2×10^{-5} M in 30% aq. Me_2SO solution) with sequential addition of Na_3PO_4 (1×10^{-2} M in H_2O). Inset plots represent absorption variation with anion addition

Fig. S26 The absorption variations of the receptor N4R3 (2×10^{-5} M in 30% aq. Me_2SO solution) with sequential addition of $NaAsO_2$ (1×10^{-2} M in H_2O). Inset plots represent absorption variation with anion addition

Fig. S27 The absorption variations of the receptor N4R3 (2×10^{-5} M in 30% aq. Me_2SO solution) with sequential addition of Na_3AsO_4 (1×10^{-2} M in H_2O). Inset plots represent absorption variation with anion addition

Fig. S28 The absorption variations of the receptor N4R3 (2×10^{-5} M in 30% aq. Me_2SO solution) with sequential addition of Na_3PO_4 (1×10^{-2} M in H_2O). Inset plots represent absorption variation with anion addition

Fig. S29 (a) The absorption variations of the receptor N4R2 (2×10^{-5} M in Me_2SO - H_2O, 1:1 v/v) with sequential addition $NaAsO_2$ (1×10^{-2} M in water) (b) Color change of N4R2 (2×10^{-5} M, 50% aq. Me_2SO) on adding 2 equiv. of anions. Inset plots represent absorption variations with arsenite addition

Fig. S30 (a) The absorption variations of the receptor N4R3 (2×10^{-5} M in Me_2SO - H_2O, 1:1 v/v) with sequential addition Na salts of arsenite (1×10^{-2} M in water). Inset plot represents absorption variation with arsenite addition (b) Color change of receptor N4R3 (2×10^{-5} M, 50% aq. Me_2SO) on adding 2 equivalence of Na salts of anions (1×10^{-2} M, in water)

Fig. S31 Effect of competing anions in the occurrence of 3 equiv. of different anions in the (a) 30% aq. Me_2SO solution (2×10^{-5} M) Black bar: N4R1 + AsO_2^- ion, Blue bar: N4R1 + AsO_2^-+ competing anions, (b) 30% aq. Me_2SO solution (2×10^{-5} M) Black bar: N4R1 + AsO_4^{3-} ion, Sky blue bar: N4R1 + AsO_4^{3-} + competing anions, and (c) 30% aq. Me_2SO solution (2×10^{-5} M) Black bar: N4R1 + PO_4^{3-} ion, Red bar: N4R1 + PO_4^{3-} + competing anions

Fig. S32 Effect of competing anions in the occurrence of 3 equiv. of different anions in the (a) 30% aq. Me_2SO solution (2×10^{-5} M) Black bar: N4R2 + AsO_2^- ion, pink bar: N4R2 + AsO_2^-+

competing anions, (b) 30% aq. Me_2SO solution (2×10^{-5} M) Black bar: N4R2 + AsO_4^{3-} ion, Green bar: N4R2 + AsO_4^{3-} + competing anions, and (c) 30% aq. Me_2SO solution (2×10^{-5} M) Black bar: N4R2 + PO_4^{3-} ion, Violet bar: N4R2 + PO_4^{3-} + competing anions

Fig. S33 Effect of competing anions in the occurrence of 3 equiv. of different anions in the (a) 30% aq. Me_2SO solution (2×10^{-5} M) Black bar: N4R3 + AsO_2^- ion, Green bar: N4R3 + AsO_2^-+ competing anions, (b) 30% aq. Me_2SO solution (2×10^{-5} M) Black bar: N4R3 + AsO_4^{3-} ion, Purple bar: N4R3 + AsO_4^{3-} + competing anions, and (c) 30% aq. Me_2SO solution (2×10^{-5} M) Black bar: N4R3 + PO_4^{3-} ion, Cyan bar: N4R3 + PO_4^{3-} + competing anions

Fig. S34 Outcome of competing cations in the occurrence of 3 equiv. of different cations in the (a) 50% aq. Me_2SO solution (2×10^{-5} M) Black bar: N4R1 + AsO_2^- ion, Green bar: N4R1 + AsO_2^-+ cations, and (b) 50% aq. Me_2SO solution (2×10^{-5} M) Black bar: N4R2 + AsO_2^- ion, Pink bar: N4R2 + AsO_2^-+ cations

Fig. S35 Effect of competing anions in the presence of 3 equiv. of different cations in the 50% aq. Me_2SO solution (2×10^{-5} M) Black bar: N4R3 + AsO_2^- ion, blue bar: N4R3 + AsO_2^-+ cations

Fig. S36 pH effect on the UV- Vis absorption spectra of N4R1 and N4R1+ AsO_4^{3-} in Me_2SO - H_2O (7: 3, v/v)

Fig. S37 pH effect on the UV- Vis absorption spectra of (a) N4R2 and N4R2+ AsO_2^- and (b) N4R2 and N4R2+ AsO_4^{3-} in Me_2SO - H_2O (7: 3, v/v)

Fig. S38 pH effect on the UV- Vis absorption spectra of N4R2 and N4R2+ PO_4^{3-} in Me_2SO - H_2O (7: 3, v/v)

Fig. S39 pH effect on the UV- Vis absorption spectra of (a) N4R3 and N4R3+ AsO_2^- and (b) N4R3 and N4R3+ AsO_4^{3-} in Me_2SO - H_2O (7: 3, v/v)

Fig. S40 pH effect on the UV- Vis absorption spectra of N4R3 and N4R3+ PO_4^{3-} in Me_2SO - H_2O (7: 3, v/v)

Fig. S41 Rariometric color change of 30% aq. Me_2SO receptor N4R1 on 0.5- 2.0 equiv. of $NaAsO_2$ addition and (b) Ratiometric plot of A_{618}/A_{440} for N4R1 with the increasing concentration of arsenite ion

Fig. S42 Ratiometric color change of 30% aq. Me_2SO receptor N4R2 on 0.5- 2.0 equivalents of sodium arsenite addition and (b) Ratiometric plot of A_{675}/A_{448} for receptor N4R2 with the increasing concentration of AsO_2^- ion

Fig. S43 Ratiometric color change of 30% aq. Me_2SO receptor N4R3 on 0.5- 2.0 equivalents of sodium arsenite addition and (b) Ratiometric plot of A_{668}/A_{446} for receptor N4R3 with the increasing concentration of AsO_2^- ion

Fig. S44 (a) B-H plot for N4R1—AsO_2^- complex in MeCN - H_2O (7:3, v/v) and (b) B-H plot for N4R1- AsO_4^{3-} complex in MeCN - H_2O (7: 3 v/v)

Fig. S45 (a) B-H plot for N4R1—AsO_2^- complex in Me_2SO - H_2O (7:3, v/v) and (b) B-H plot for N4R1- AsO_4^{3-} complex in Me_2SO - H_2O (7: 3 v/v)

Fig. S46 (a) B-H plot for N4R2—AsO_2^- complex in Me_2SO - H_2O (7:3, v/v) and (b) B-H plot for N4R2- AsO_4^{3-} complex in Me_2SO - H_2O (7: 3 v/v)

Fig. S47 (a) B-H plot for N4R3—AsO_2^- complex in Me_2SO - H_2O (7:3, v/v) and (b) B-H plot for N4R3- AsO_4^{3-} complex in Me_2SO - H_2O (7: 3 v/v)

Fig. S48 (a) B-H plot for N4R2—AsO_2^- complex in Me_2SO - H_2O (1:1, v/v) and (b) B-H plot for N4R3- AsO_2^- complex in Me_2SO - H_2O (1: 1 v/v)

Fig. S49 B-H plot for N4R1—PO_4^{3-} complex in **(**a) MeCN- H_2O (7: 3, v/v) and (b) Me_2SO - H_2O (7: 3, v/v)

Fig. S50 (a) B-H plot for N4R2—PO_4^{3-} complex in Me_2SO - H_2O (7: 3, v/v) and (b) B-H plot for N4R3- PO_4^{3-} complex in Me_2SO - H_2O (7: 3, v/v)

Fig. S51 (a) Calibration curve for N4R1—AsO_2^- complex in MeCN - H_2O (7: 3, v/v) and (b) calibration curve for N4R1- AsO_4^{3-} complex in MeCN - H_2O (7: 3, v/v)

Fig. S52 (a) Calibration curve for N4R1—AsO_2^- complex in Me_2SO- H_2O (7: 3, v/v) and (b) calibration curve for N4R1- AsO_4^{3-} complex in Me_2SO - H_2O (7: 3, v/v)

Fig. S53 (a) Calibration curve for N4R2—AsO_2^- complex in Me_2SO - H_2O (7: 3, v/v) and (b) calibration curve for N4R2- AsO_4^{3-} complex in Me_2SO - H_2O (7: 3, v/v)

Fig. S54 (a) Calibration curve for N4R3—AsO_2^- complex in Me_2SO - H_2O (7: 3, v/v) and (b) calibration curve for N4R3- AsO_4^{3-} complex in Me_2SO - H_2O (7: 3, v/v)

Fig. S55 (a) Calibration curve for N4R2—AsO_2^- complex in Me_2SO - H_2O (1: 1, v/v) and (b) calibration curve for N4R3- AsO_2^- complex in Me_2SO - H_2O (1: 1, v/v)

Fig. S56 Calibration curve for N4R1—PO_4^{3-} complex in **(**a) MeCN- H_2O (7: 3, v/v) and (b) Me_2SO - H_2O (7: 3, v/v)

Fig. S57 (a) Calibration curve for N4R2—PO_4^{3-} complex in Me_2SO - H_2O (7: 3, v/v) and (b) calibration curve for N4R3- PO_4^{3-} complex in Me_2SO - H_2O (7: 3, v/v)

Fig. S58 CV diagram of (a) N4R2 and (b) N4R3 with the sequential addition of AsO_2^-

Fig. S59 CV diagram of (a) N4R2 and (b) N4R3 with the sequential addition of PO_4^{3-}

Fig. S60 CV diagram of (a) N4R1 and (b) N4R2 with the sequential addition of AsO_4^{3-}

Fig. S61 CV diagram of receptor N4R3 with the serial addition of AsO_4^{3-} ion

Fig. S62 ^1H NMR titration of receptor N4R2 in a Me_2SO -d_6 solvent with incremental addition of (0-1 equiv.) of $NaAsO_2$ (1×10^{-2} M in H_2O)

Fig. S63 ^1H NMR titration of receptor N4R3 in a Me_2SO -d_6 solvent with incremental addition of (0-1 equiv.) of $NaAsO_2$ (1×10^{-2} M in H_2O)

Fig. S64 Blank ^1H NMR titration of receptor N4R1 in a Me_2SO -d_6 solvent with incremental addition of H_2O

Fig. S65 Blank ^1H NMR titration of receptor N4R2 in a Me_2SO -d_6 solvent with incremental addition of H_2O

Fig. S66 LC- MS spectrum of N4R1- AsO_2^- complex in negative mode

Fig. S67 LC- MS spectrum of N4R1- AsO_4^{3-} complex in negative mode

Fig. S68 LC- MS spectrum of N4R2- AsO_2^- complex in negative mode

Fig. S69 LC- MS spectrum of N4R2- AsO_4^{3-} complex in negative mode

Fig. S70 HOMO's and LUMO's diagrams for receptor N4R3 and receptor N4R3-AsO_2^- obtained by B3LYP/def- TZVPP method

Fig. S71 HOMO's and LUMO's diagrams for receptor N4R1 and receptor N4R1-AsO_2^- obtained by B3LYP/def- TZVPP method

Fig. S72 UV-visible absorption spectra of receptor N4R1 and complexation with AsO_2^- ion calculated by using TD-DFT calculation in solvent phase

Fig. S73 Reversible cycles and reproducible colorimetric switch of receptor (2×10^{-5} M, 30% aq. Me_2SO) (a) N4R1 reversed and reproduced by the addition of AsO_4^{3-} and 40 µL Ca^{2+}, (b) N4R1 reversed and reproduced by the addition of PO_4^{3-} and 40 µL Ca^{2+}, (c) N4R2 reversed and reproduced by the addition of AsO_4^{3-} and 20 µL Ca^{2+}, (d) N4R2 reversed and reproduced by the addition of PO_4^{3-} and 20 µL Ca^{2+}, (e) N4R3 reversed and reproduced by the addition of AsO_4^{3-} and 20 µL Ca^{2+}, and (f) N4R3 reversed and reproduced by the addition of PO_4^{3-} and 20 µL Ca^{2+}

Fig. S74 UV- Vis absorption of receptor (2×10^{-5} M, 30% aq. Me_2SO) (a) N4R1 circulated with addition of 40 µL Ca^{2+} and AsO_4^{3-} by turns, (b) N4R1 circulated with addition of 40 µL Ca^{2+} and PO_4^{3-} by turns, (c) N4R2 circulated with addition of 20 µL Ca^{2+} and AsO_4^{3-} by turns, (d) N4R2 circulated with addition of 20 µL Ca^{2+} and PO_4^{3-} by turns, (e) N4R3 circulated with addition of 20 µL Ca^{2+} and AsO_4^{3-} by turns, and (f) N4R1 circulated with addition of 20 µL Ca^{2+} and PO_4^{3-} by turns

Fig. S75 (a) Addition of (i) 50 µL, (ii) 100 µL, (iii) 150 µL, (iv) 200 µL and (v) 300 µL Cu^{2+} solution to N4R1 containing 2 equiv. AsO_2^-, (b) Addition of (i) 20 µL, (ii) 40 µL, (iii) 60 µL, (iv) 80 µL, (v) 100 µL, (vi) 120 µL and (vii) 140 µL Cu^{2+} solution to N4R2 containing 2 equiv. AsO_2^-, and (c) Addition of (i) 20 µL, (ii) 40 µL, (iii) 60 µL, (iv) 80 µL, (v) 100 µL, and (vi) 120 µL Cu^{2+} solution to N4R3 containing 2 equiv. AsO_2^-

Fig. S76 UV- Vis absorption intensity changes on stepwise addition of Cu^{2+} solution to (a) N4R1 containing 2 equivalence of AsO_2^-, (b) N4R3 containing 2 equivalence of AsO_2^-, and (c) N4R3 containing 2 equivalence of AsO_2^-

Fig. S77 Observed color changes on adding 2 equivalences of PO_4^{3-} ions on test strips with (a) N4R1 in 30% aq. Me_2SO, (b) N4R2 in 30% aq. Me_2SO and (c) N4R3 in 30% aq. Me_2SO

Fig. S78 A linear calibration plot of (a) N4R1–AsO_2^- vs. the amount of AsO_2^- ions and (b) N4R2–AsO_2^- vs. the amount of AsO_2^- ions for the quantitative analysis of food and water samples

Fig. S79 A linear calibration plot of N4R3–AsO_2^- vs. the amount of AsO_2^- ions for the quantitative analysis of food and water samples

Fig. S80 A linear calibration plot of (a) N4R1–PO_4^{3-} vs. the amount of PO_4^{3-} ions and (b) N4R2– PO_4^{3-} vs. the amount of PO_4^{3-} ions for the quantitative analysis of food and water samples

Fig. S81 A linear calibration plot of N4R3 $-PO_4^{3-}$ vs. the amount of PO_4^{3-} ions for the quantitative analysis of food and water samples

Table S1 Absorption maximum difference ($\Delta\lambda_{max}$) of N4R1-N4R3 (2×10^{-5} M) in the presence of AsO_2^-, AsO_4^{3-} , PO_4^{3-} ions (2 equiv.)

Table S2 Binding ratio, binding constant, and detection limit of receptors N4R2 and N4R3 in the presence of arsenite, arsenate and phosphate ions

Table S3 Oscillator strength of Receptor- arsenite complexes

Table S4 λ_{max} of N4R1- N4R3 and complexes calculated from the theoretical DFT method and experimental UV- Vis spectroscopy

Table S5 Determination of AsO_2^- spiked into different food and water samples using N4R2 and N4R3

Table S6 Determination of PO_4^{3-} spiked into different food and water samples using N4R2 and N4R3

Table S7: Determination of arsenite spiked into different food and water samples with one equivalent of various anions spiked (F^-+ AcO^-+ $H_2PO_4^-$+ NO_3^-)

Table S8: Determination of phosphate spiked into different food and water samples with one equivalent of various anions spiked (F^-+ AcO^-+ $H_2PO_4^-$+ NO_3^-)

Materials and methods

The chemicals, anions, and solvents used in the study were procured from Sigma- Aldrich and TCI and used without further purification. ^{1}H- NMR and ^{13}C- NMR spectra of the synthesized receptors were recorded using JASCO (400 MHz) NMR spectrometer. Infrared spectra were noted on Bruker- alpha FT- IR spectrometer with a resolution of 4 cm^{-1}. UV- Vis spectral studies were performed using Analytikjena Specord S600 spectrometer in a 3.5 mL glass cuvette with a path length of 1 cm. The cyclic voltammograms were recorded on an Ivium electrochemical workstation with a scan rate of 20 mV/s, and a potential range of -1.5 to +1.5 V. Mass spectra of the receptors were recorded using Xevo QToF, Waters mass spectrometer. The melting point of the synthesized products was recorded using Stuart- SMP3 melting point apparatus. pKa values were calculated using ChemAxon's Chemicalize software.

Colorimetric detection of anions: A fixed concentration (2×10^{-5} M) of receptor in MeCN/ Me_2SO and anions in water (1×10^{-2} M) have been used for the colorimetric detection of anions.

2 equivalence of each anion is added to the receptor and the color changes have been noted. The detection has been verified by shift in the UV- Vis spectroscopy.

UV- Vis titration: Anions of 1×10^{-2} M in water have been sequentially added to the receptors of 2×10^{-5} M concentration in MeCN/ Me_2SO. UV- Vis spectra has been monitored in the each addition.

pH of the solutions was maintained 7- 7.2 and distilled water were used.

Synthesis of receptors (N4R1, N4R2 and N4R3)

An equimolar quantity of 5- nitro-2-furaldehyde and substituted phenyl hydrazine (2,4-dinitrophenylhydrazine, 4-cyanophenylhydrazine and 2,4- dichlorophenylhydrazine) were dissolved in 20 mL of ethanol, and a catalytic quantity of glacial acetic acid was added into it. The reaction mixture was refluxed for 3 hours, followed by checking the completion of the reaction using TLC plates.

Structural characterization of the receptors N4R1- N4R3

(E)-1-(2,4-dinitrophenyl)-2-((5-nitrofuran-2-yl)methylene)hydrazine (**N4R1**): Yield: 83%, Melting point: 271.5^{0}C, FT IR (KBr) (cm^{-1}): 3258.51 (N-H), 1507.03 (NO_2), 1609.13 (CH=N). ^{1}H NMR (DMSO-d_6, 400 MHz, Me_4Si): 11.91 (s, 1H), 8.82-8.80 (d, 1H), 8.65 (s, 1H), 8.44-8.41 (dd, 1H), 7.99- 7.97 (d, 1H), 7.80- 7.78 (d, 1H), 7.31- 7.30 (d,1H). ^{13}C NMR (DMSO-d_6, 400MHz): 152.61, 151.94, 144.31, 138.73, 136.85, 131.15, 130.54, 123.31, 117.53, 116.17, 115.35. Mass (LC-MS): m/z calculated for $C_{11}H_7N_5O_7$: 321.03 Obtained: 320.02 $[M-H]^+$.

(E)-4-(2-((5-nitrofuran-2-yl)methylene)hydrazinyl)benzonitrile (**N4R2**): Yield: 81%, Melting point: 221.4^{0}C, FT IR (KBr) (cm^{-1}): 3309.84 (N-H), 1470.82 (NO_2), 1602.79 (CH=N), 2209.26 (-CN). ^{1}H NMR (DMSO-d_6, 400 MHz, Me_4Si): 11.51 (s,1H), 7.87 (s, 1H), 7.76- 7.75(d, 1H), 7.68- 7.65(dd, 2H), 7.19- 7.16 (dd, 2H), 7.11-7.10 (d, 1H). ^{13}C NMR (DMSO-d_6, 400MHz): 153.74, 151.88, 147.97, 134.38, 128.18, 120.26, 116.01, 113.50, 113.16, 101.82. Mass (LC-MS): m/z calculated for $C_{12}H_8N_4O_3$: 256.22 Obtained: 255.05 $[M-H]^+$.

(E)-1-(2,4-dichlorophenyl)-2-((5-nitrofuran-2-yl)methylene)hydrazine (**N4R3**): Yield: 82%, Melting point: 223.8^{0}C, FT IR (KBr) (cm^{-1}): 3298.05 (N-H), 1464.98 (NO_2), 1570.07 (CH=N). ^{1}H NMR (DMSO-d_6, 400 MHz, Me_4Si): 10.75 (s, 1H), 8.22 (s, 1H), 7.76- 7.75 (d, 1H), 7.51-7.49 (m, 2H), 7.36- 7.33 (dd, 1H), 7.10- 7.09 (d, 1H). ^{13}C NMR (DMSO-d_6, 400MHz): 154.00, 151.82, 140.02, 129.39, 128.95, 128.86, 124.55, 118.07, 116.24, 116.03, 112.72. Mass (LC-MS): m/z calculated for $C_{11}H_7Cl_2N_3O_3$: 298.99 Obtained: 298.03 $[M-H]^+$.

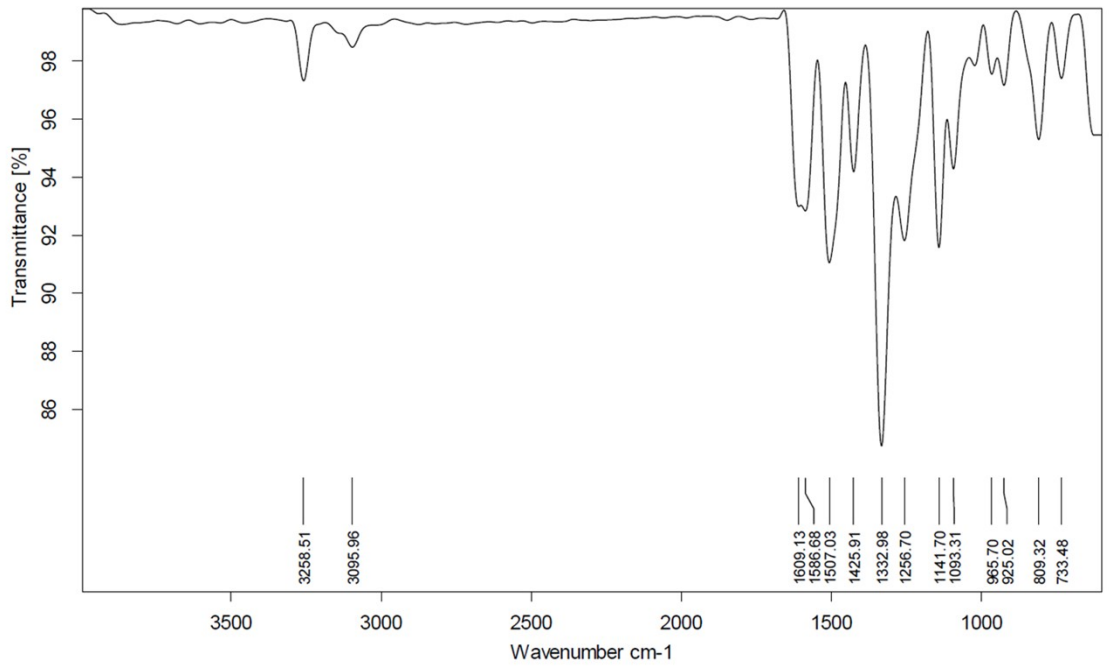

Fig. S1 FT- IR spectrum of the receptor N4R1

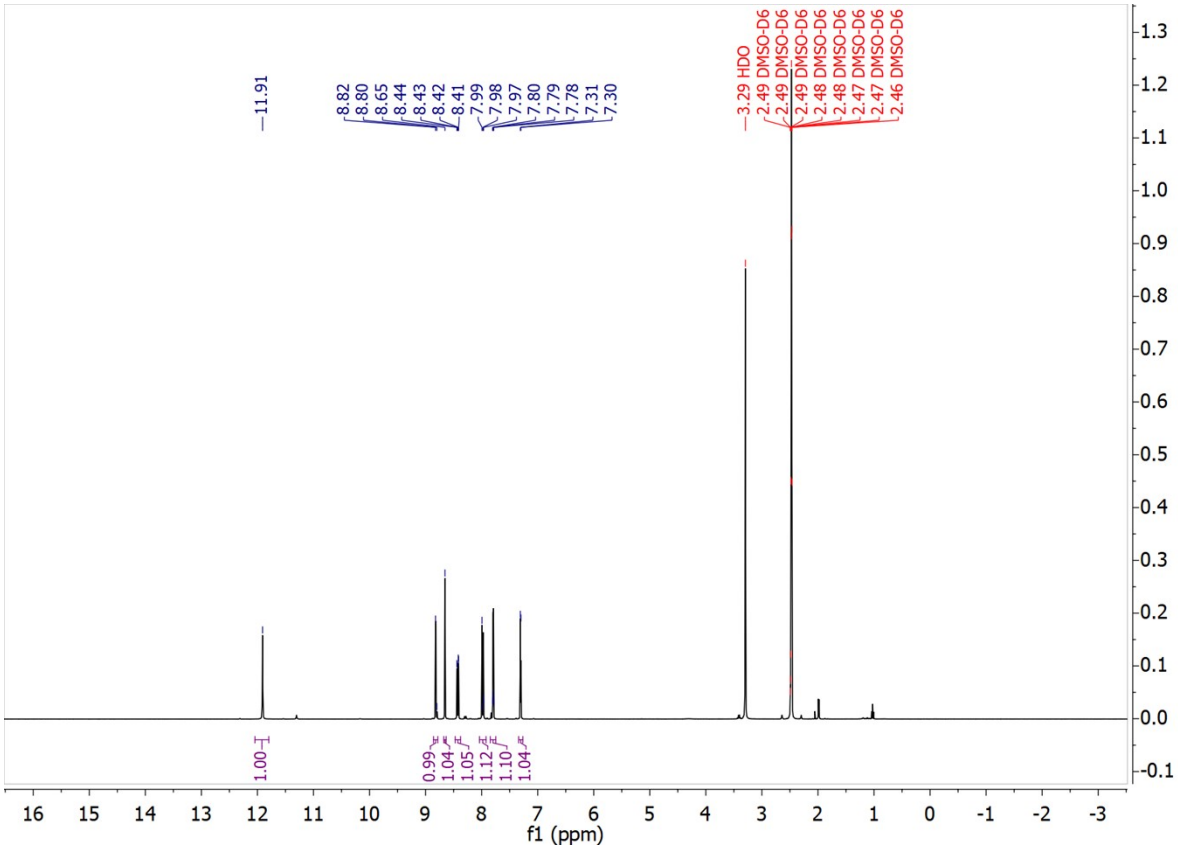

Fig. S2 ^{1}H- NMR spectrum of N4R1

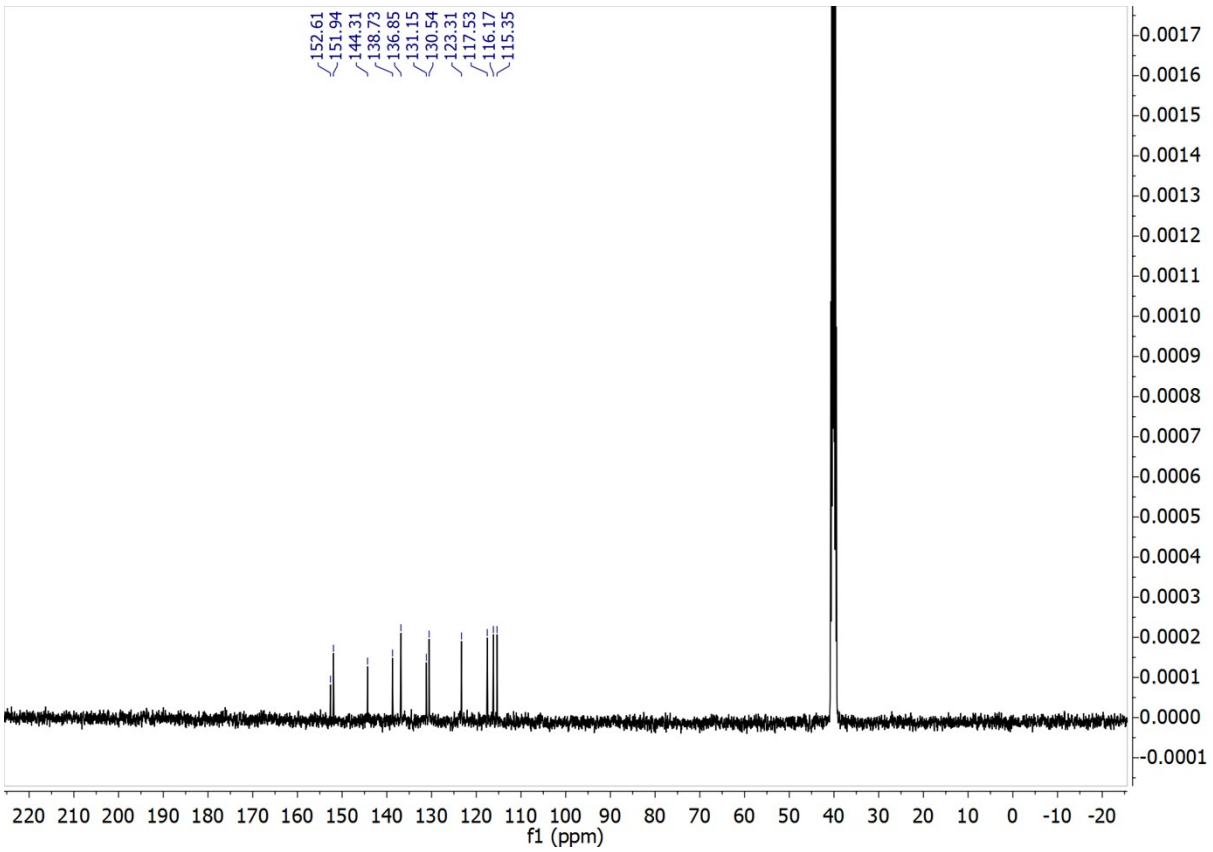

Fig. S3 ^{13}C- NMR spectrum of receptor N4R1

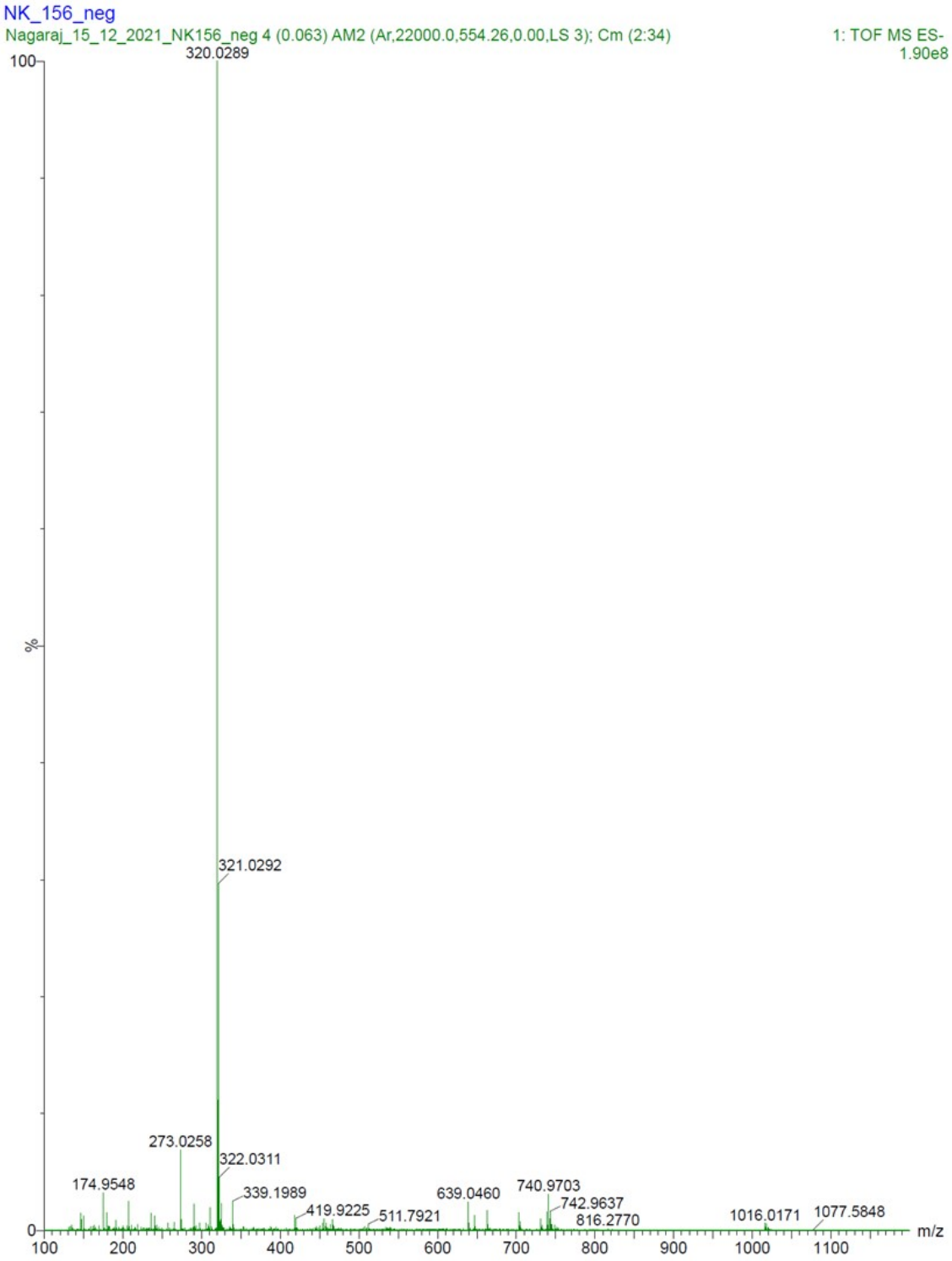

Fig. S4 LC- MS spectrum of receptor N4R1

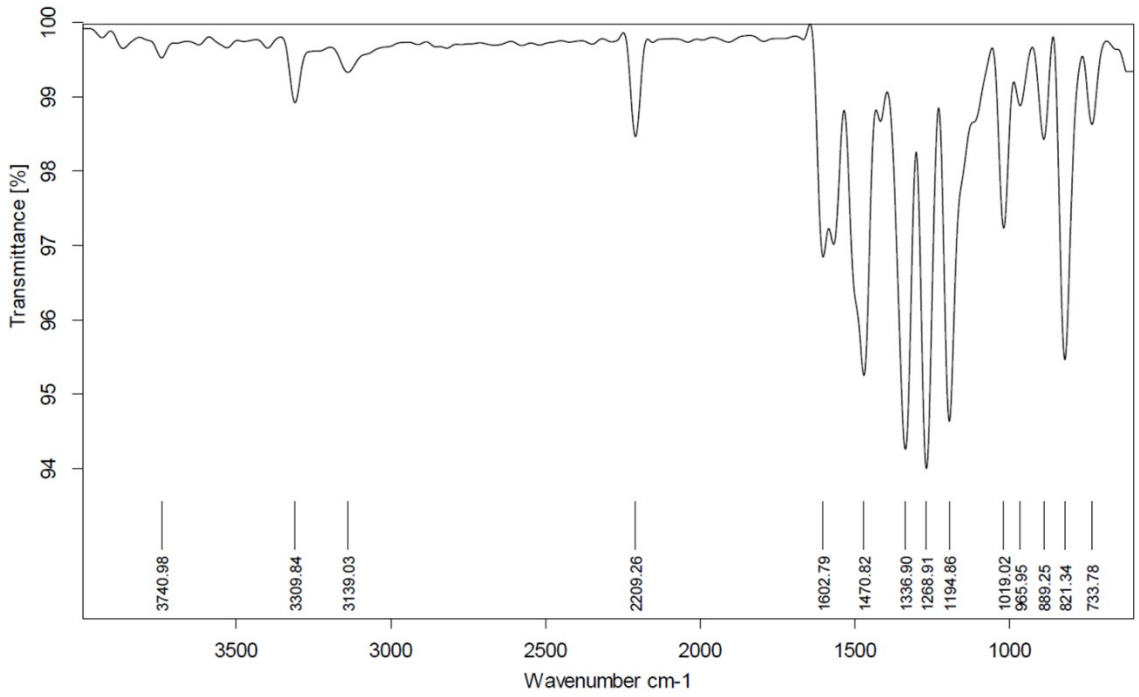

Fig. S5 FT- IR spectrum of receptor N4R2

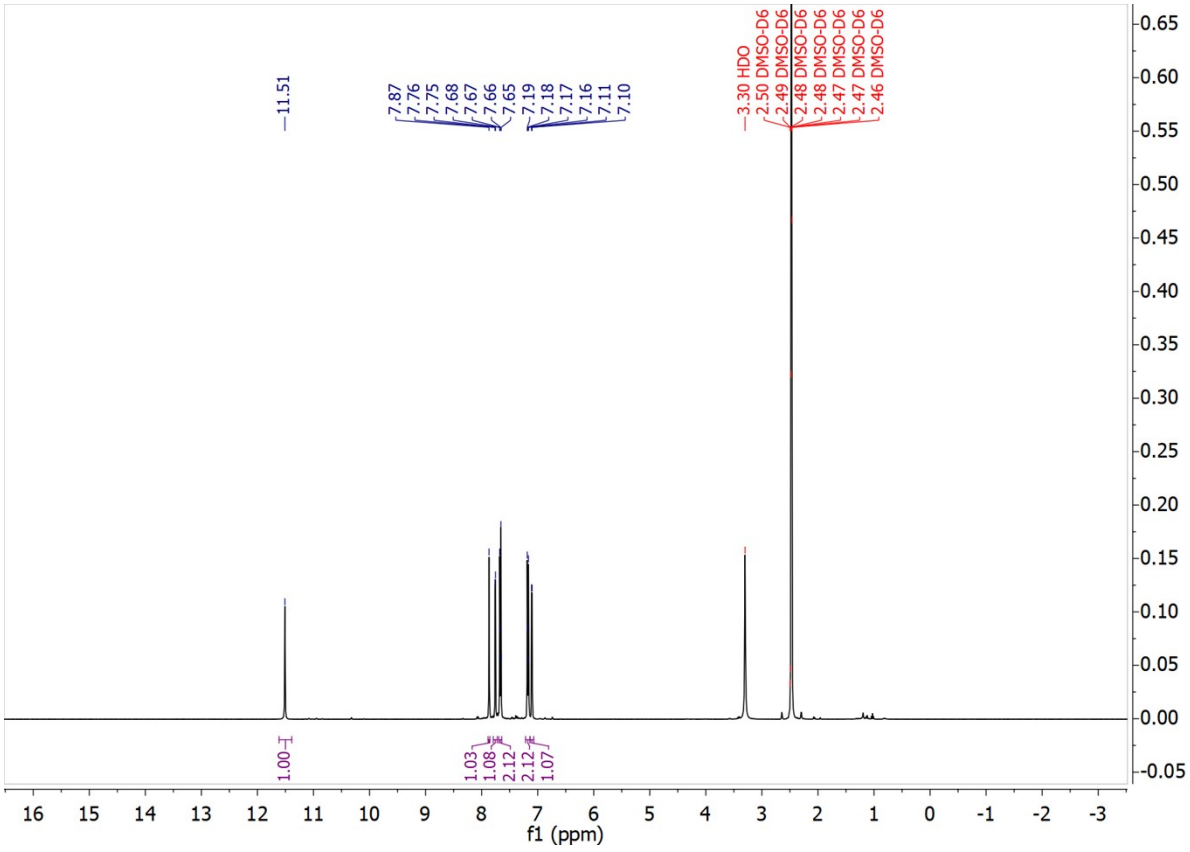

Fig. S6 ^{1}H- NMR spectrum of receptor N4R2

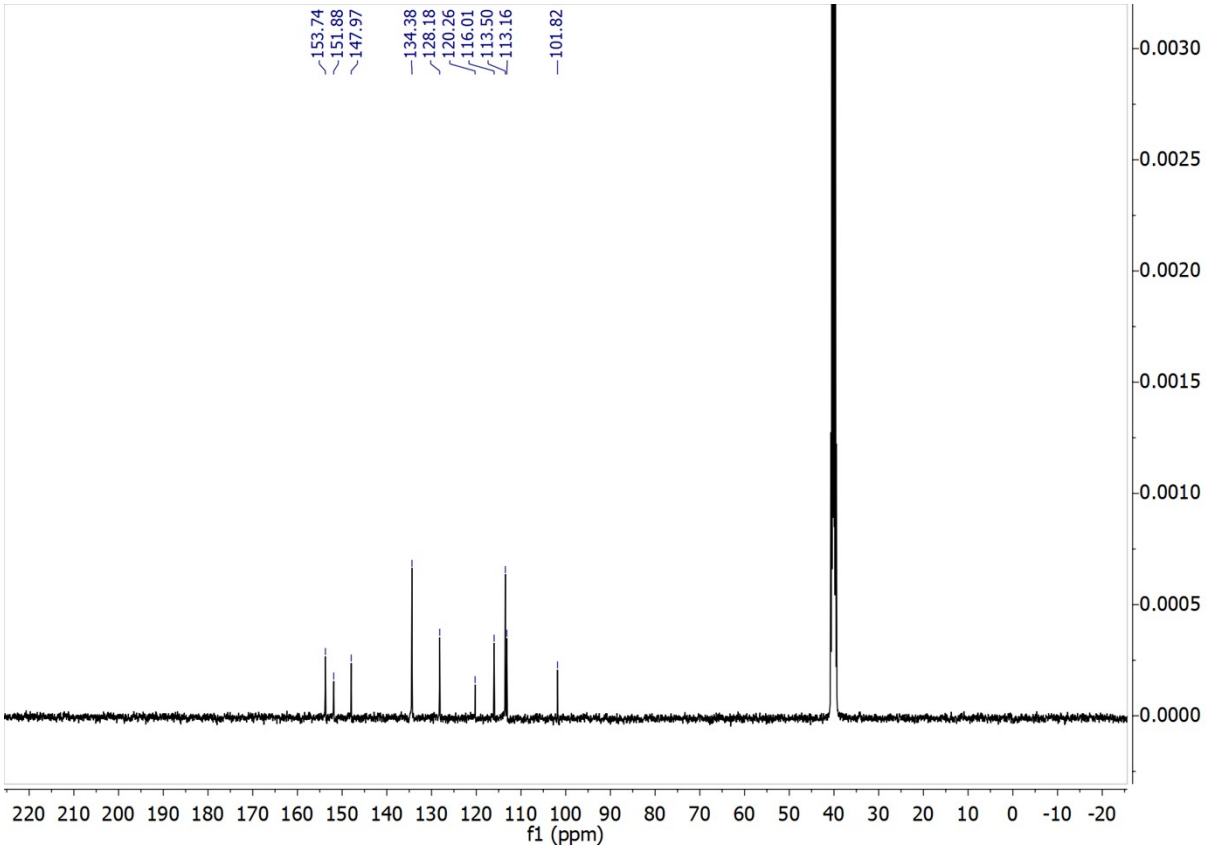

Fig. S7 ^{13}C- NMR spectrum of receptor N4R2

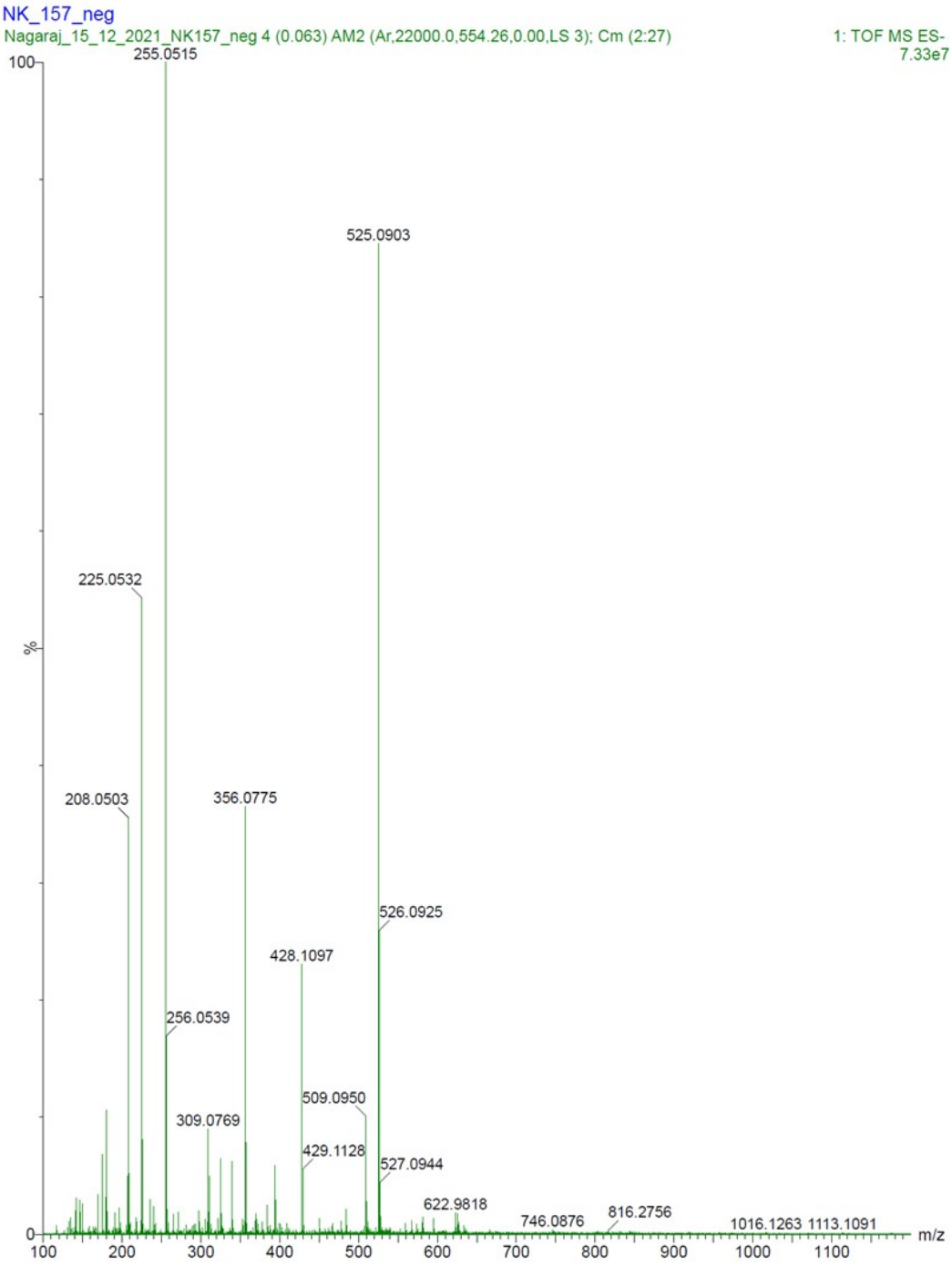

Fig. S8 LC- MS spectrum of receptor N4R2

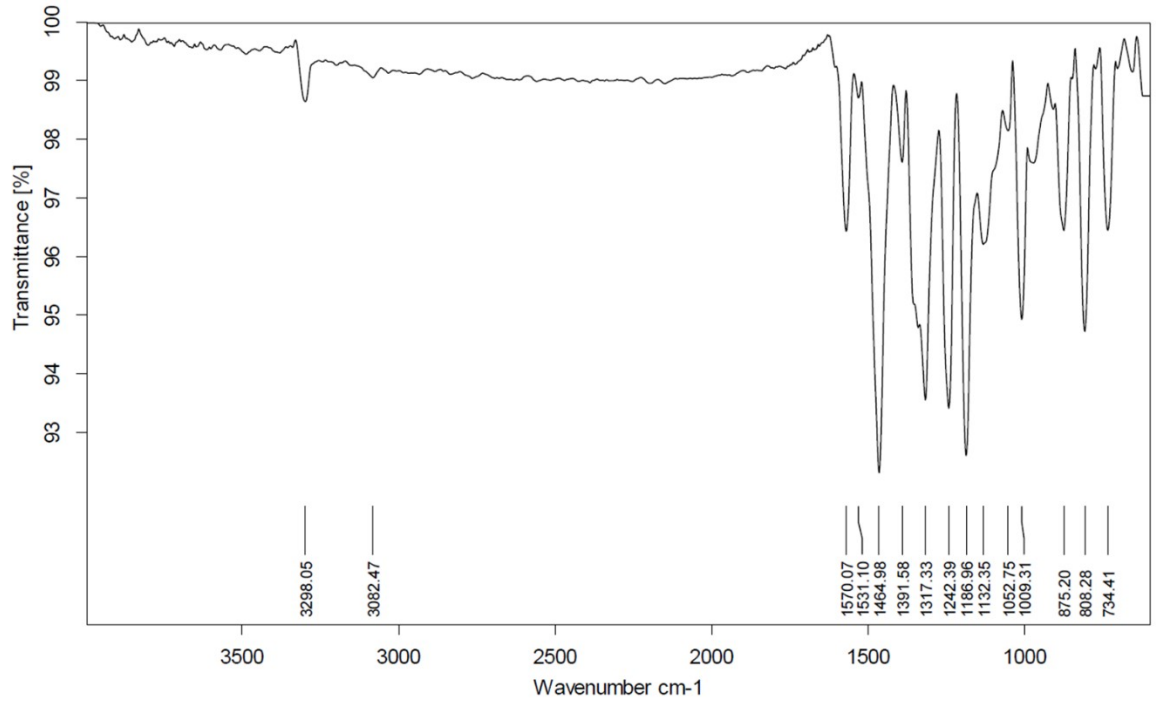

Fig. S9 FT- IR spectrum of the receptor N4R3

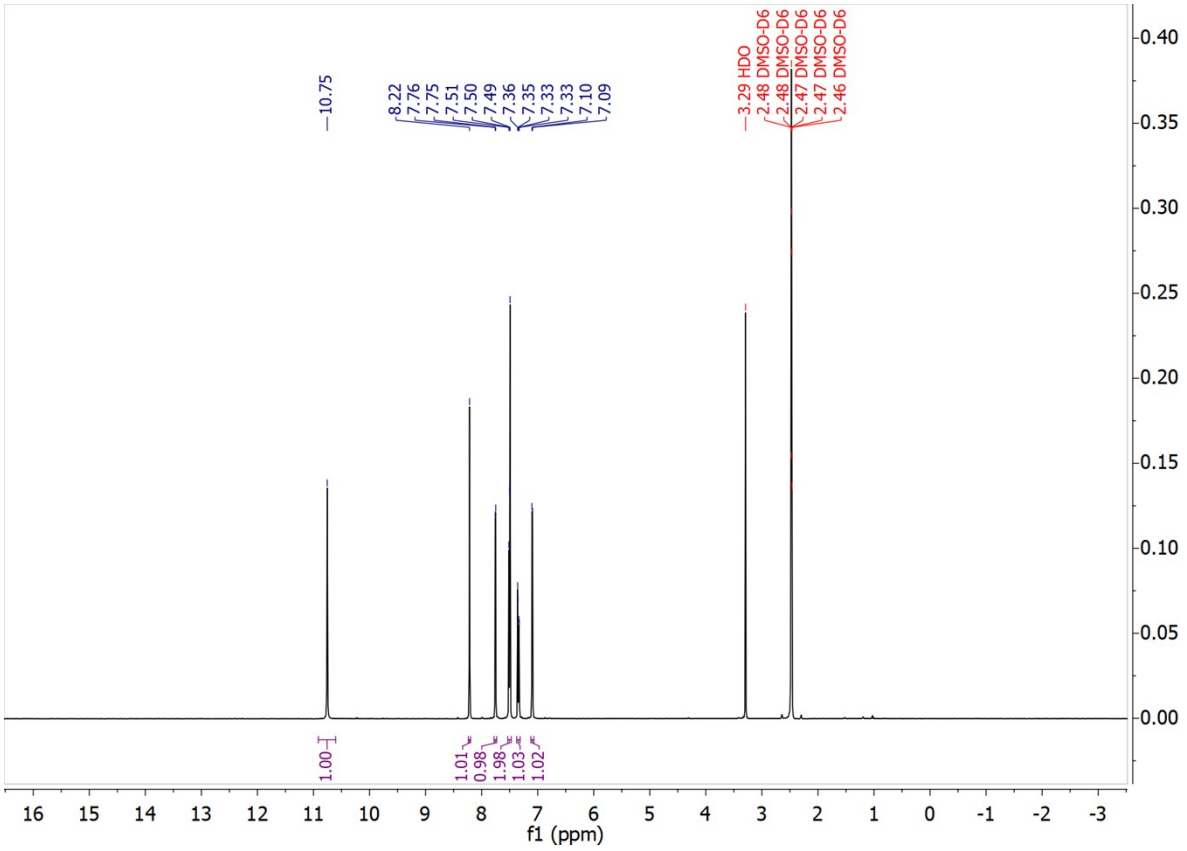

Fig. S10 ^{1}H- NMR spectrum of receptor N4R3

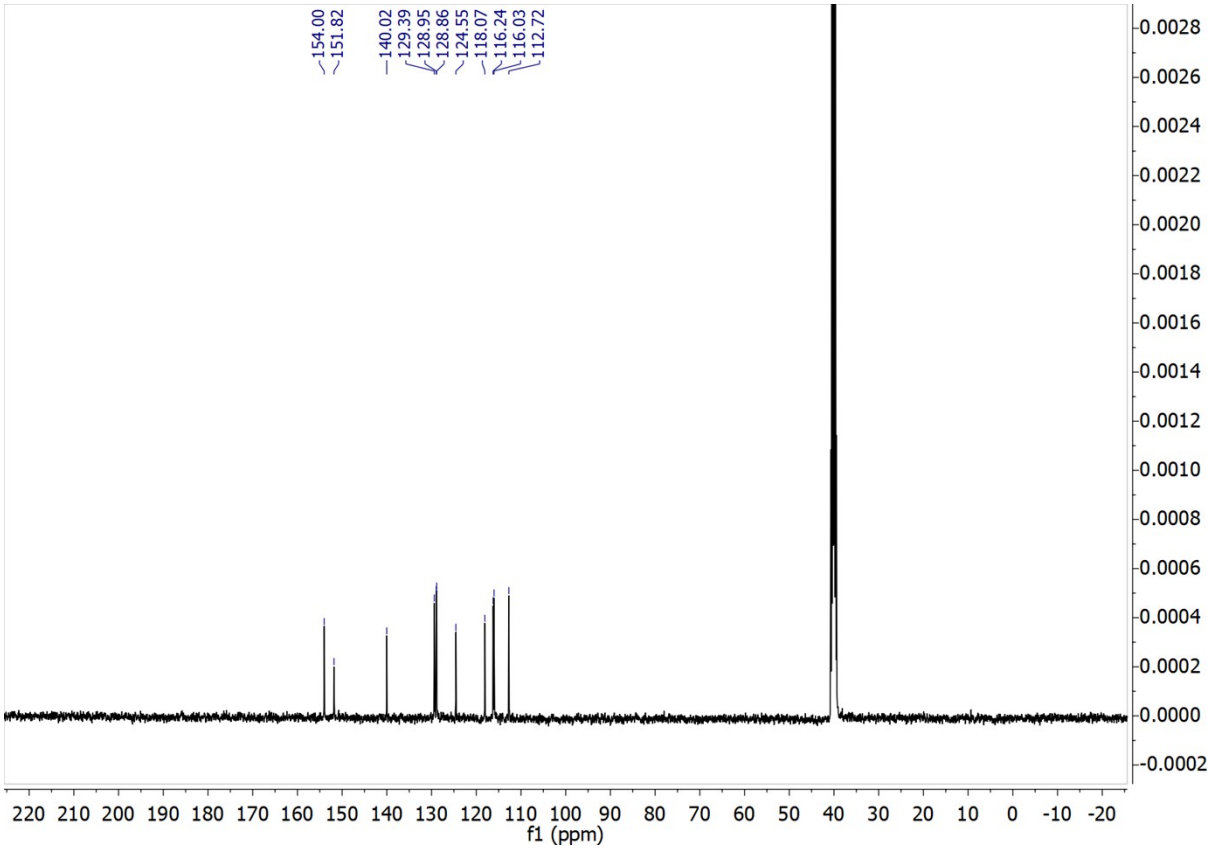

Fig. S11 ^{13}C- NMR spectrum of receptor N4R3

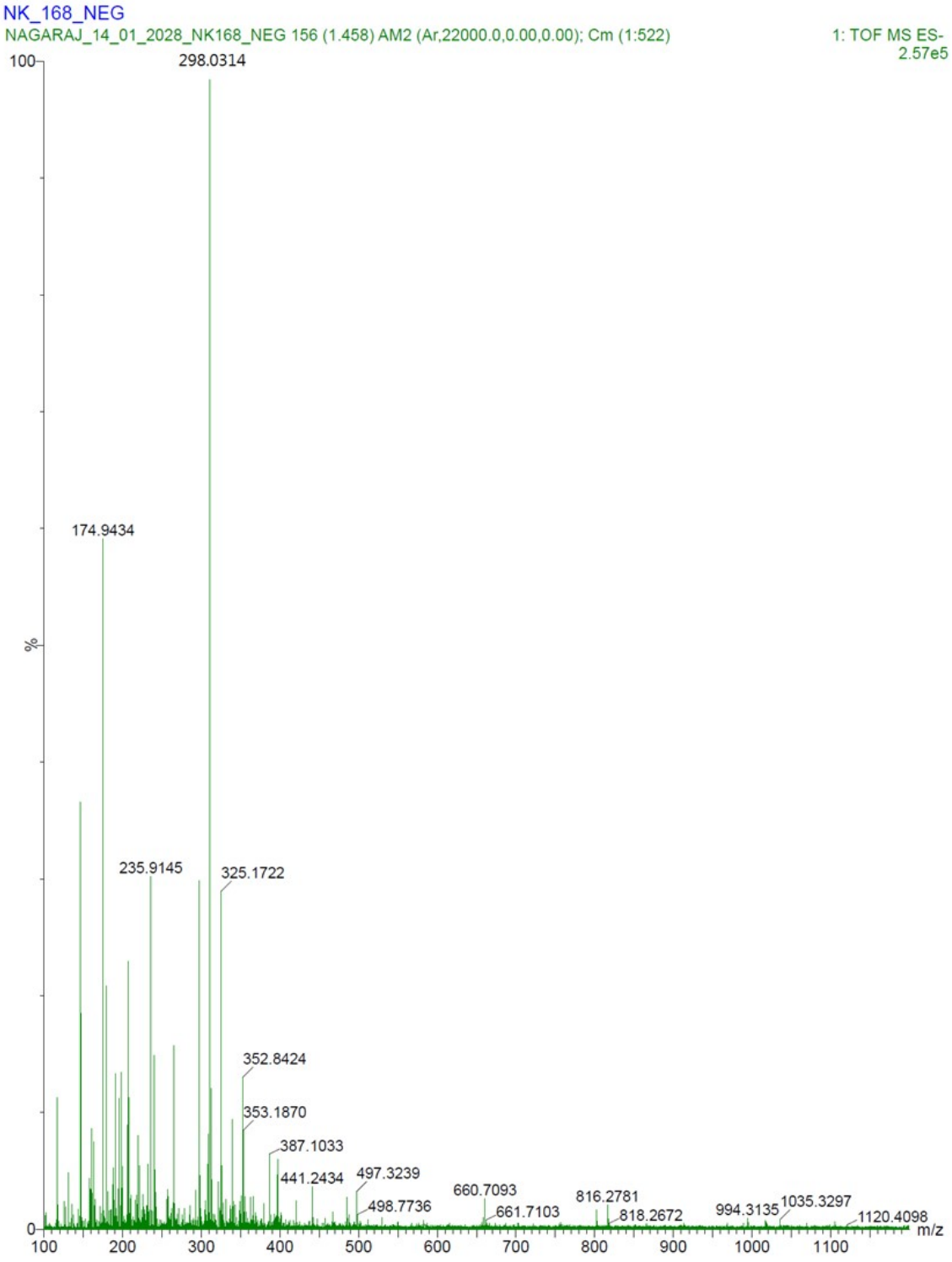

Fig. S12 LC- MS spectrum of receptor N4R3

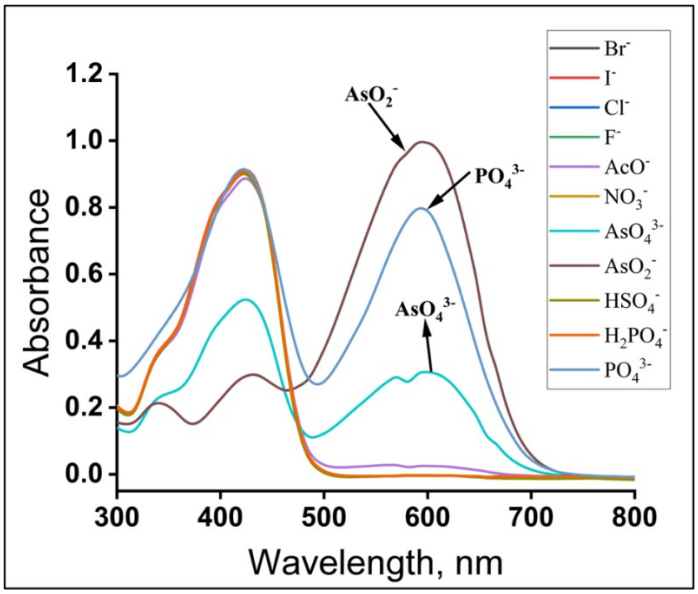

Fig. S13 UV- Vis absorption spectrum of receptor N4R1 in the presence of 2 equivalence of different anions in 30% aq. MeCN (MeCN- H_2O, 7:3, v/v)

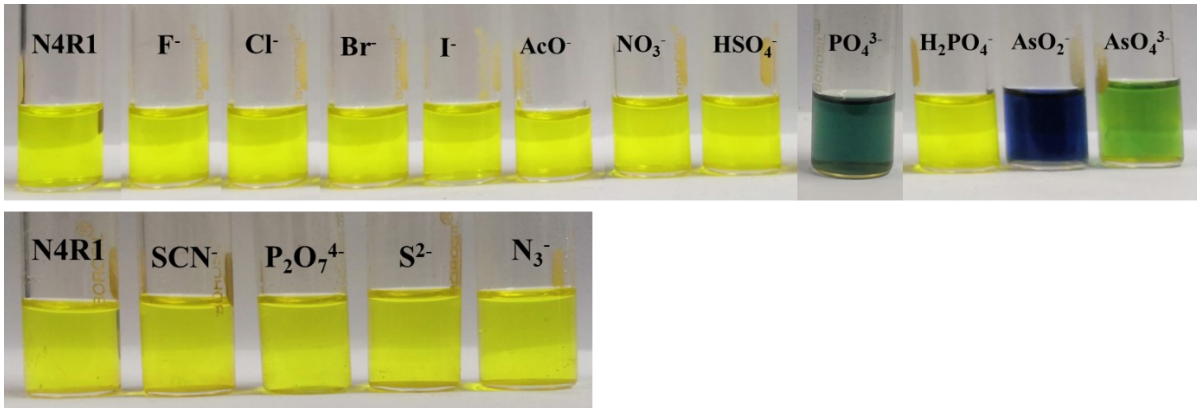

Fig. S14 Change in color observed for receptor N4R1 (2×10^{-5} M, MeCN: H_2O, 7:3, v/v) with an addition of 2 equivalent NaF, NaCl, NaBr, NaI, NaAcO, $NaNO_3$, $NaHSO_4$, Na_3PO_4, NaH_2PO_4, $NaAsO_2$, Na_3AsO_4, SCN^-, $P_2O_7^{4-}$, S^{2-}, and N_3^- (1×10^{-2} M, H_2O)

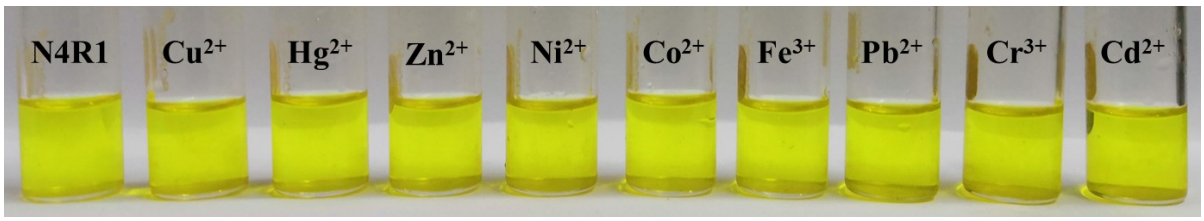

Fig. S15 Change in color observed for receptor N4R1 (2×10^{-5} M, MeCN: H_2O, 7:3, v/v) with an addition of 2 equivalent metal ions as its nitrates Cu^{2+}, Hg^{2+}, Zn^{2+}, Ni^{2+}, Co^{2+}, Fe^{3+}, Pb^{2+}, Cd^{2+}, and Cr^{3+} (1×10^{-2} M, H_2O)

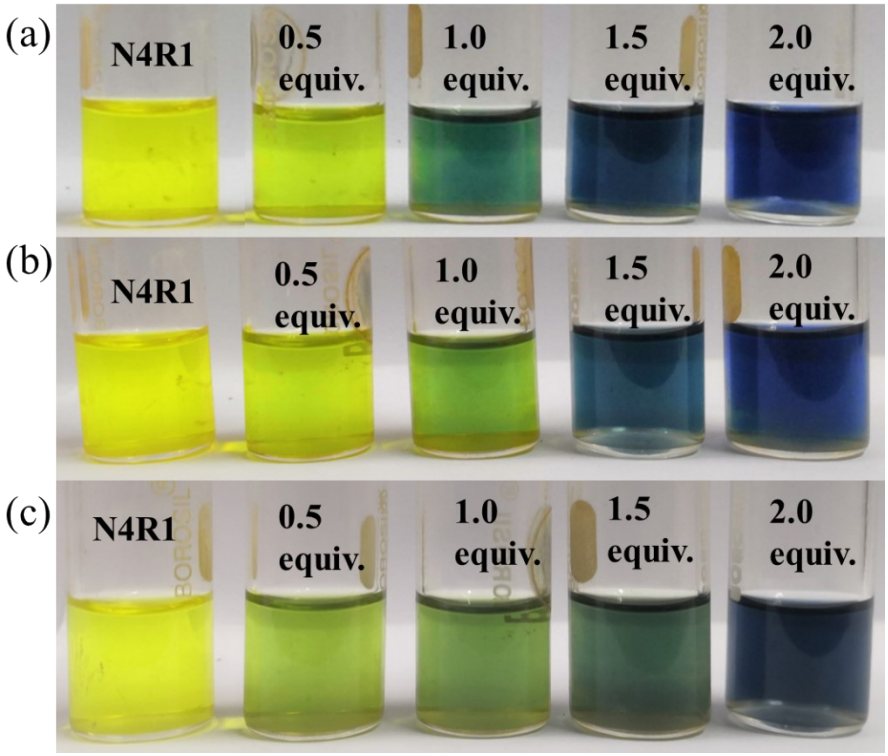

Fig. S16 Ratiometric color change of receptor N4R1 (2×10^{-5} M, 30% aq. MeCN) on addition of (i) 0.5 equivalent, (ii) 1 equivalent and (iii) 1.5 equivalent and (iv) 2 equivalent of $NaAsO_2$ (a) 1×10^{-3} M, (b) 1×10^{-4} M, (c) 1×10^{-5} M in H_2O

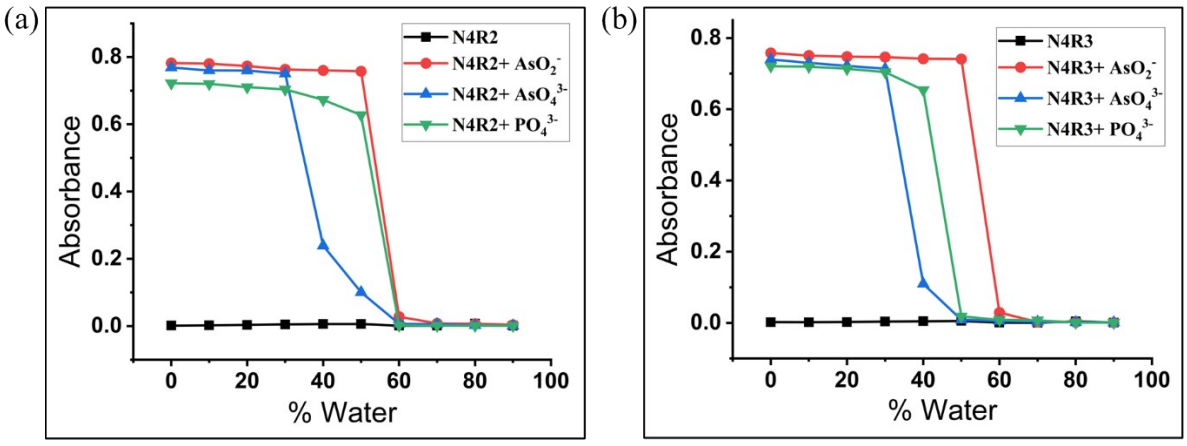

Fig. S17 UV- Vis spectral response of (a) N4R2 and N4R2+ AsO_2^-/ AsO_4^{3-}/ PO_4^{3-} and (b) N4R3 and N4R3+ AsO_2^-/ AsO_4^{3-}/ PO_4^{3-} in various percentage of water content in Me_2SO

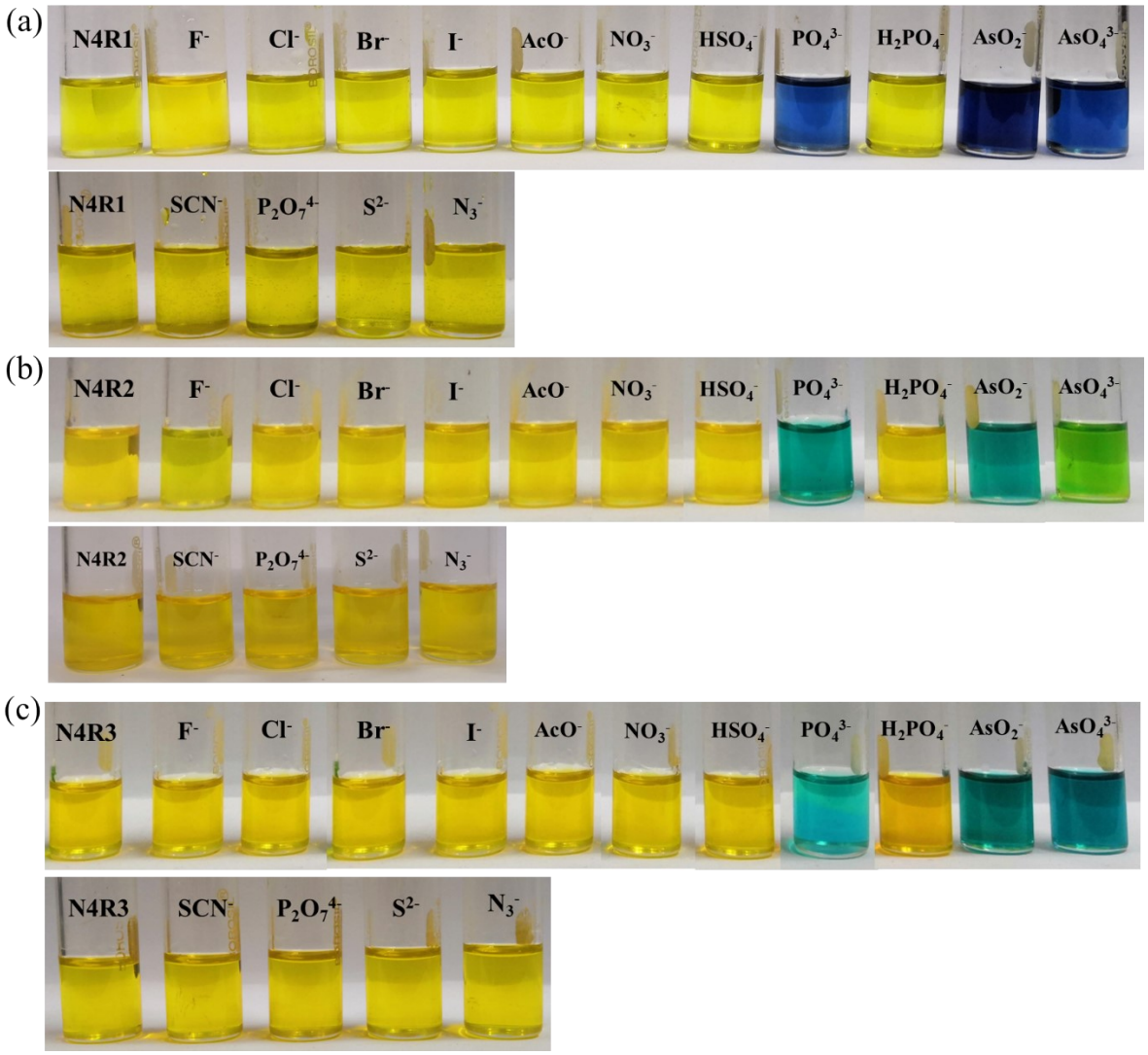

Fig. S18 Color change of receptors (2×10^{-5} M, 30% aq. Me_2SO) (a) N4R1, (b) N4R2 and (c) N4R3 on adding 2 equivalence of Na salts of anions (1×10^{-2} M, in water)

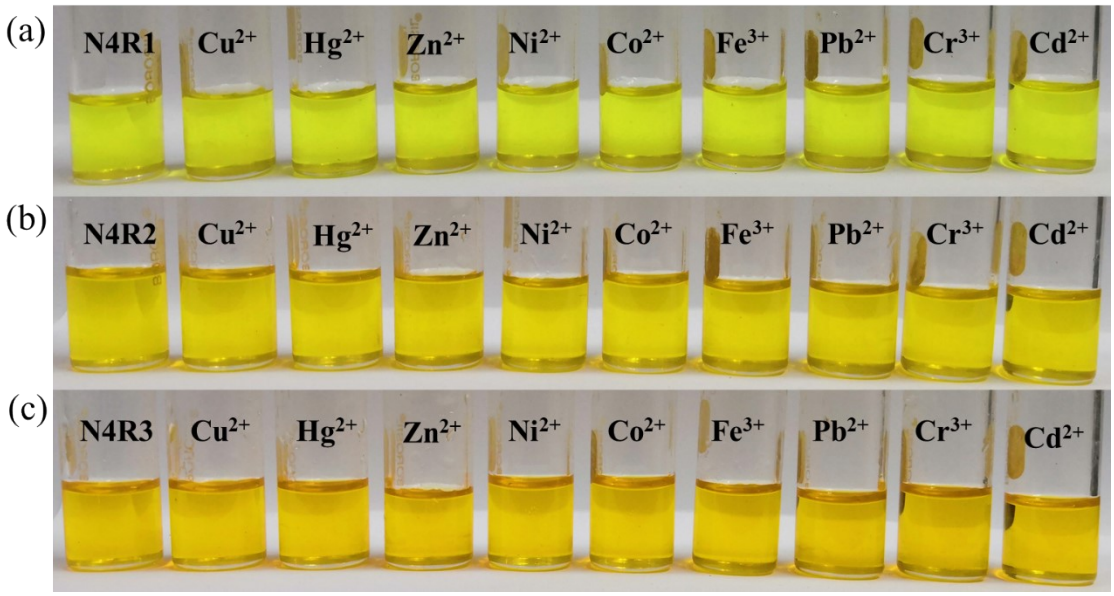

Fig. S19 Color change of receptors (2×10^{-5} M, 30% aq. Me_2SO) (a) N4R1, (b) N4R2 and (c) N4R3 on adding 2 equivalence of metal ions (1×10^{-2} M, in water)

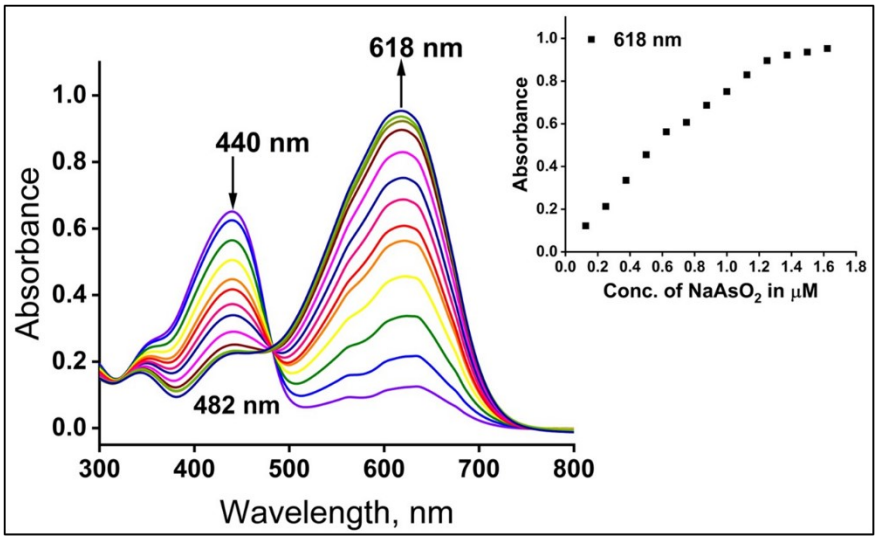

Fig. S20 The absorption variations of the receptor N4R1 (2×10^{-5} M in 30% aq. Me_2SO solution) with stepwise addition of $NaAsO_2$ (1×10^{-2} M in H_2O). Inset plots represent absorption variation with anion addition

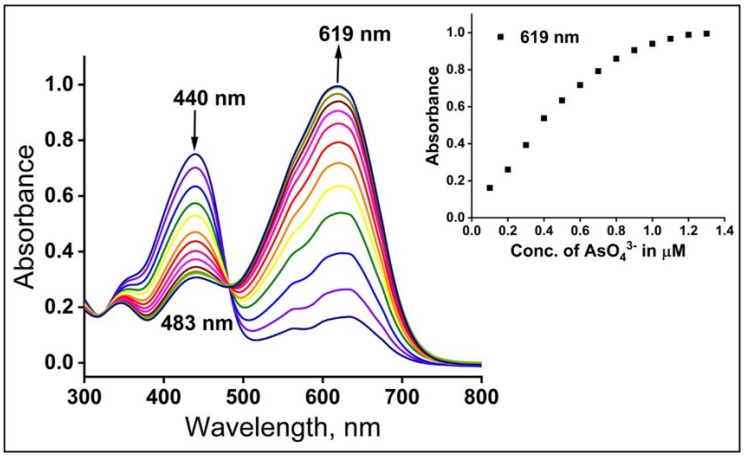

Fig. S21 The absorption variations of the receptor N4R1 (2×10^{-5} M in 30% aq. Me_2SO solution) with sequential addition of Na_3AsO_4 (1×10^{-2} M in H_2O). Inset plots represent absorption variation with anion addition

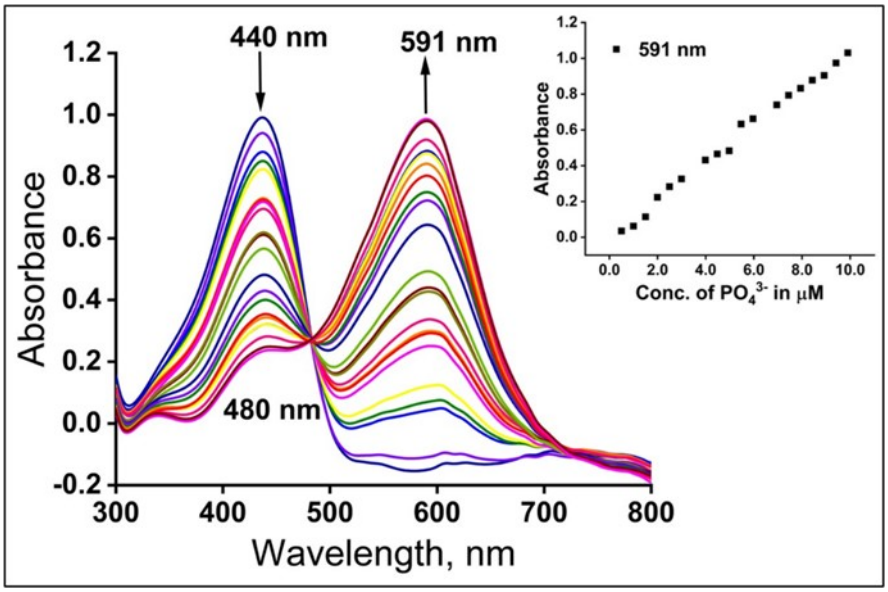

Fig. S22 The absorption variations of the receptor N4R1 (2×10^{-5} M in 30% aq. Me_2SO solution) with sequential addition of Na_3PO_4 (1×10^{-2} M in H_2O). Inset plots represent absorption variation with anion addition

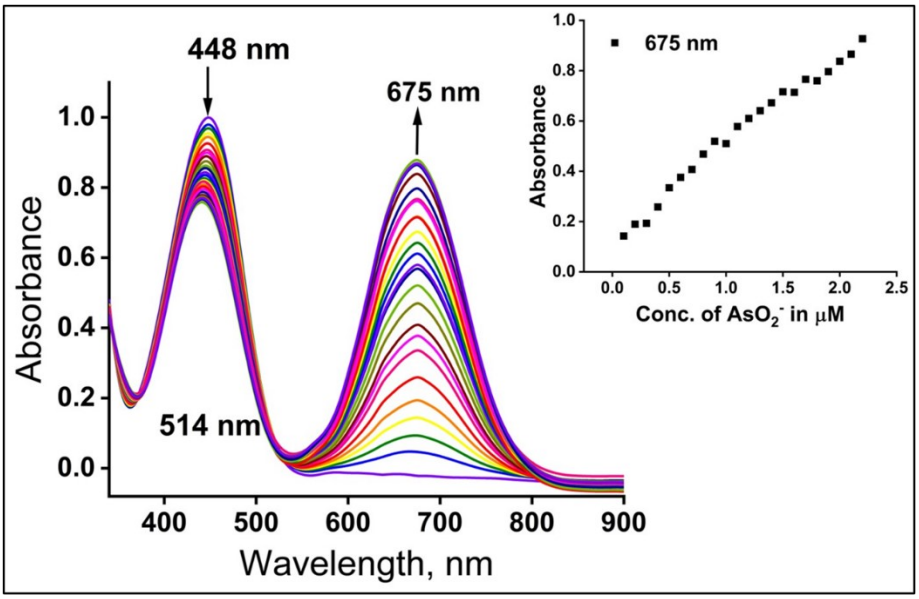

Fig. S23 The absorption variations of the receptor N4R2 (2×10^{-5} M in 30% aq. Me_2SO solution) with sequential addition of $NaAsO_2$ (1×10^{-2} M in H_2O). Inset plots represent absorption variation with anion addition

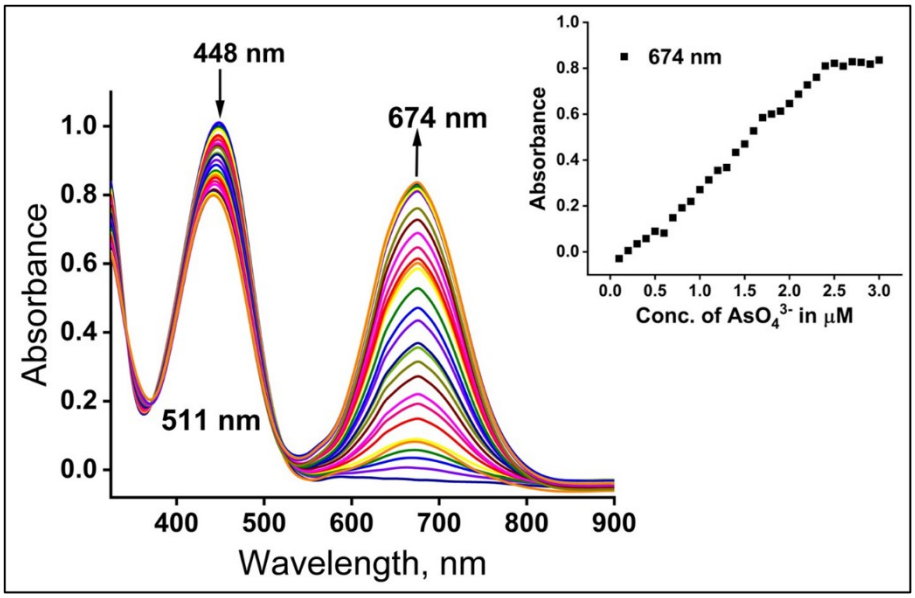

Fig. S24 The absorption variations of the receptor N4R2 (2×10^{-5} M in 30% aq. Me_2SO solution) with sequential addition of Na_3AsO_4. Inset plots represent absorption variation with anion addition

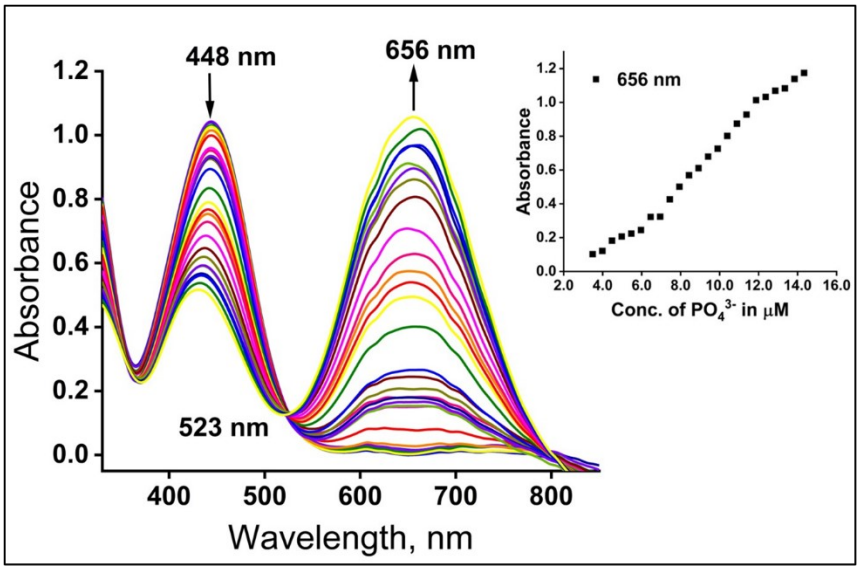

Fig. S25 The absorption variations of the receptor N4R2 (2×10^{-5} M in 30% aq. Me_2SO solution) with sequential addition of Na_3PO_4 (1×10^{-2} M in H_2O). Inset plots represent absorption variation with anion addition

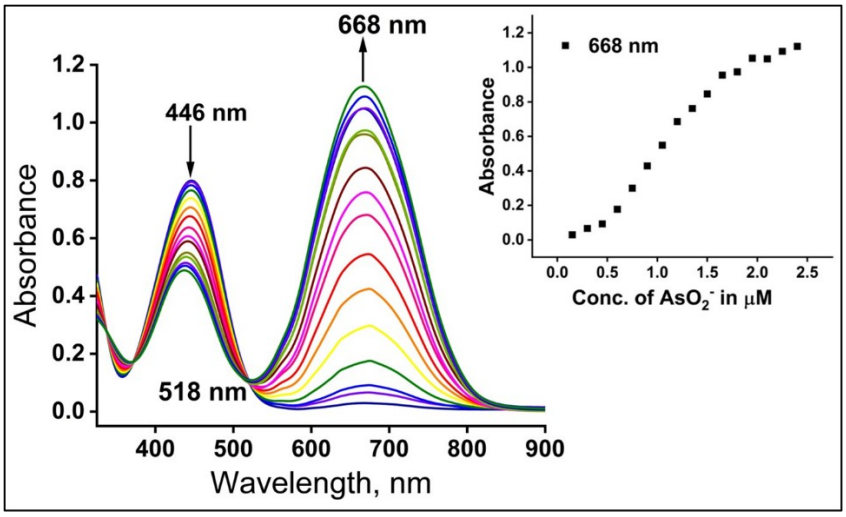

Fig. S26 The absorption variations of the receptor N4R3 (2×10^{-5} M in 30% aq. Me_2SO solution) with sequential addition of $NaAsO_2$ (1×10^{-2} M in H_2O). Inset plots represent absorption variation with anion addition

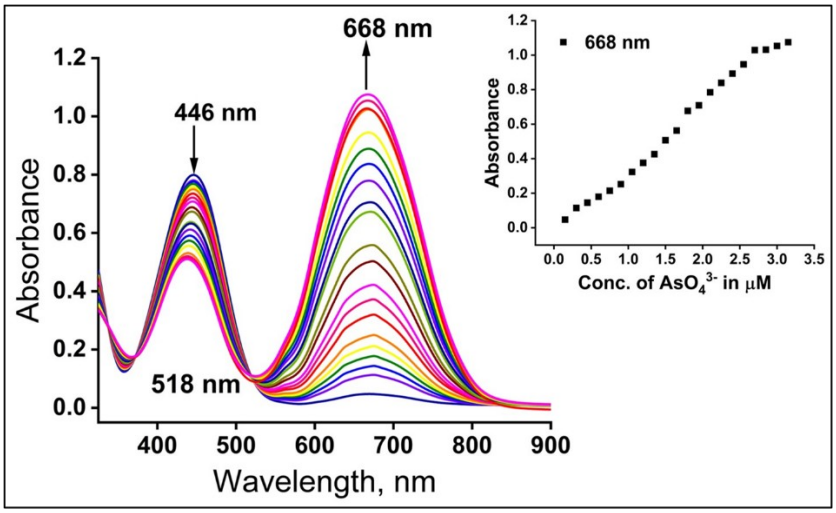

Fig. S27 The absorption variations of the receptor N4R3 (2×10^{-5} M in 30% aq. Me_2SO solution) with sequential addition of Na_3AsO_4 (1×10^{-2} M in H_2O). Inset plots represent absorption variation with anion addition

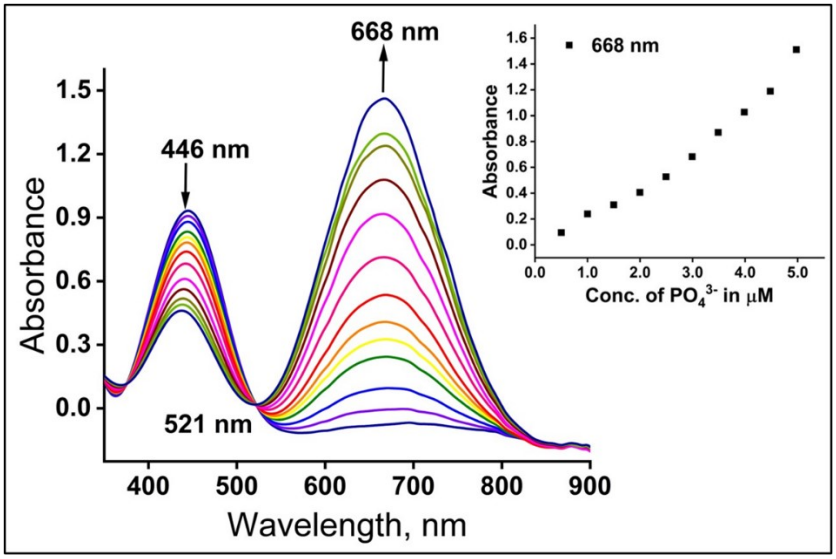

Fig. S28 The absorption variations of the receptor N4R3 (2×10^{-5} M in 30% aq. Me_2SO solution) with sequential addition of Na_3PO_4 (1×10^{-2} M in H_2O). Inset plots represent absorption variation with anion addition

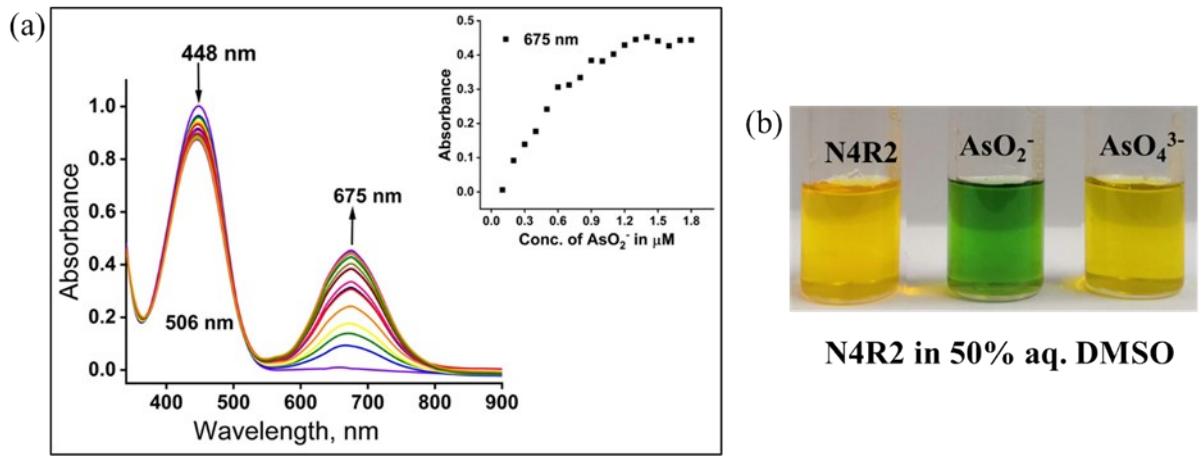

Fig. S29 (a) The absorption variations of the receptor N4R2 (2 ×10^{-5} M in Me_2SO - H_2O, 1:1 v/v) with sequential addition $NaAsO_2$ (1×10^{-2} M in water) (b) Color change of N4R2 (2 × 10^{-5} M, 50% aq. Me_2SO) on adding 2 equiv. of anions. Inset plots represent absorption variations with arsenite addition

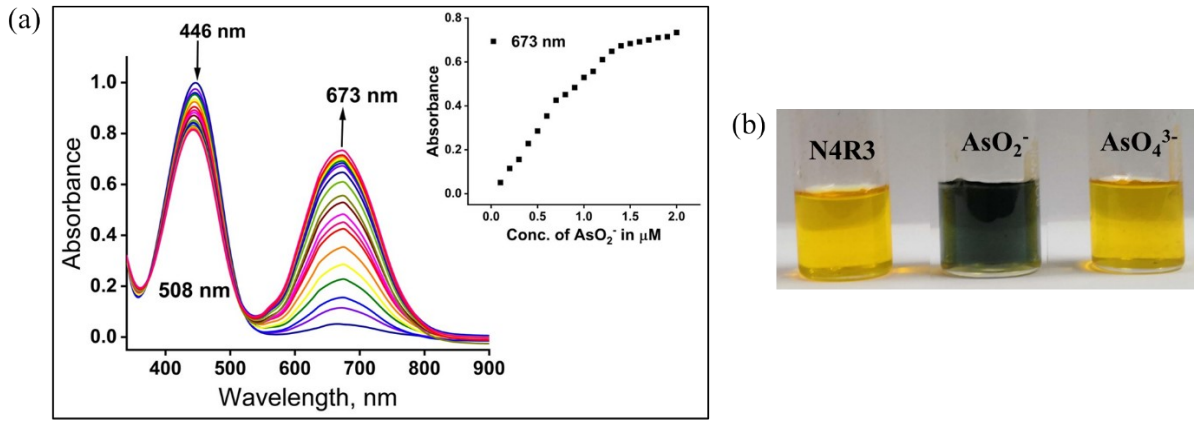

Fig. S30 (a) The absorption variations of the receptor N4R3 (2 ×10^{-5} M in Me_2SO - H_2O, 1:1 v/v) with sequential addition Na salts of arsenite (1×10^{-2} M in water). Inset plot represents absorption variation with arsenite addition (b) Color change of receptor N4R3 (2 × 10^{-5} M, 50% aq. Me_2SO) on adding 2 equivalence of Na salts of anions (1× 10^{-2} M, in water)

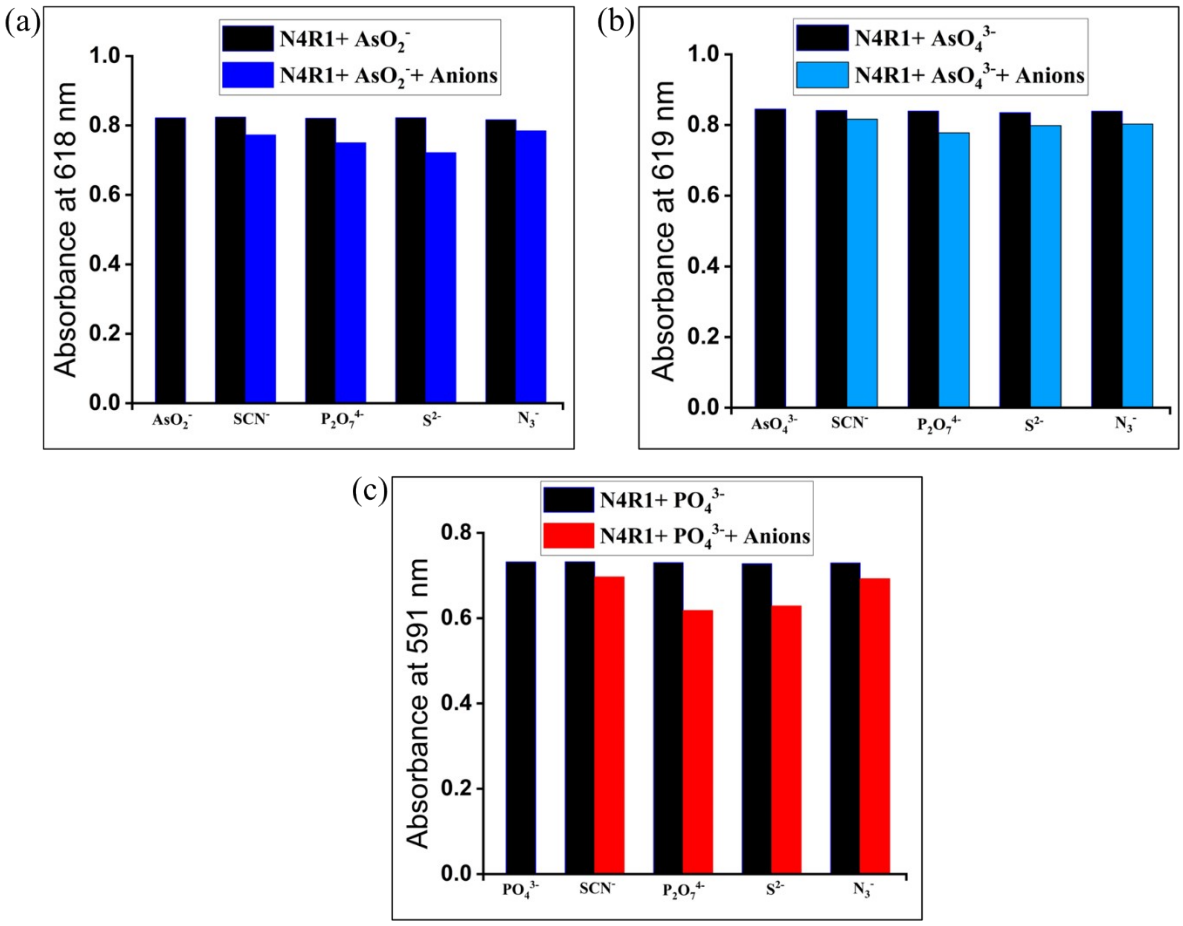

Fig. S31 Effect of competing anions in the occurrence of 3 equiv. of different anions in the (a) 30% aq. Me_2SO solution (2×10^{-5} M) Black bar: N4R1 + AsO_2^- ion, Blue bar: N4R1 + AsO_2^-+ competing anions, (b) 30% aq. Me_2SO solution (2×10^{-5} M) Black bar: N4R1 + AsO_4^{3-} ion, Sky blue bar: N4R1 + AsO_4^{3-} + competing anions, and (c) 30% aq. Me_2SO solution (2×10^{-5} M) Black bar: N4R1 + PO_4^{3-} ion, Red bar: N4R1 + PO_4^{3-} + competing anions

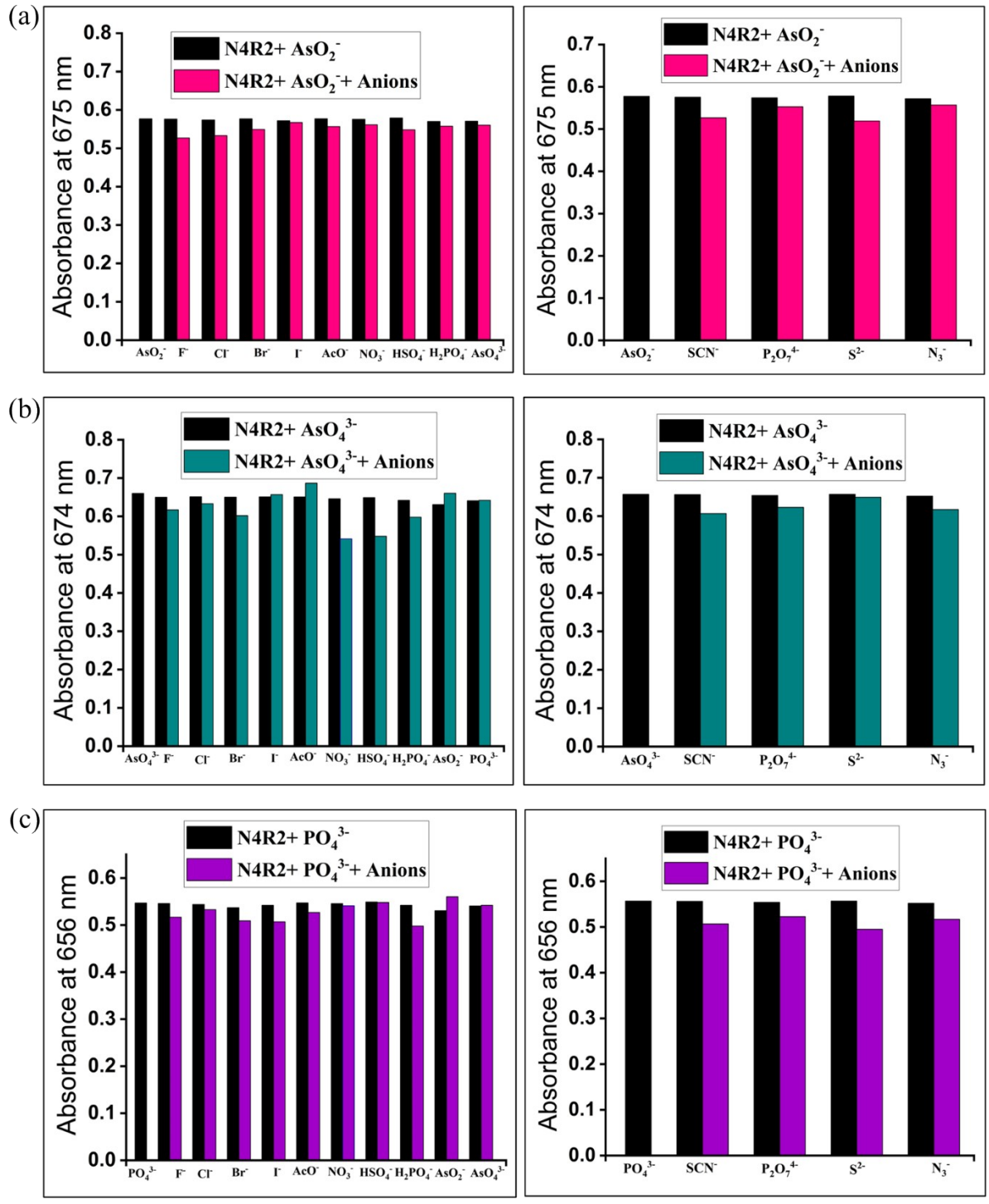

Fig. S32 Effect of competing anions in the occurrence of 3 equiv. of different anions in the (a) 30% aq. Me_2SO solution (2×10^{-5} M) Black bar: N4R2 + AsO_2^- ion, pink bar: N4R2 + AsO_2^-+ competing anions, (b) 30% aq. Me_2SO solution (2×10^{-5} M) Black bar: N4R2 + AsO_4^{3-} ion, Green bar: N4R2 + AsO_4^{3-} + competing anions, and (c) 30% aq. Me_2SO solution (2×10^{-5} M) Black bar: N4R2 + PO_4^{3-} ion, Violet bar: N4R2 + PO_4^{3-} + competing anions

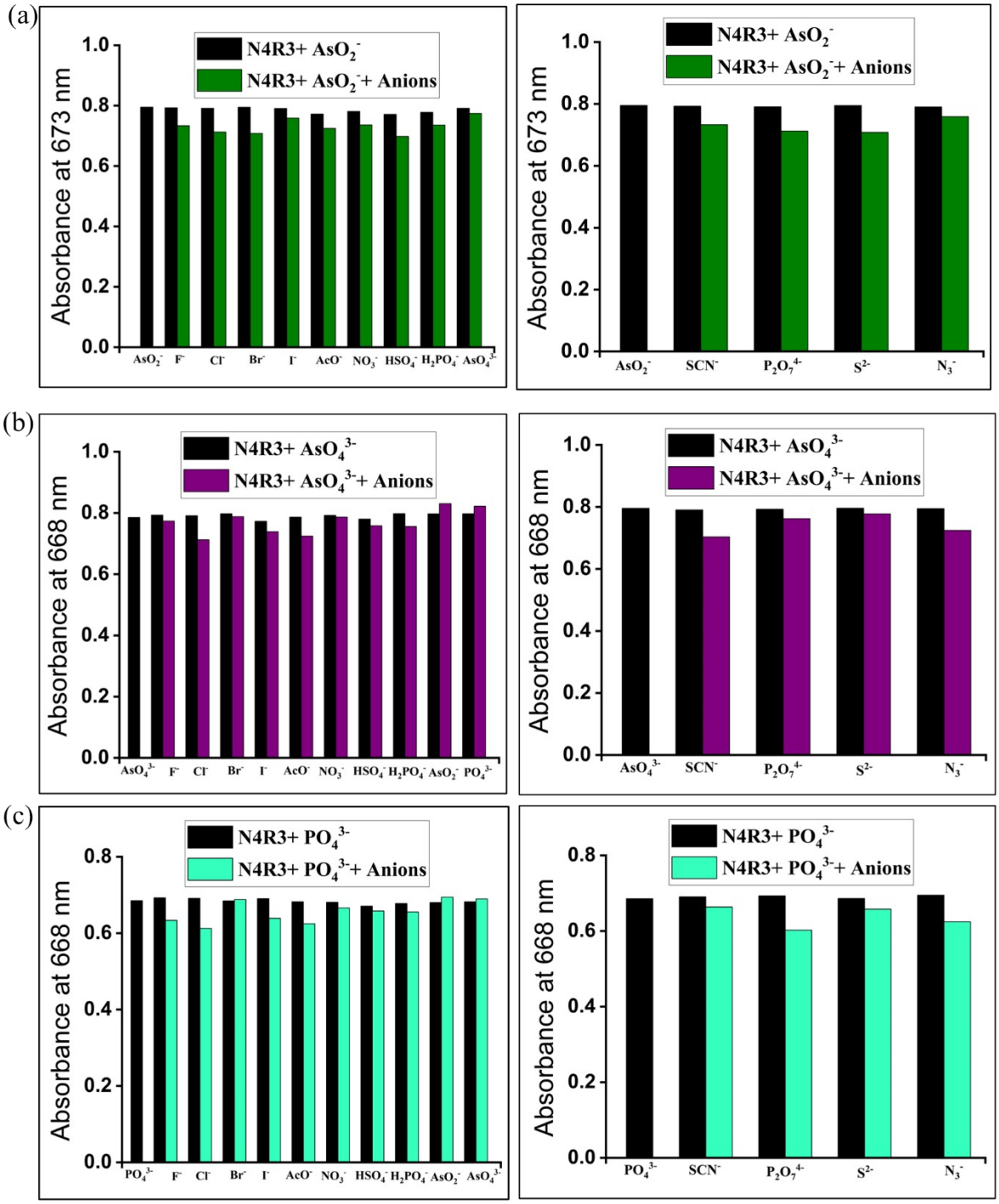

Fig. S33 Effect of competing anions in the occurrence of 3 equiv. of different anions in the (a) 30% aq. Me_2SO solution (2×10^{-5} M) Black bar: N4R3 + AsO_2^- ion, Green bar: N4R3 + AsO_2^-+ competing anions, (b) 30% aq. Me_2SO solution (2×10^{-5} M) Black bar: N4R3 + AsO_4^{3-} ion, Purple bar: N4R3 + AsO_4^{3-} + competing anions, and (c) 30% aq. Me_2SO solution (2×10^{-5} M) Black bar: N4R3 + PO_4^{3-} ion, Cyan bar: N4R3 + PO_4^{3-} + competing anions

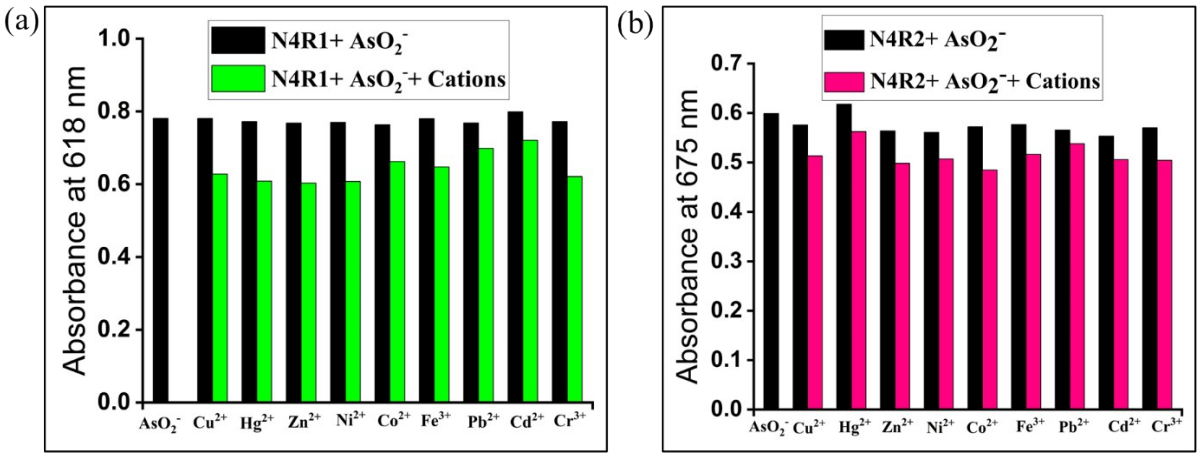

Fig. S34 Outcome of competing cations in the occurrence of 3 equiv. of different cations in the (a) 50% aq. Me_2SO solution (2×10^{-5} M) Black bar: N4R1 + AsO_2^- ion, Green bar: N4R1 + AsO_2^-+ cations, and (b) 50% aq. Me_2SO solution (2×10^{-5} M) Black bar: N4R2 + AsO_2^- ion, Pink bar: N4R2 + AsO_2^-+ cations

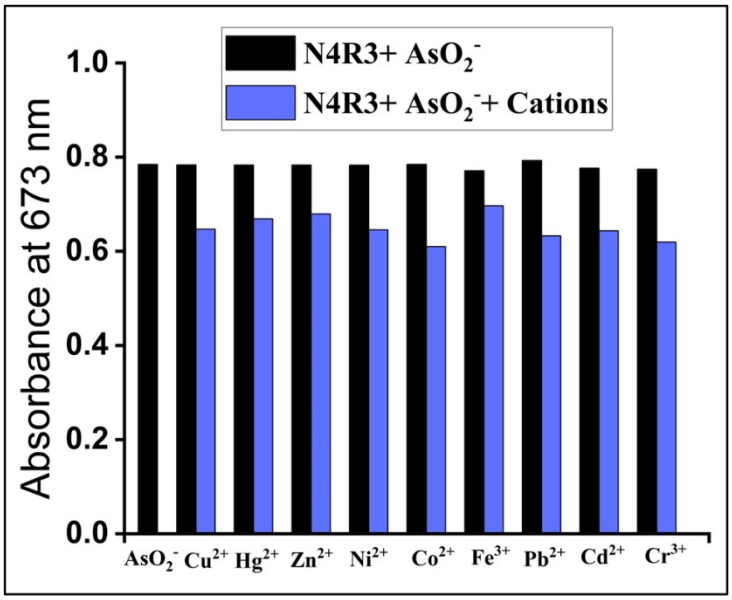

Fig. S35 Effect of competing anions in the presence of 3 equiv. of different cations in the 50% aq. Me_2SO solution (2×10^{-5} M) Black bar: N4R3 + AsO_2^- ion, blue bar: N4R3 + AsO_2^-+ cations

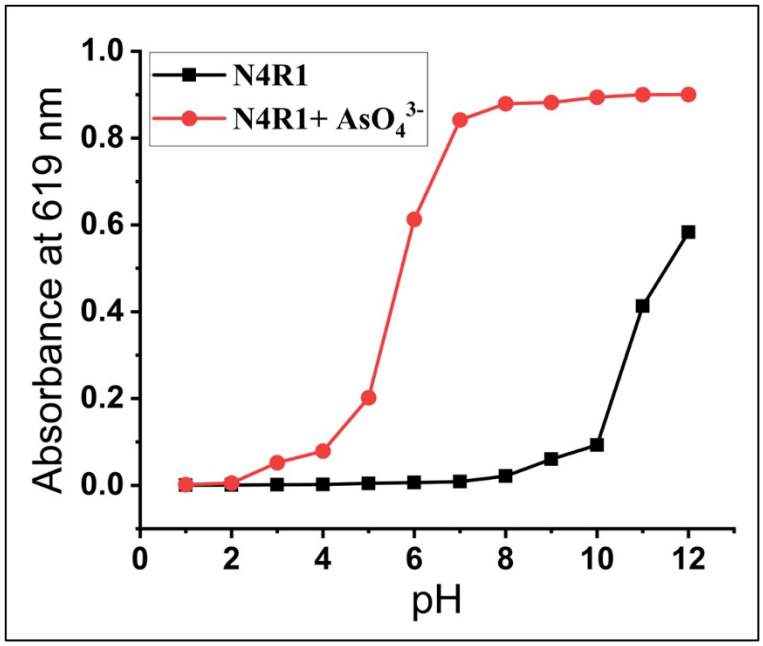

Fig. S36 pH effect on the UV- Vis absorption spectra of N4R1 and N4R1+ AsO_4^{3-} in Me_2SO - H_2O (7: 3, v/v)

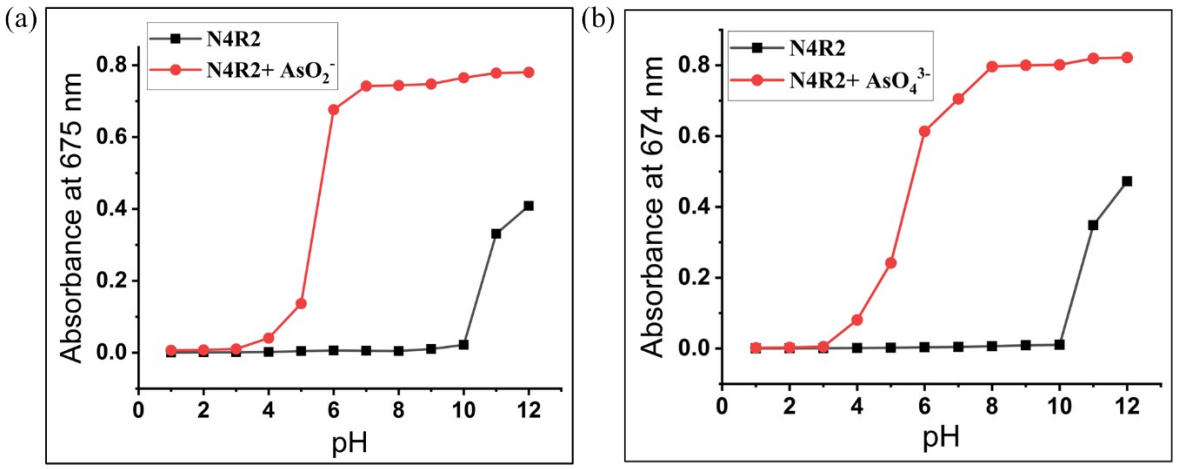

Fig. S37 pH effect on the UV- Vis absorption spectra of (a) N4R2 and N4R2+ AsO_2^- and (b) N4R2 and N4R2+ AsO_4^{3-} in Me_2SO - H_2O (7: 3, v/v)

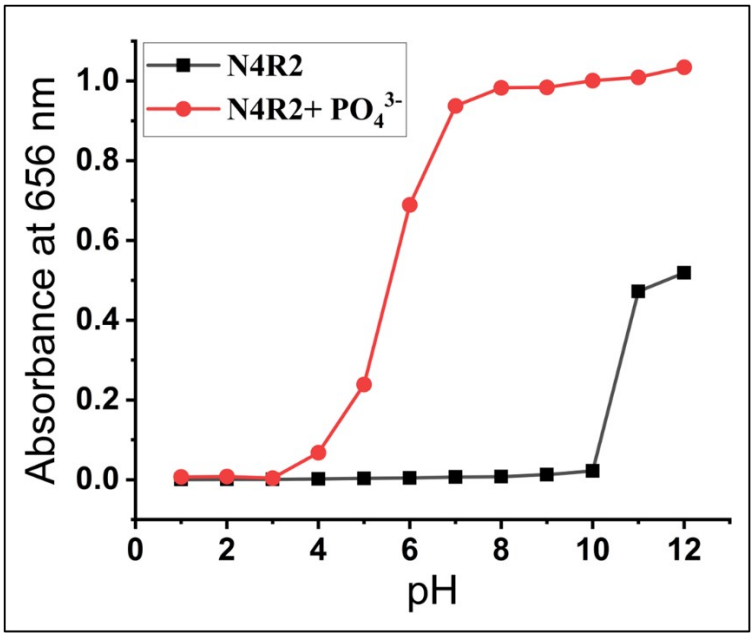

Fig. S38 pH effect on the UV- Vis absorption spectra of N4R2 and N4R2+ PO_4^{3-} in Me_2SO - H_2O (7: 3, v/v)

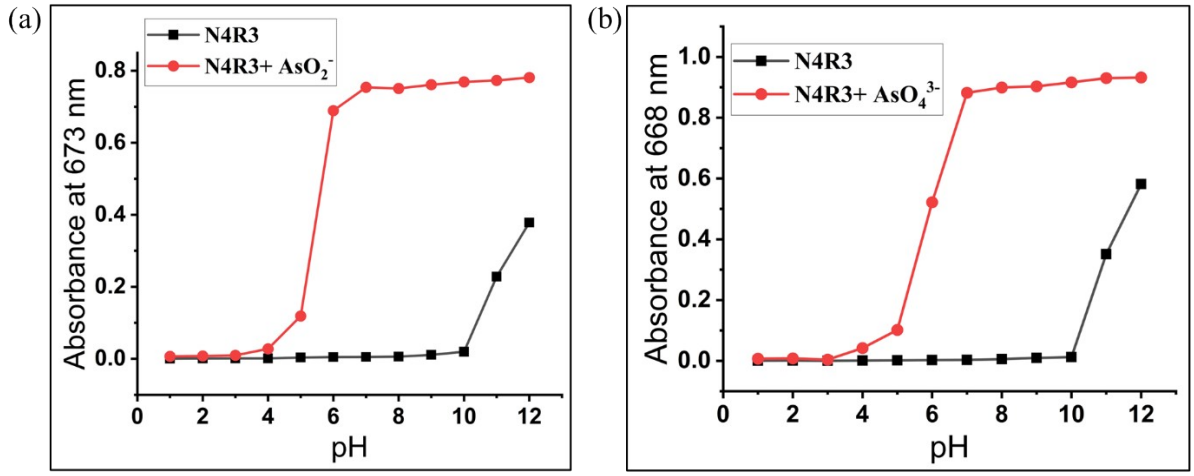

Fig. S39 pH effect on the UV- Vis absorption spectra of (a) N4R3 and N4R3+ AsO_2^- and (b) N4R3 and N4R3+ AsO_4^{3-} in Me_2SO - H_2O (7: 3, v/v)

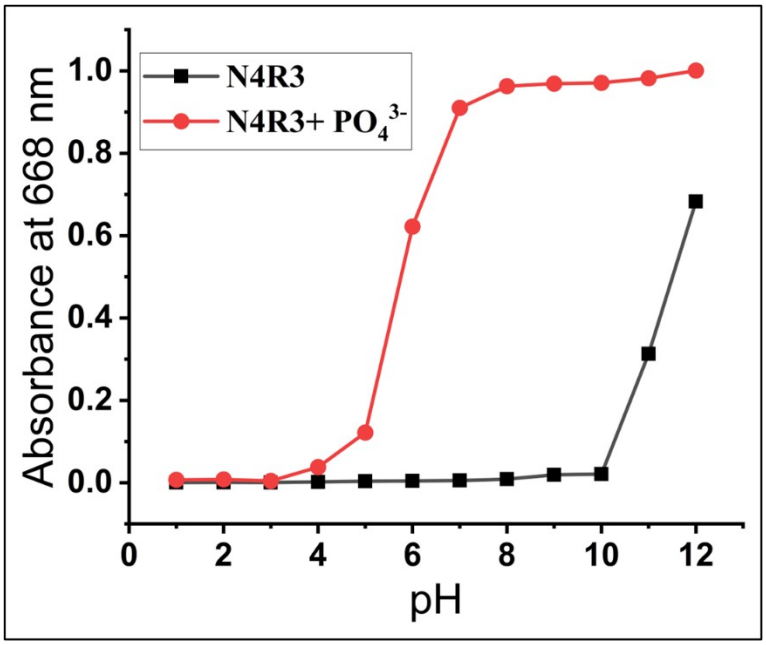

Fig. S40 pH effect on the UV- Vis absorption spectra of N4R3 and N4R3+ PO_4^{3-} in Me_2SO - H_2O (7: 3, v/v)

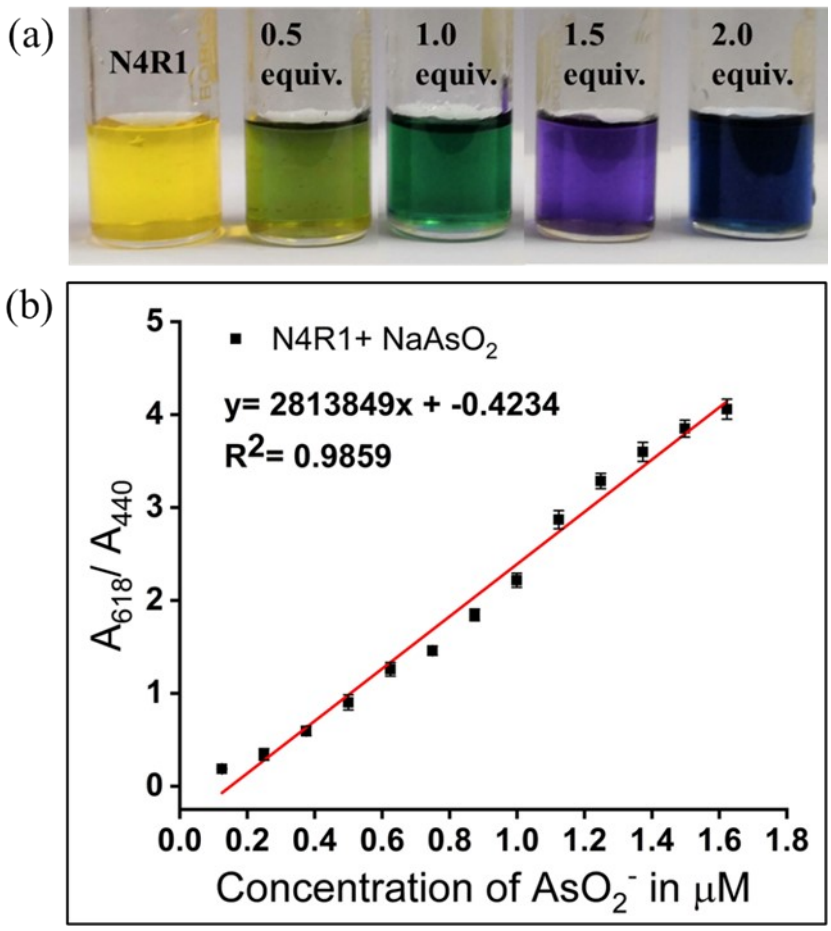

Fig. S41 Rariometric color change of 30% aq. Me_2SO receptor N4R1 on 0.5- 2.0 equiv. of $NaAsO_2$ addition and (b) Ratiometric plot of A_{618}/A_{440} for N4R1 with the increasing concentration of arsenite ion

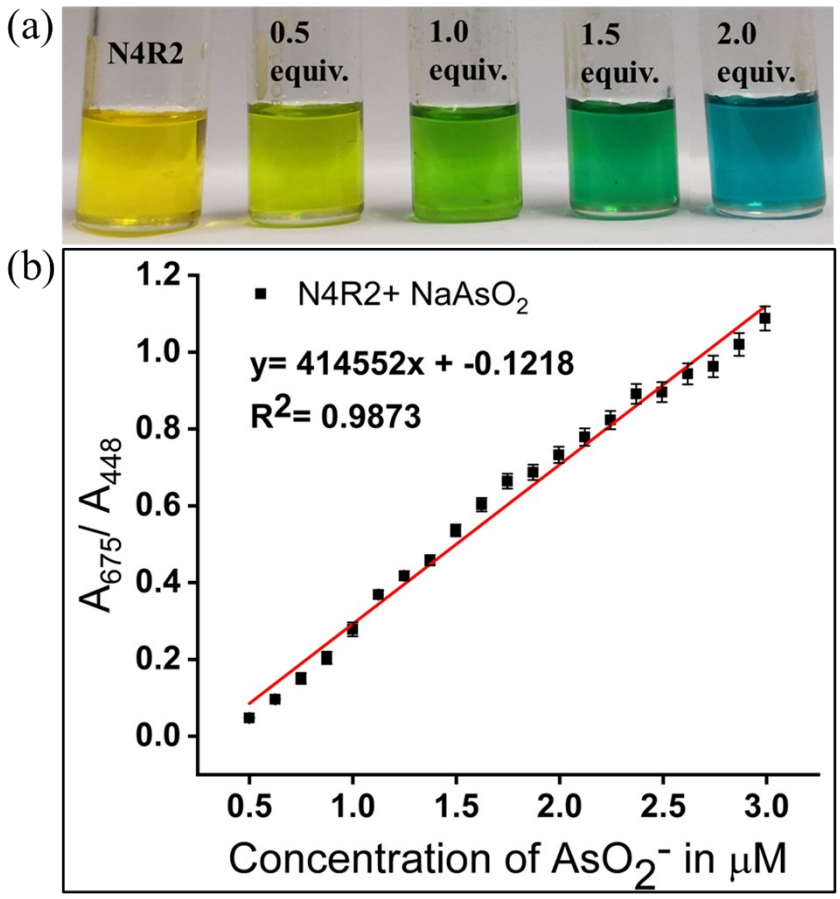

Fig. S42 Ratiometric color change of 30% aq. Me_2SO receptor N4R2 on 0.5- 2.0 equivalents of sodium arsenite addition and (b) Ratiometric plot of A_{675}/A_{448} for receptor N4R2 with the increasing concentration of AsO_2^- ion

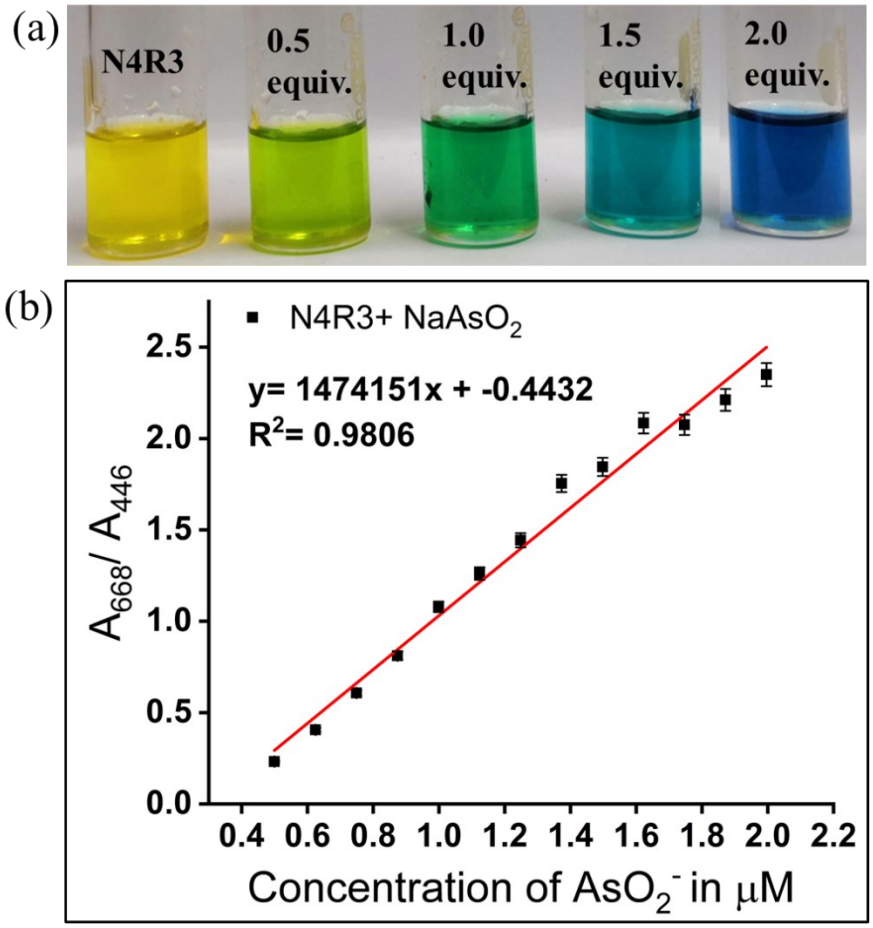

Fig. S43 Ratiometric color change of 30% aq. Me_2SO receptor N4R3 on 0.5- 2.0 equivalents of sodium arsenite addition and (b) Ratiometric plot of A_{668}/A_{446} for receptor N4R3 with the increasing concentration of AsO_2^- ion

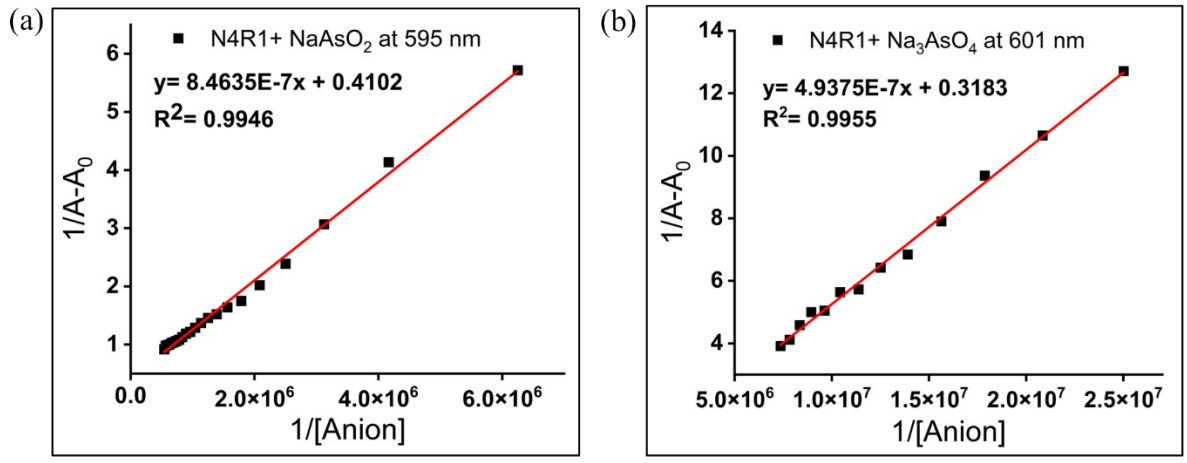

Fig. S44 (a) B-H plot for N4R1—AsO_2^- complex in MeCN - H_2O (7:3, v/v) and (b) B-H plot for N4R1- AsO_4^{3-} complex in MeCN - H_2O (7: 3 v/v)

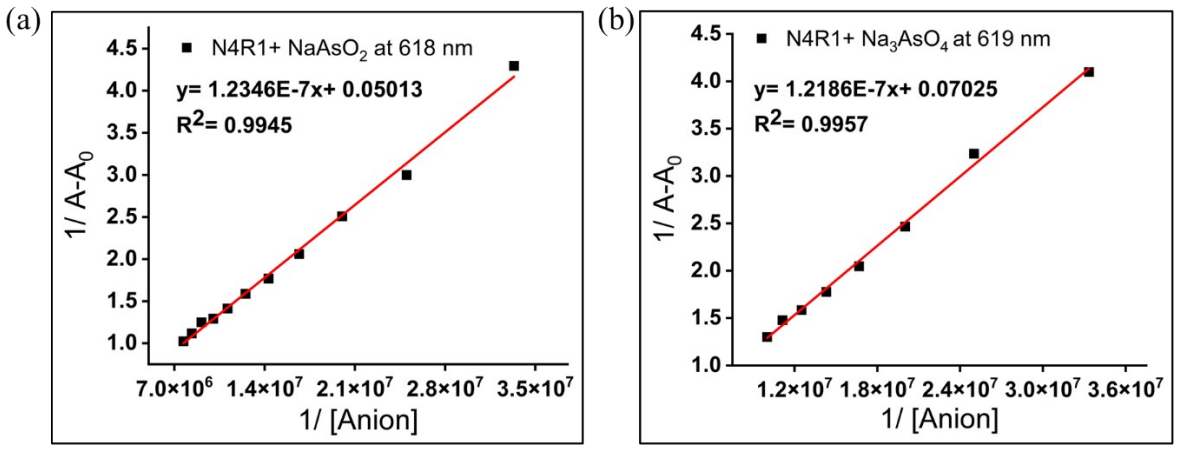

Fig. S45 (a) B-H plot for N4R1—AsO_2^- complex in Me_2SO - H_2O (7:3, v/v) and (b) B-H plot for N4R1- AsO_4^{3-} complex in Me_2SO - H_2O (7: 3 v/v)

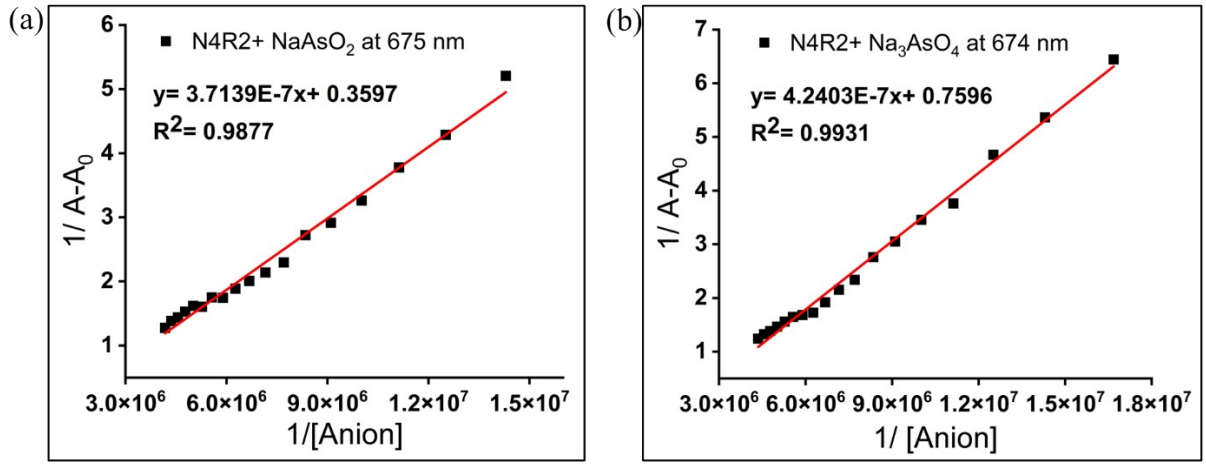

Fig. S46 (a) B-H plot for N4R2—AsO_2^- complex in Me_2SO - H_2O (7:3, v/v) and (b) B-H plot for N4R2- AsO_4^{3-} complex in Me_2SO - H_2O (7: 3 v/v)

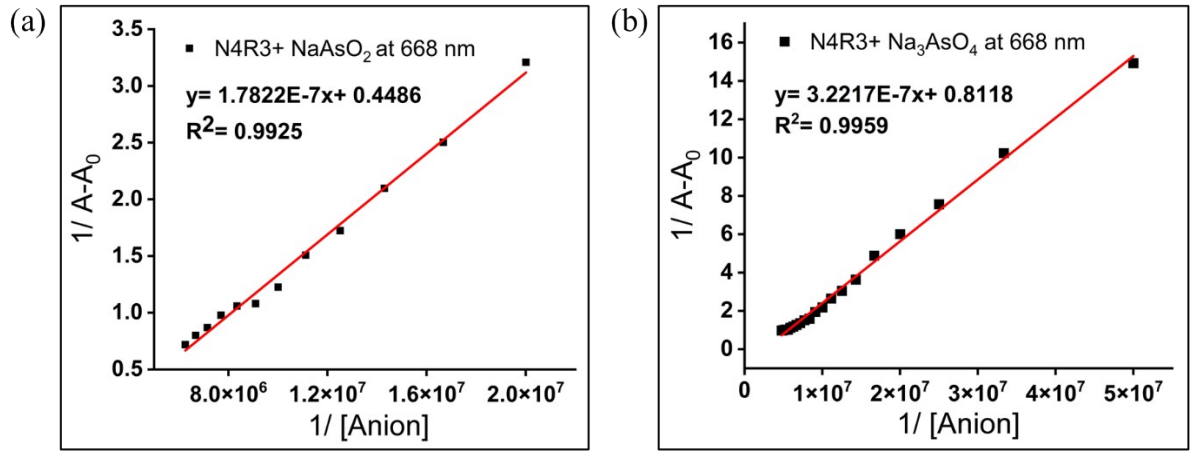

Fig. S47 (a) B-H plot for N4R3—AsO_2^- complex in Me_2SO - H_2O (7:3, v/v) and (b) B-H plot for N4R3- AsO_4^{3-} complex in Me_2SO - H_2O (7: 3 v/v)

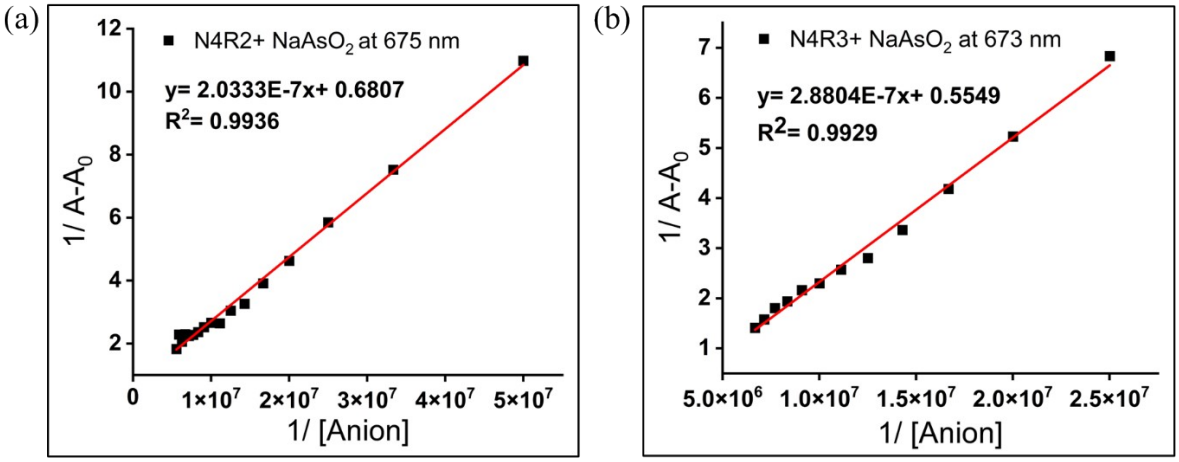

Fig. S48 (a) B-H plot for N4R2—AsO_2^- complex in Me_2SO - H_2O (1:1, v/v) and (b) B-H plot for N4R3- AsO_2^- complex in Me_2SO - H_2O (1: 1 v/v)

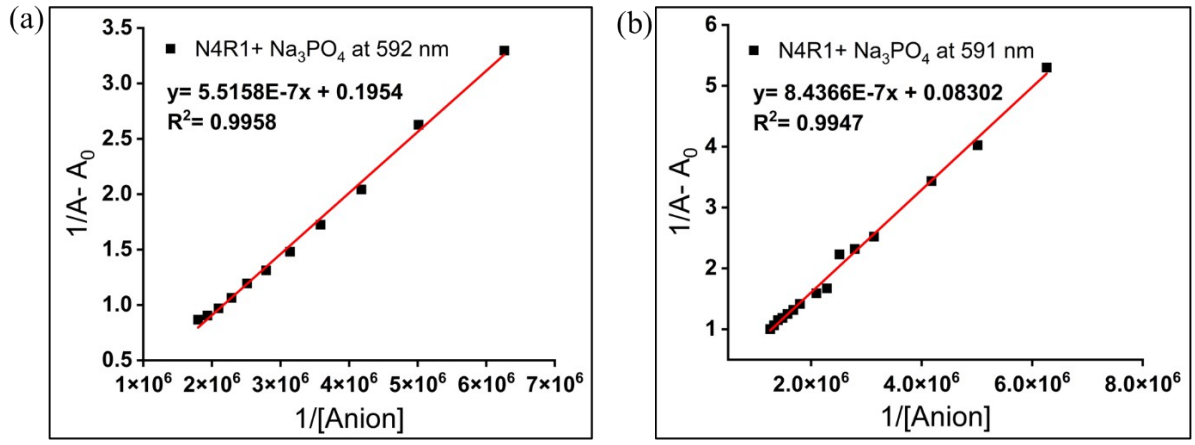

Fig. S49 B-H plot for N4R1—PO_4^{3-} complex in **(**a) MeCN- H_2O (7: 3, v/v) and (b) Me_2SO - H_2O (7: 3, v/v)

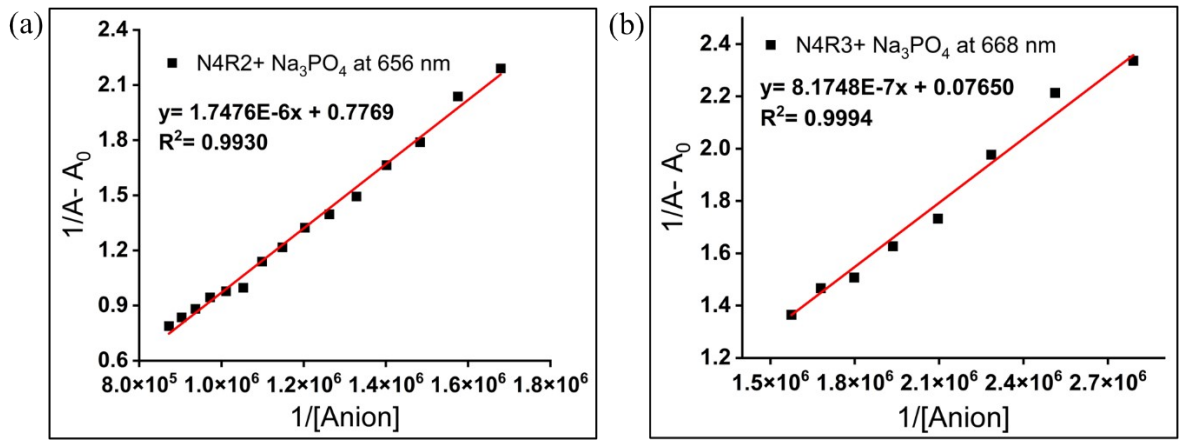

Fig. S50 (a) B-H plot for N4R2—PO_4^{3-} complex in Me_2SO - H_2O (7: 3, v/v) and (b) B-H plot for N4R3- PO_4^{3-} complex in Me_2SO - H_2O (7: 3, v/v)

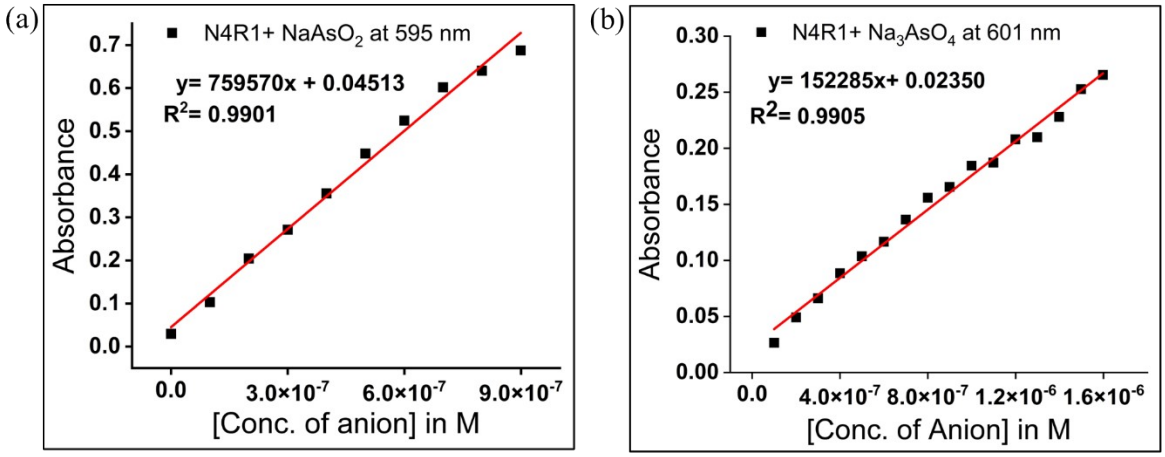

Fig. S51 (a) Calibration curve for N4R1—AsO_2^- complex in MeCN - H_2O (7: 3, v/v) and (b) calibration curve for N4R1- AsO_4^{3-} complex in MeCN - H_2O (7: 3, v/v)

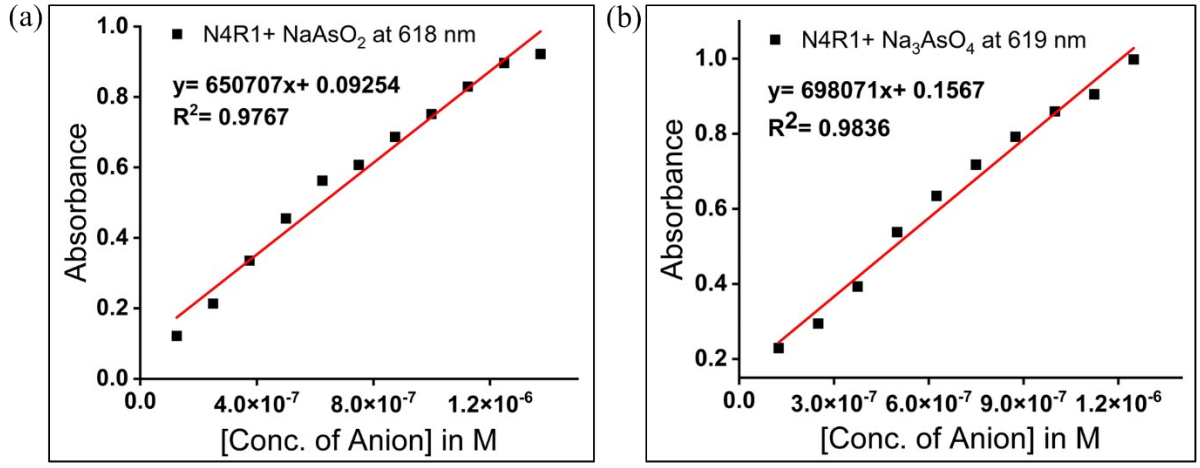

Fig. S52 (a) Calibration curve for N4R1—AsO_2^- complex in Me_2SO- H_2O (7: 3, v/v) and (b) calibration curve for N4R1- AsO_4^{3-} complex in Me_2SO - H_2O (7: 3, v/v)

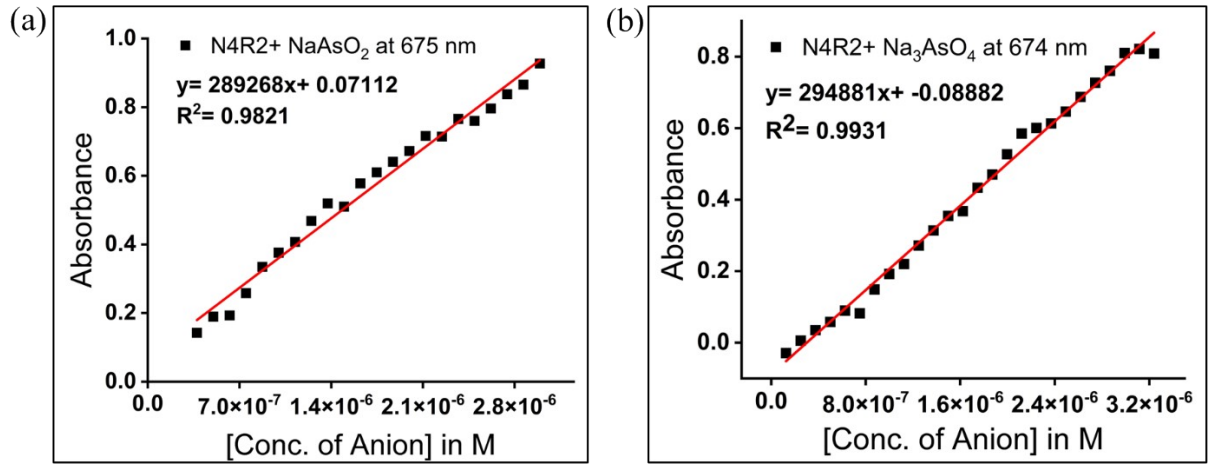

Fig. S53 (a) Calibration curve for N4R2—AsO_2^- complex in Me_2SO - H_2O (7: 3, v/v) and (b) calibration curve for N4R2- AsO_4^{3-} complex in Me_2SO - H_2O (7: 3, v/v)

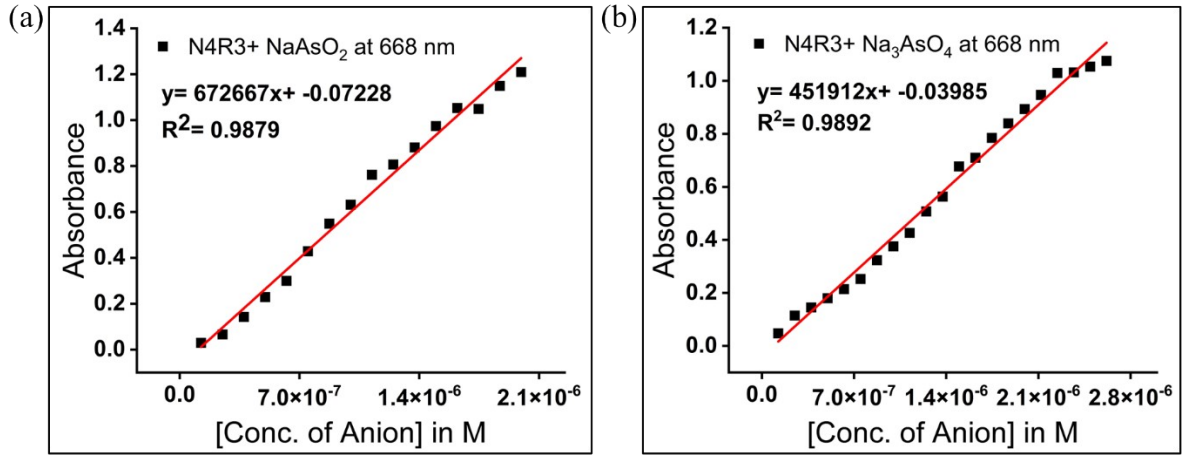

Fig. S54 (a) Calibration curve for N4R3—AsO_2^- complex in Me_2SO - H_2O (7: 3, v/v) and (b) calibration curve for N4R3- AsO_4^{3-} complex in Me_2SO - H_2O (7: 3, v/v)

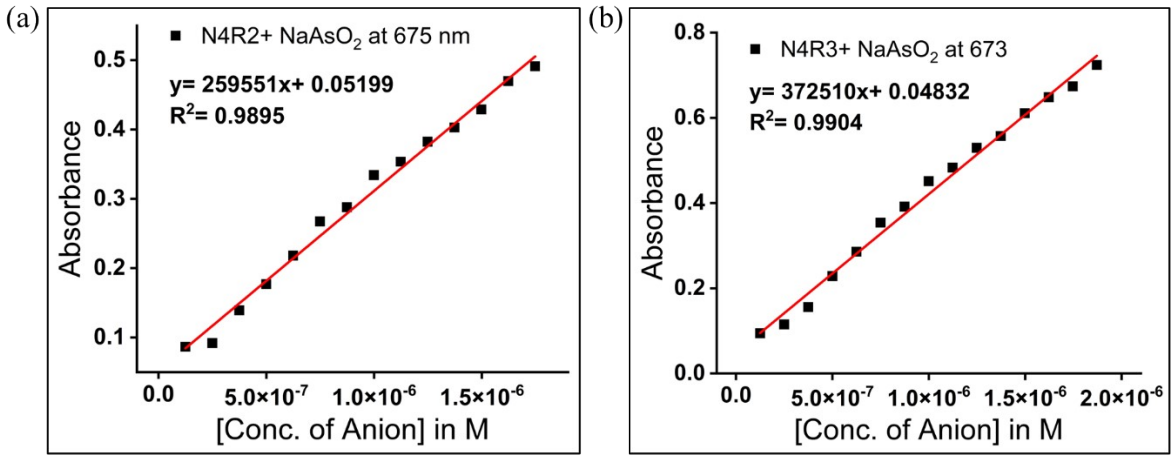

Fig. S55 (a) Calibration curve for N4R2—AsO_2^- complex in Me_2SO - H_2O (1: 1, v/v) and (b) calibration curve for N4R3- AsO_2^- complex in Me_2SO - H_2O (1: 1, v/v)

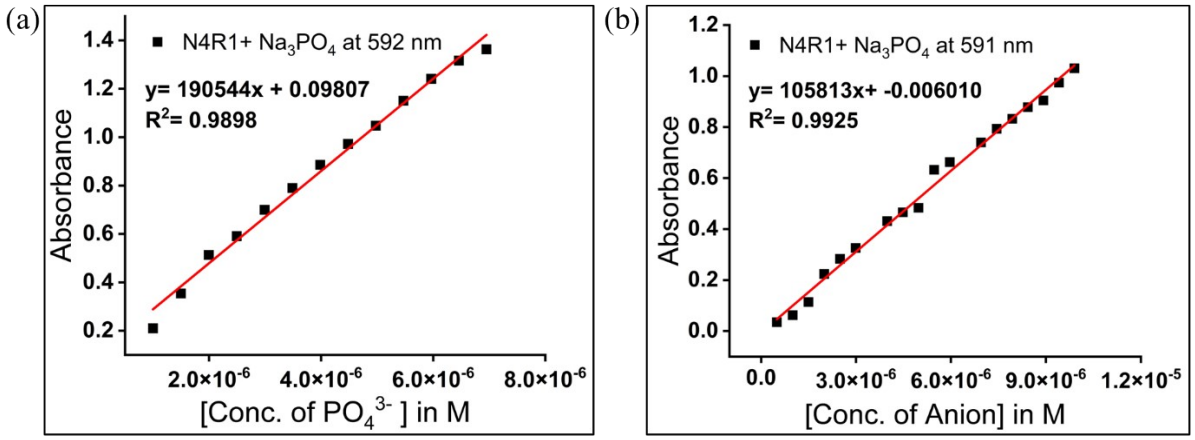

Fig. S56 Calibration curve for N4R1—PO_4^{3-} complex in **(**a) MeCN- H_2O (7: 3, v/v) and (b) Me_2SO - H_2O (7: 3, v/v)

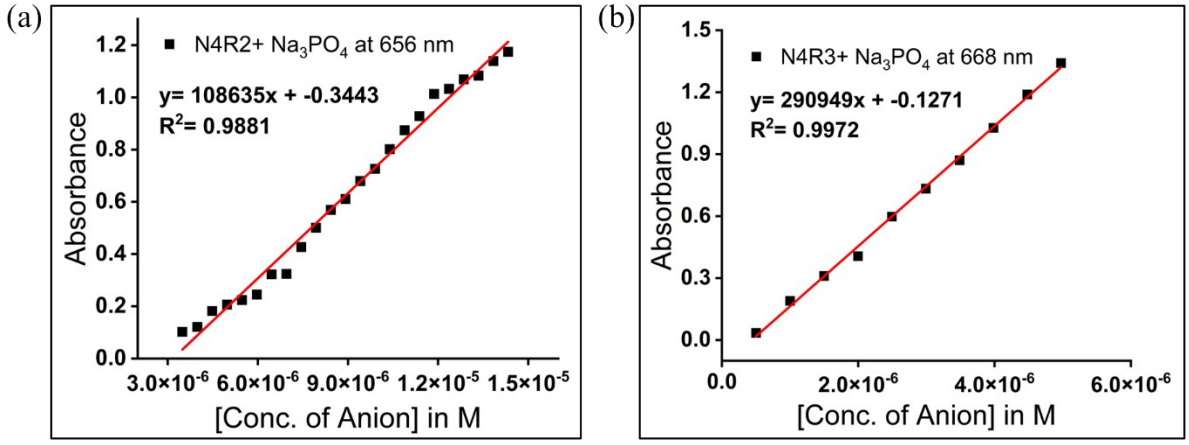

Fig. S57 (a) Calibration curve for N4R2—PO_4^{3-} complex in Me_2SO - H_2O (7: 3, v/v) and (b) calibration curve for N4R3- PO_4^{3-} complex in Me_2SO - H_2O (7: 3, v/v)

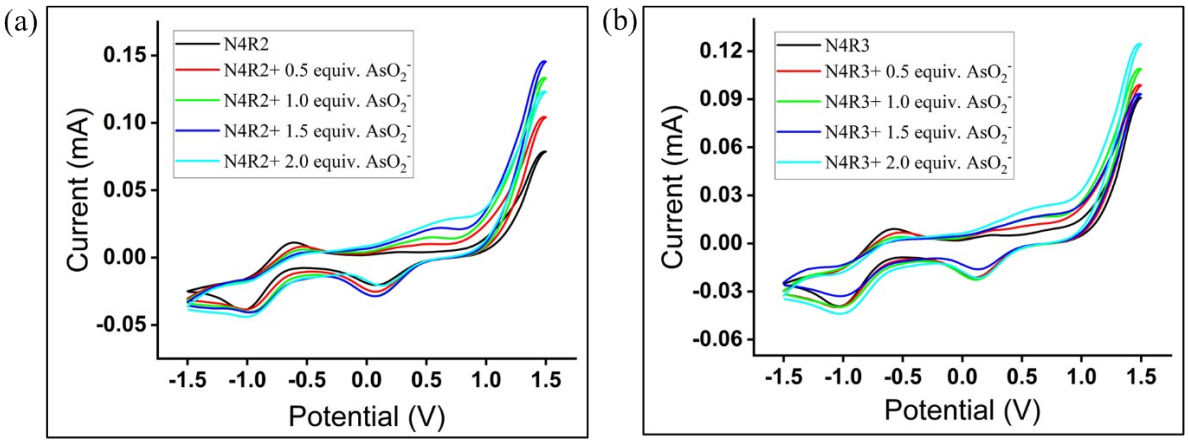

Fig. S58 CV diagram of (a) N4R2 and (b) N4R3 with the sequential addition of AsO_2^-

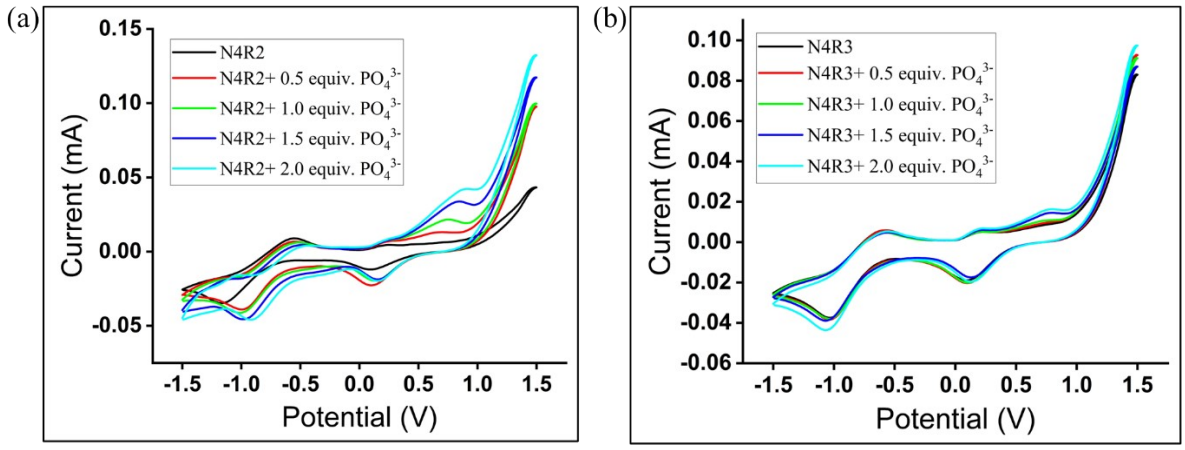

Fig. S59 CV diagram of (a) N4R2 and (b) N4R3 with the sequential addition of PO_4^{3-}

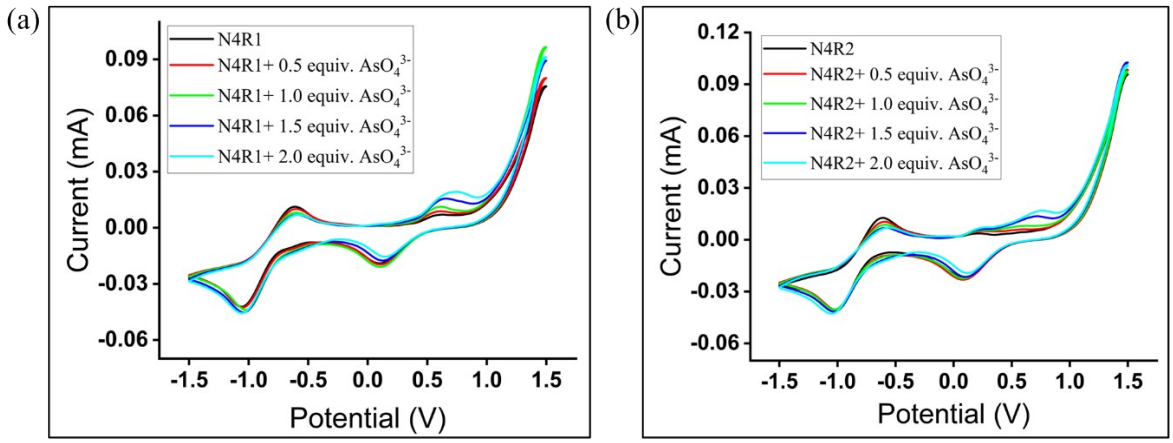

Fig. S60 CV diagram of (a) N4R1 and (b) N4R2 with the sequential addition of AsO_4^{3-}

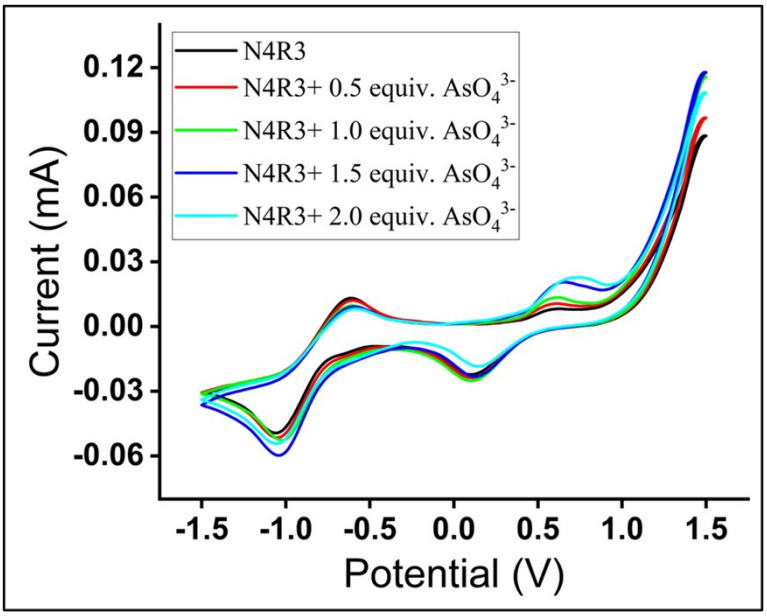

Fig. S61 CV diagram of receptor N4R3 with the serial addition of AsO_4^{3-} ion

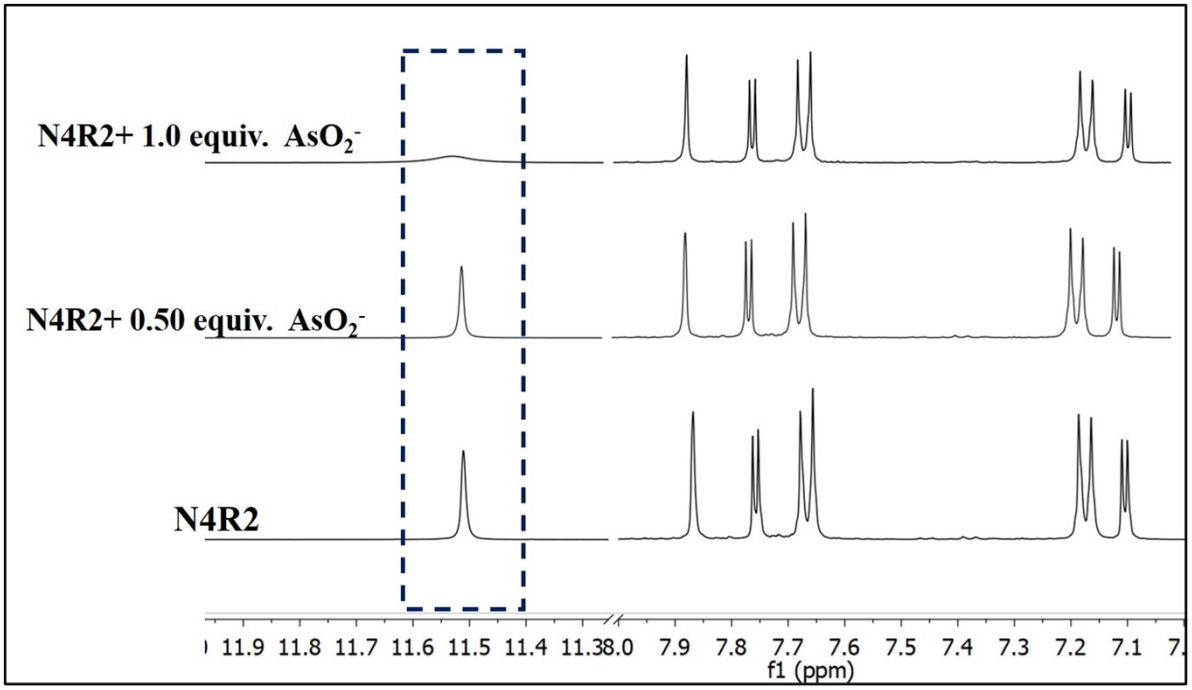

Fig. S62 ^1H NMR titration of receptor N4R2 in a Me_2SO -d_6 solvent with incremental addition of (0-1 equiv.) of $NaAsO_2$ (1×10^{-2} M in H_2O)

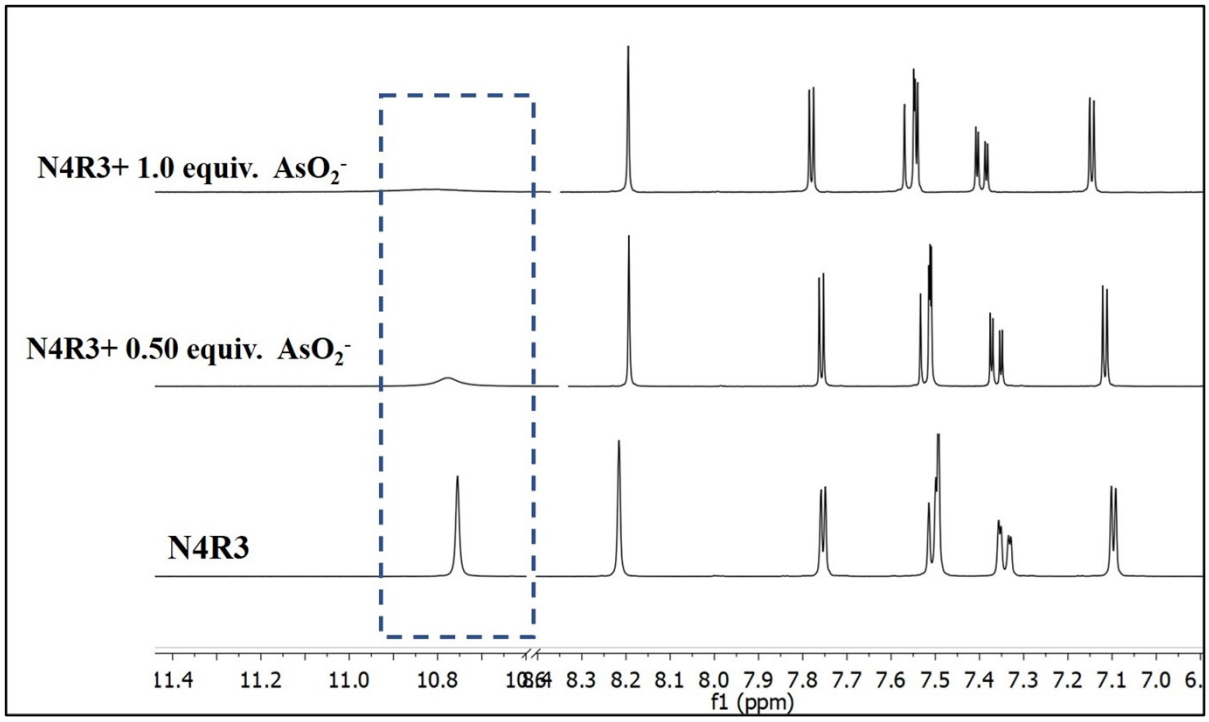

Fig. S63 ^{1}H NMR titration of receptor N4R3 in a Me_2SO -d_6 solvent with incremental addition of (0-1 equiv.) of $NaAsO_2$ (1×10^{-2} M in H_2O)

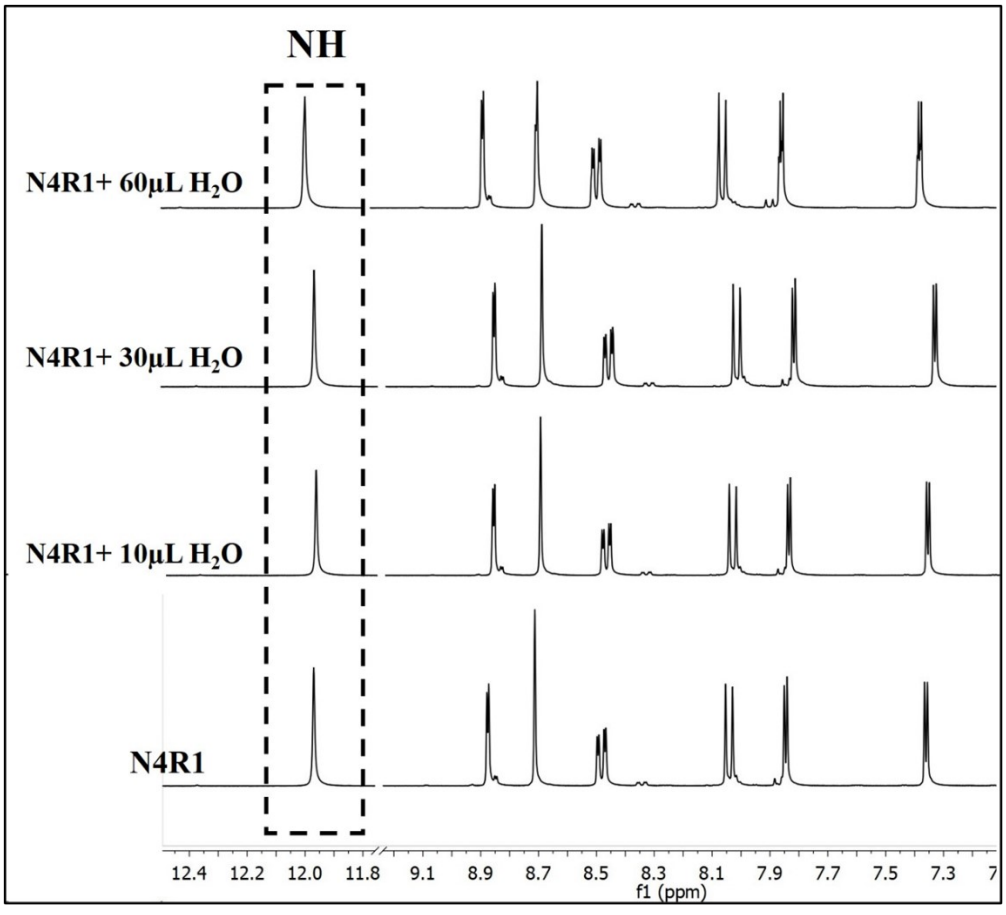

Fig. S64 Blank ^{1}H NMR titration of receptor N4R1 in a Me_2SO -d_6 solvent with incremental addition of H_2O

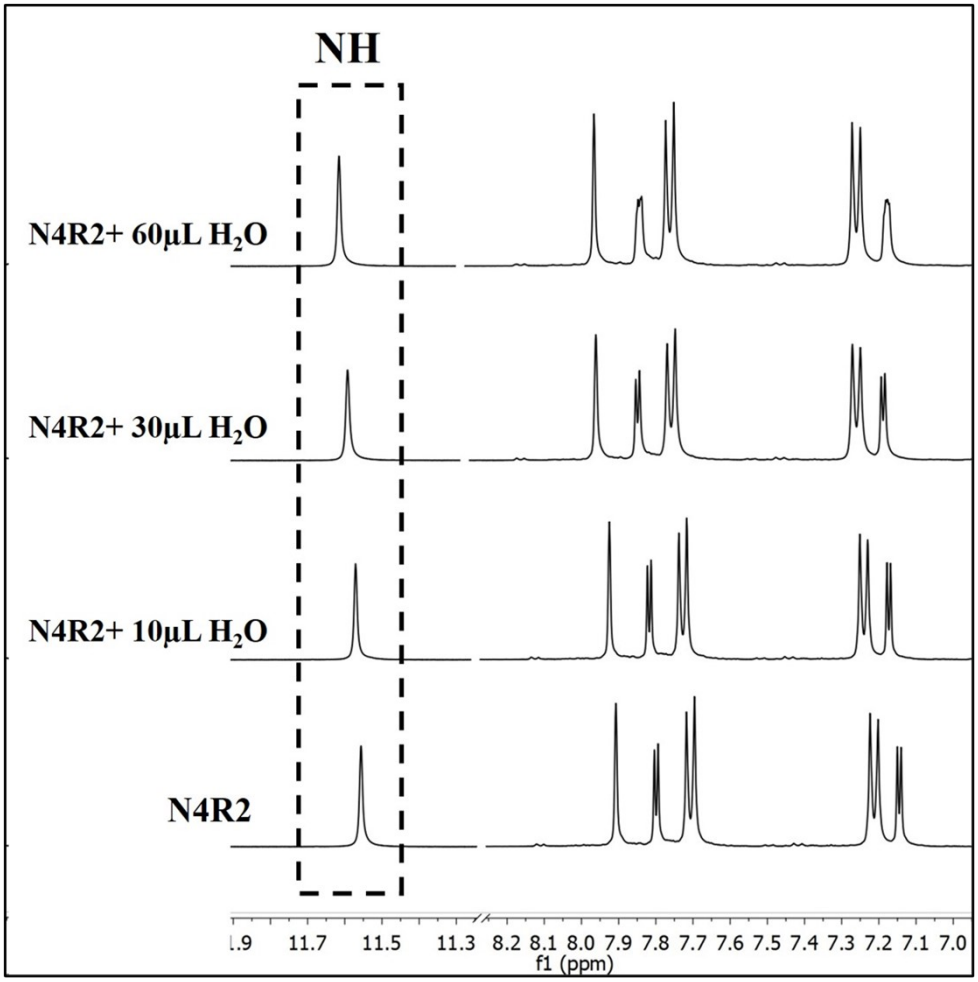

Fig. S65 Blank ^{1}H NMR titration of receptor N4R2 in a Me_2SO -d_6 solvent with incremental addition of H_2O

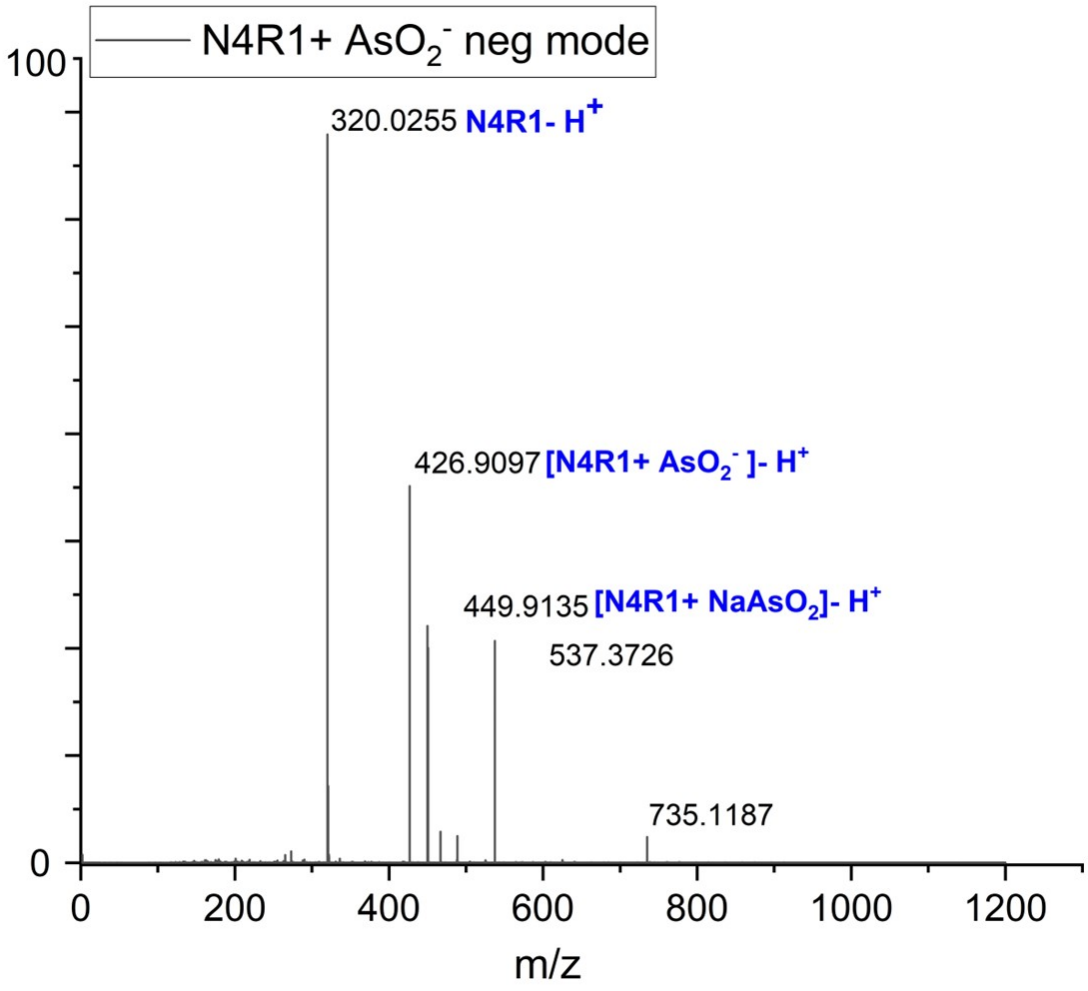

Fig. S66 LC- MS spectrum of N4R1- AsO_2^- complex in negative mode

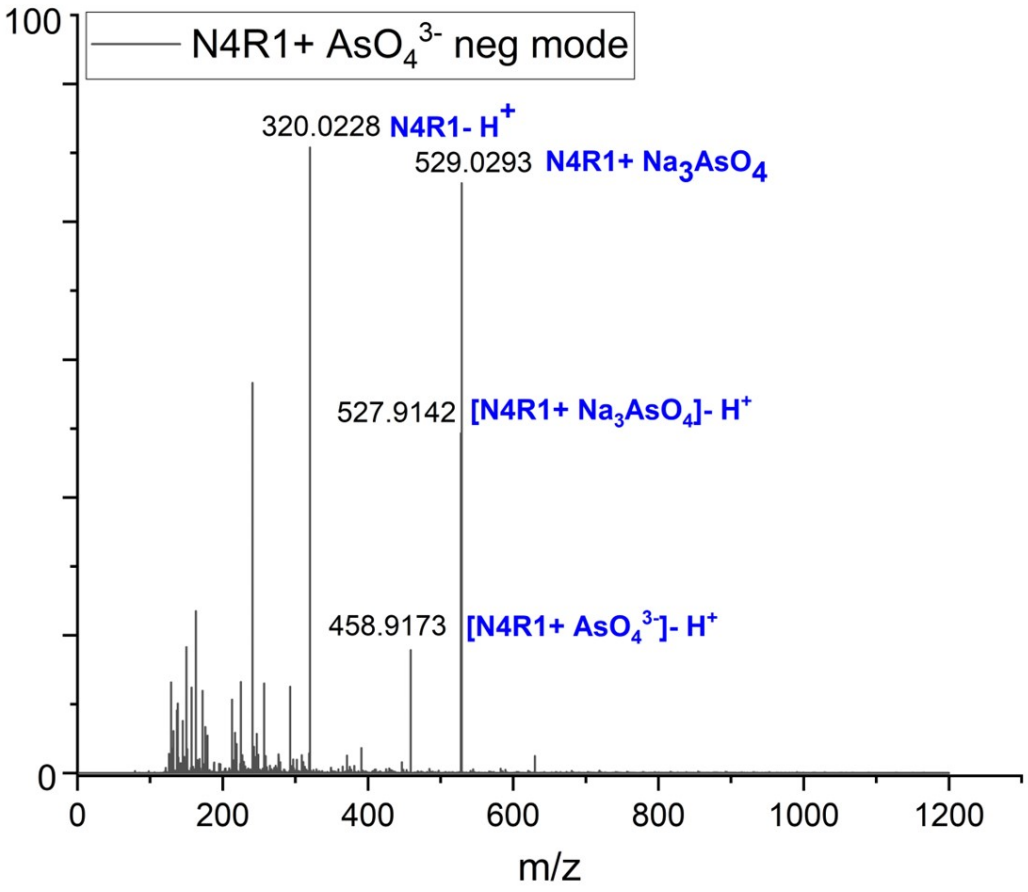

Fig. S67 LC- MS spectrum of N4R1- AsO_4^{3-} complex in negative mode

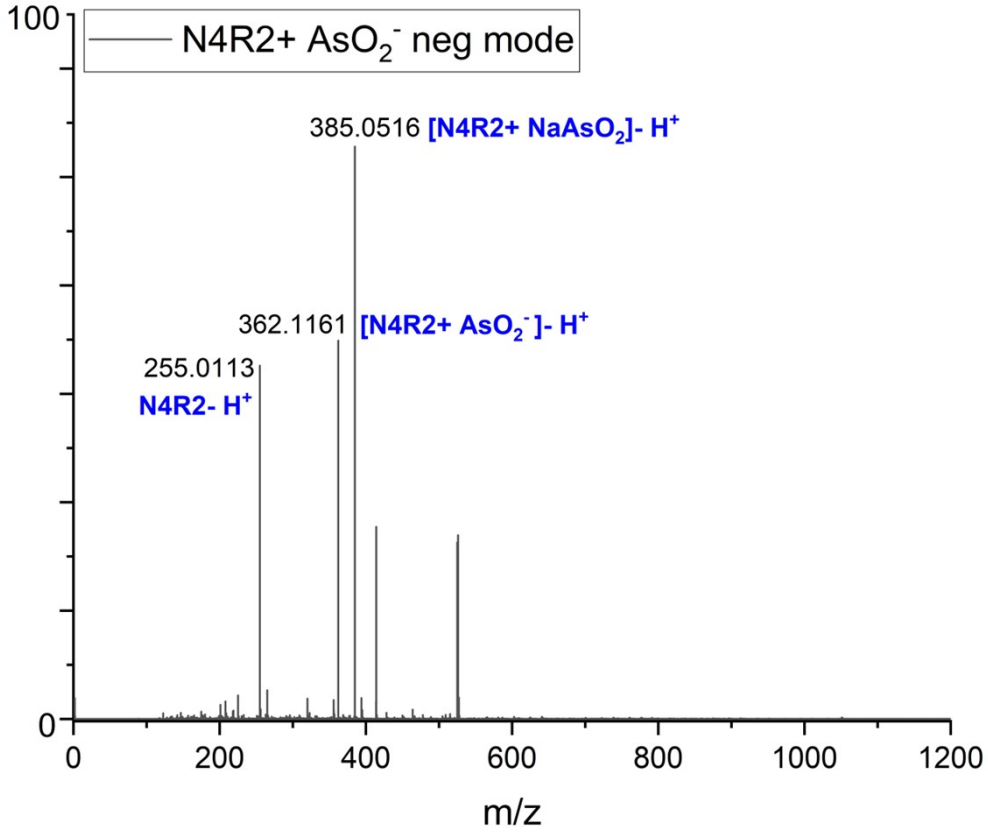

Fig. S68 LC- MS spectrum of N4R2- AsO_2^- complex in negative mode

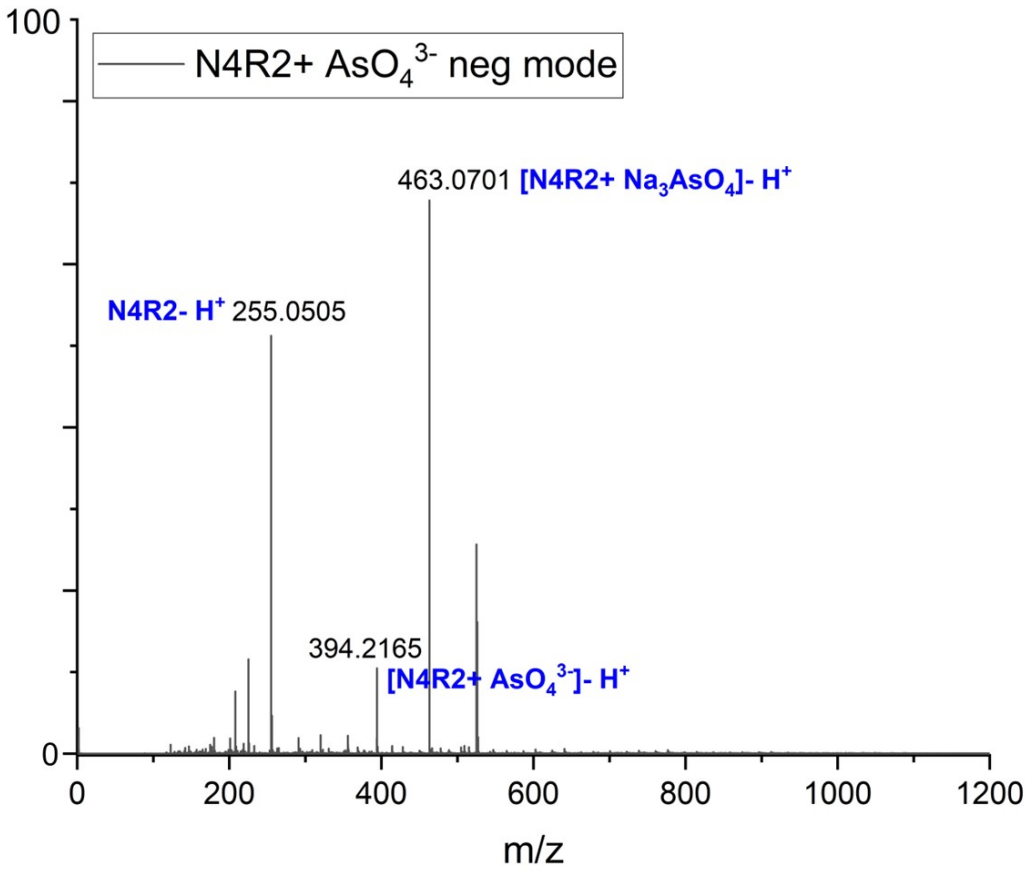

Fig. S69 LC- MS spectrum of N4R2- AsO_4^{3-} complex in negative mode

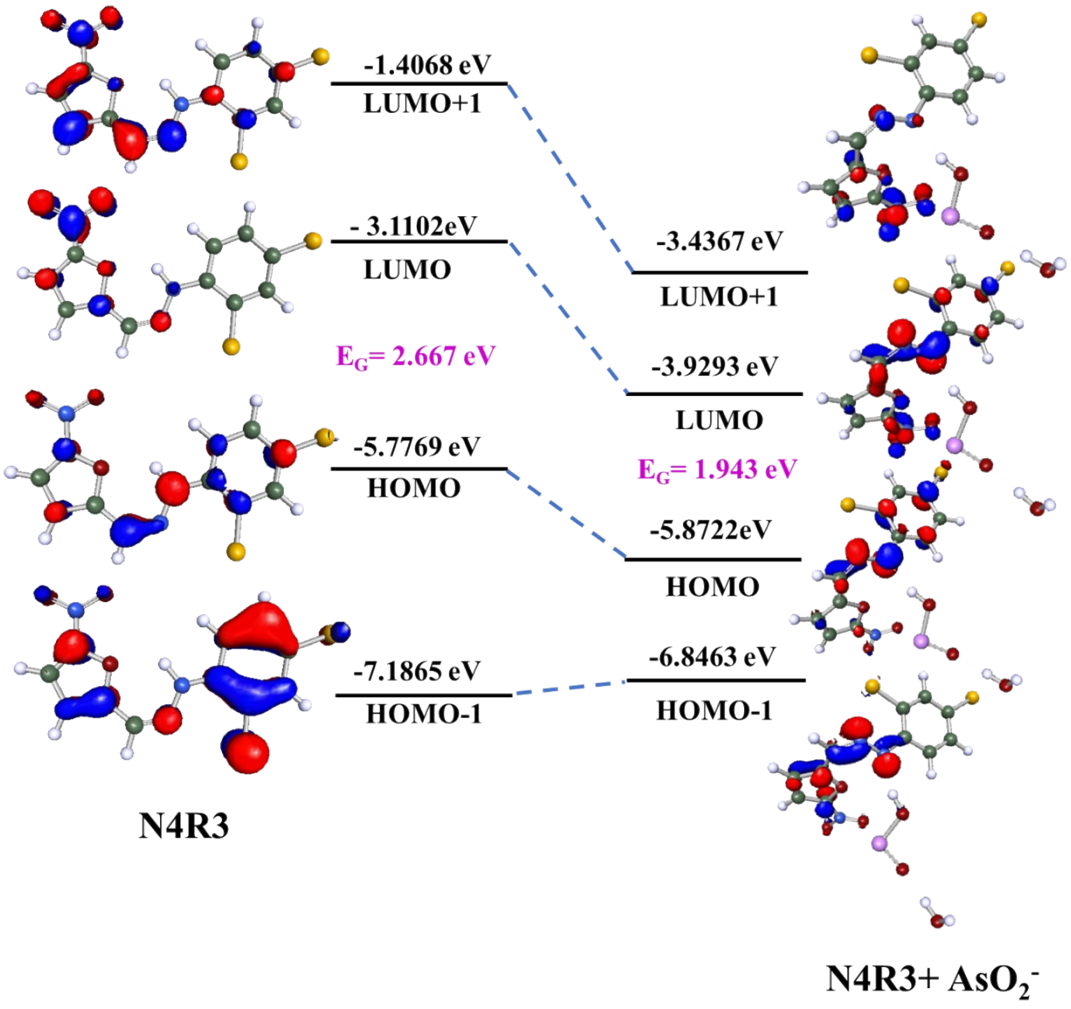

Fig. S70 HOMO's and LUMO's diagrams for receptor N4R3 and receptor N4R3-AsO_2^- obtained by B3LYP/def- TZVPP method

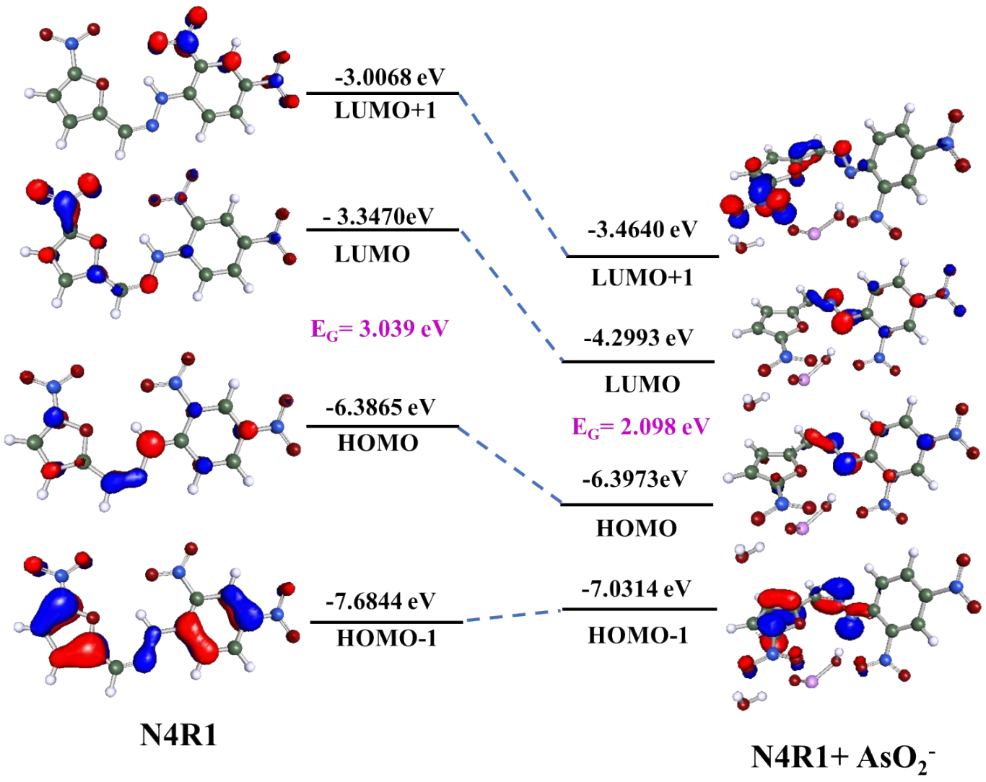

Fig. S71 HOMO's and LUMO's diagrams for receptor N4R1 and receptor N4R1-AsO_2^- obtained by B3LYP/def- TZVPP method

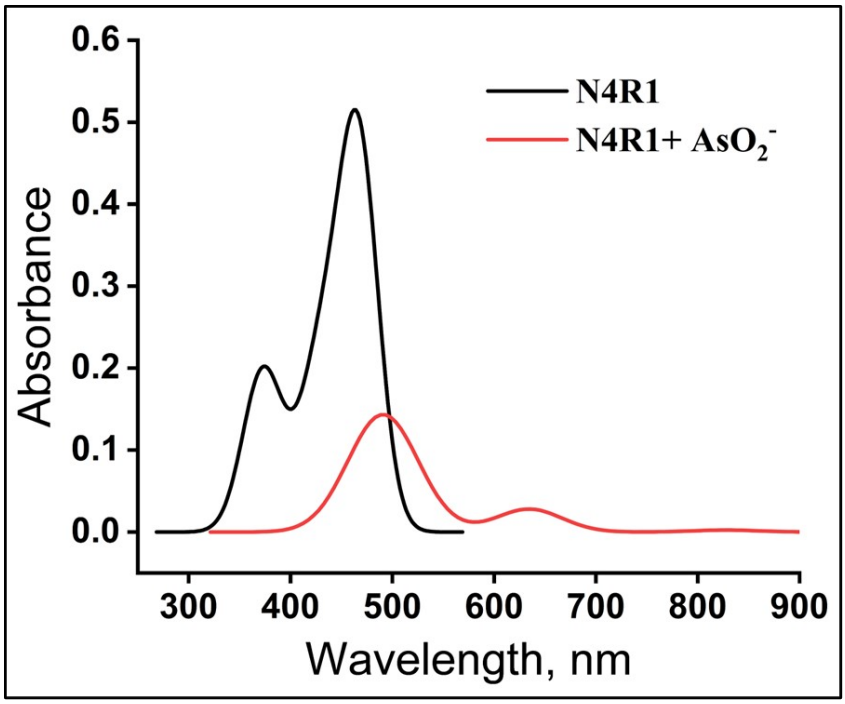

Fig. S72 UV-visible absorption spectra of receptor N4R1 and complexation with AsO_2^- ion calculated by using TD-DFT calculation in solvent phase

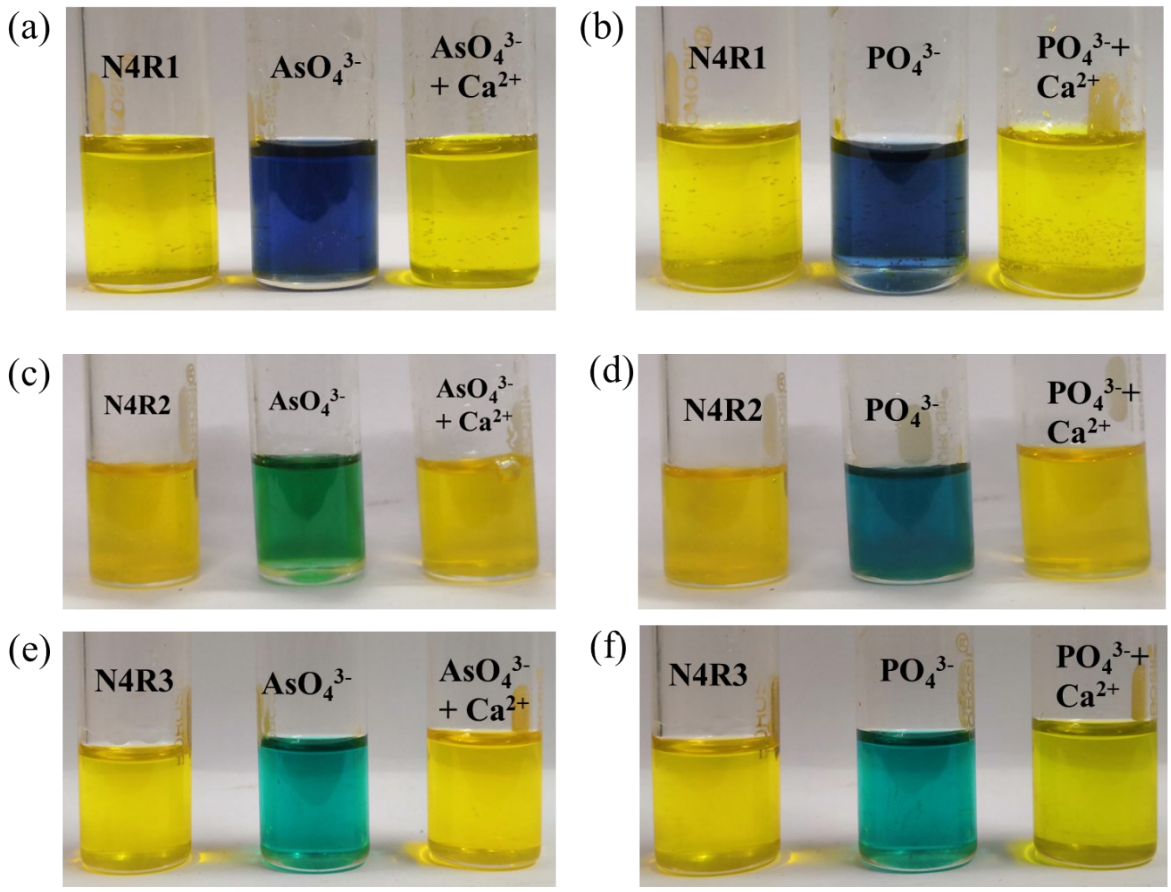

Fig. S73 Reversible cycles and reproducible colorimetric switch of receptor (2×10^{-5} M, 30% aq. Me_2SO) (a) N4R1 reversed and reproduced by the addition of AsO_4^{3-} and 40 µL Ca^{2+}, (b) N4R1 reversed and reproduced by the addition of PO_4^{3-} and 40 µL Ca^{2+}, (c) N4R2 reversed and reproduced by the addition of AsO_4^{3-} and 20 µL Ca^{2+}, (d) N4R2 reversed and reproduced by the addition of PO_4^{3-} and 20 µL Ca^{2+}, (e) N4R3 reversed and reproduced by the addition of AsO_4^{3-} and 20 µL Ca^{2+}, and (f) N4R3 reversed and reproduced by the addition of PO_4^{3-} and 20 µL Ca^{2+}

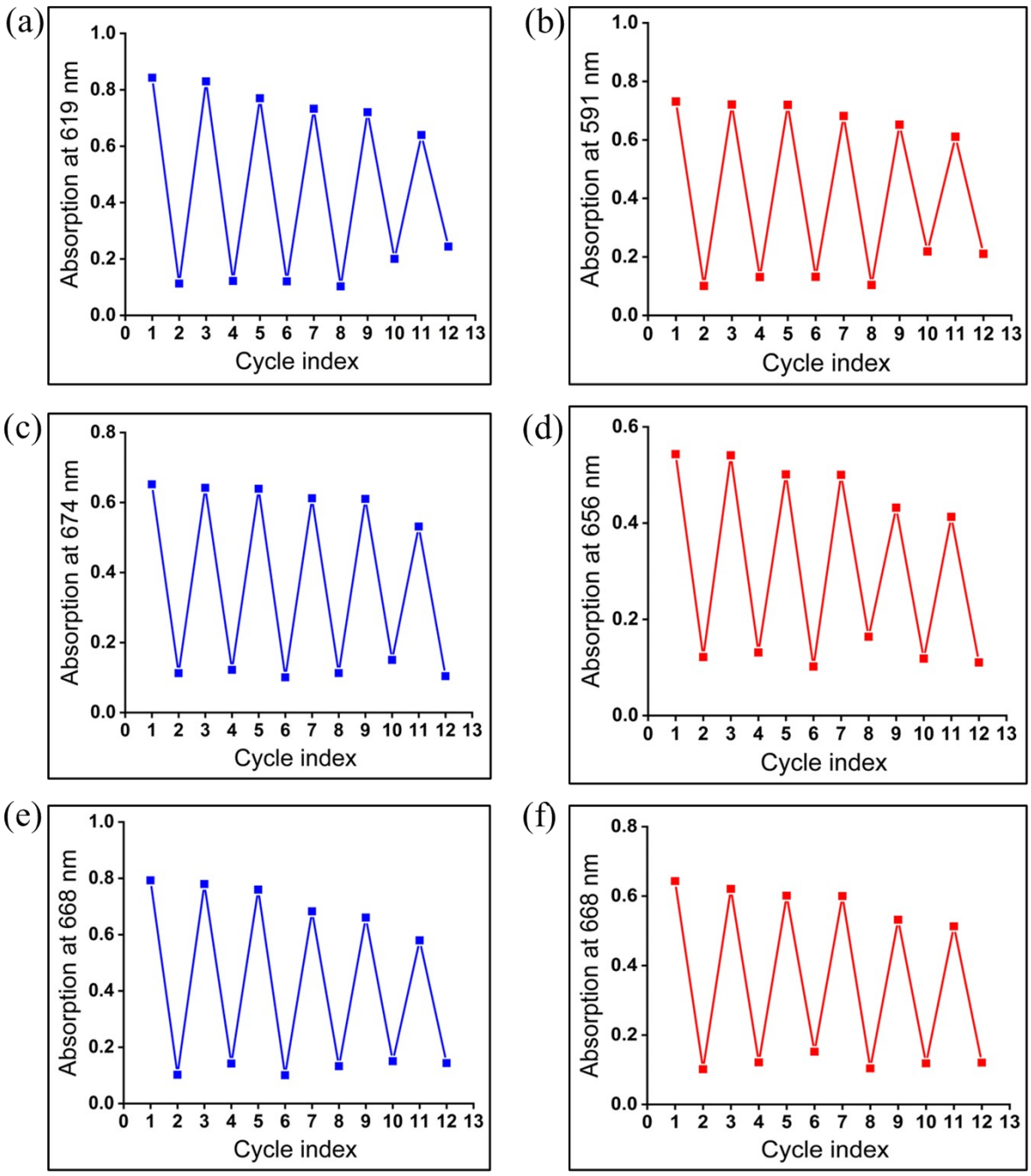

Fig. S74 UV- Vis absorption of receptor (2×10^{-5} M, 30% aq. Me_2SO) (a) N4R1 circulated with addition of 40 µL Ca^{2+} and AsO_4^{3-} by turns, (b) N4R1 circulated with addition of 40 µL Ca^{2+} and PO_4^{3-} by turns, (c) N4R2 circulated with addition of 20 µL Ca^{2+} and AsO_4^{3-} by turns, (d) N4R2 circulated with addition of 20 µL Ca^{2+} and PO_4^{3-} by turns, (e) N4R3 circulated with addition of 20 µL Ca^{2+} and AsO_4^{3-} by turns, and (f) N4R1 circulated with addition of 20 µL Ca^{2+} and PO_4^{3-} by turns

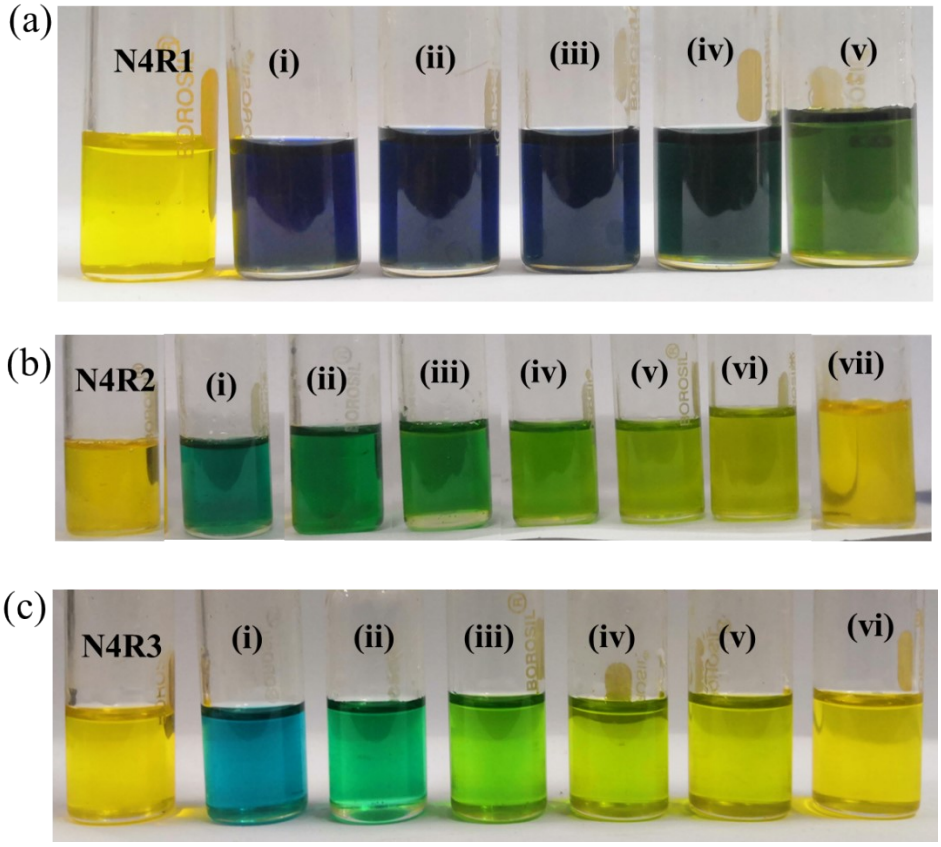

Fig. S75 (a) Addition of (i) 50 µL, (ii) 100 µL, (iii) 150 µL, (iv) 200 µL and (v) 300 µL Cu^{2+} solution to N4R1 containing 2 equiv. AsO_2^-, (b) Addition of (i) 20 µL, (ii) 40 µL, (iii) 60 µL, (iv) 80 µL, (v) 100 µL, (vi) 120 µL and (vii) 140 µL Cu^{2+} solution to N4R2 containing 2 equiv. AsO_2^-, and (c) Addition of (i) 20 µL, (ii) 40 µL, (iii) 60 µL, (iv) 80 µL, (v) 100 µL, and (vi) 120 µL Cu^{2+} solution to N4R3 containing 2 equiv. AsO_2^-

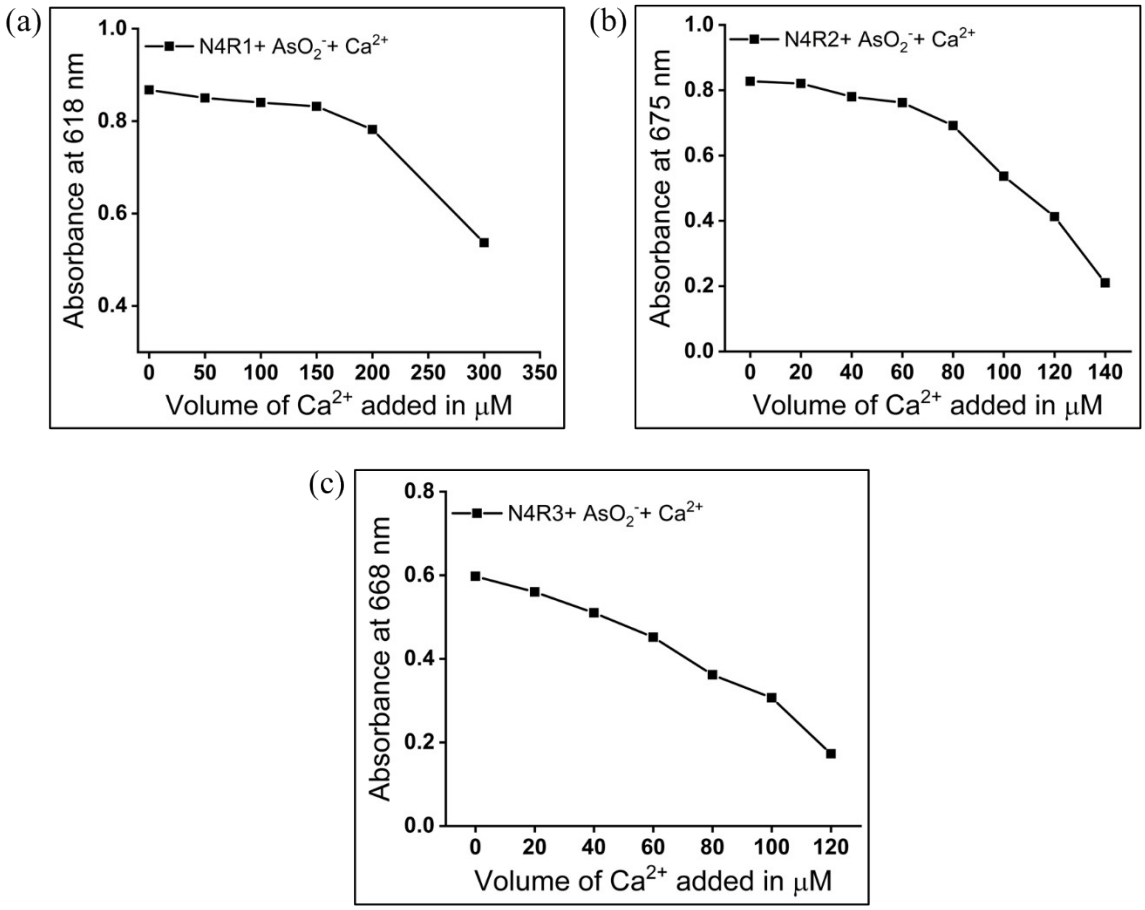

Fig. S76 UV- Vis absorption intensity changes on stepwise addition of Cu^{2+} solution to (a) N4R1 containing 2 equivalence of AsO_2^-, (b) N4R3 containing 2 equivalence of AsO_2^-, and (c) N4R3 containing 2 equivalence of AsO_2^-

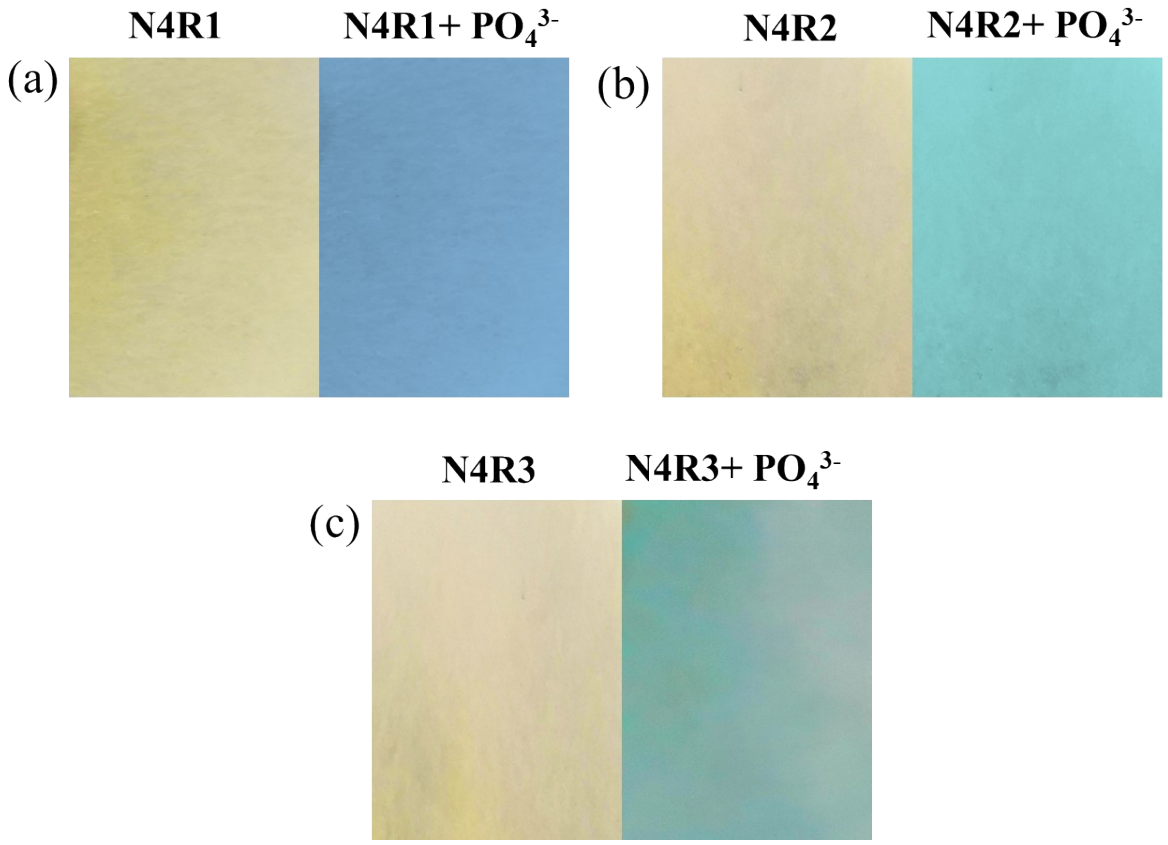

Fig. S77 Observed color changes on adding 2 equivalences of PO_4^{3-} ions on test strips with (a) N4R1 in 30% aq. Me_2SO, (b) N4R2 in 30% aq. Me_2SO and (c) N4R3 in 30% aq. Me_2SO

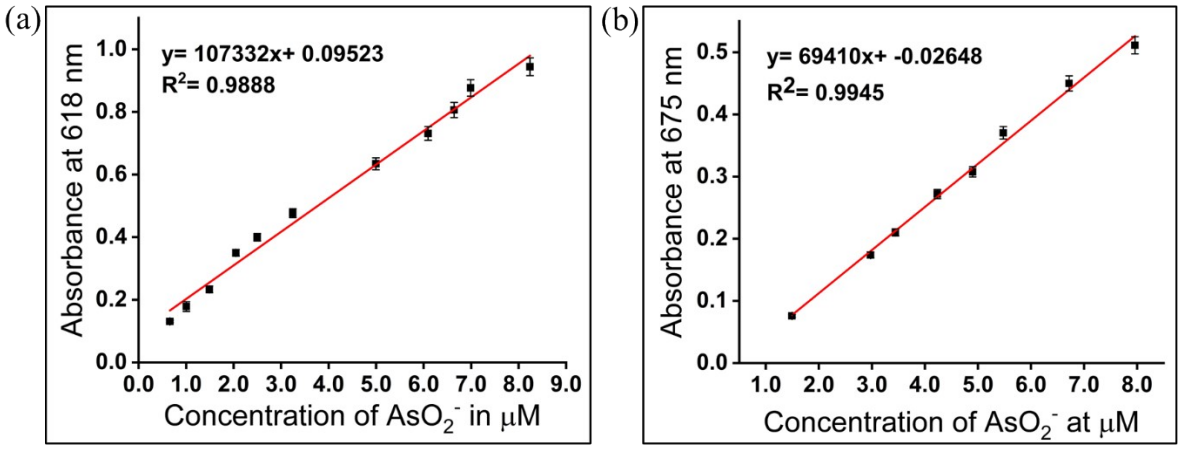

Fig. S78 A linear calibration plot of (a) N4R1–AsO_2^- vs. the amount of AsO_2^- ions and (b) N4R2–AsO_2^- vs. the amount of AsO_2^- ions for the quantitative analysis of food and water samples

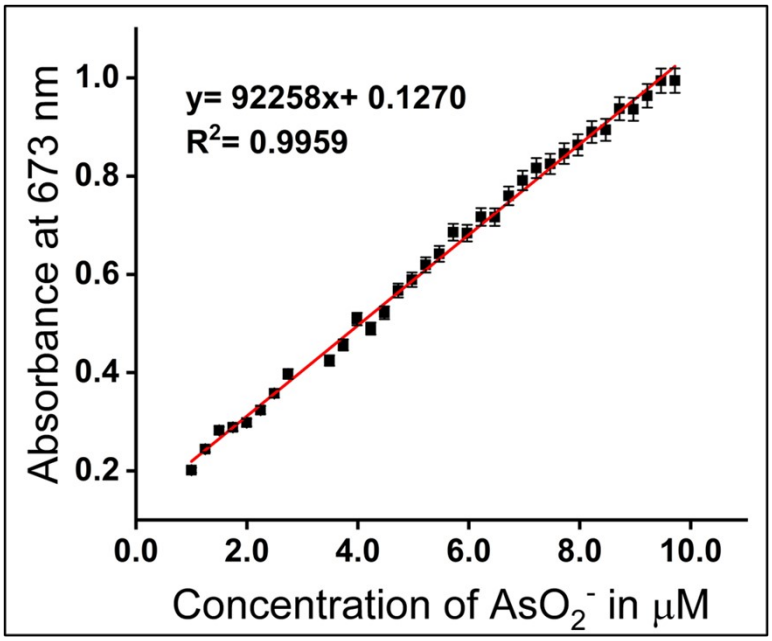

Fig. S79 A linear calibration plot of N4R3–AsO_2^- vs. the amount of AsO_2^- ions for the quantitative analysis of food and water samples

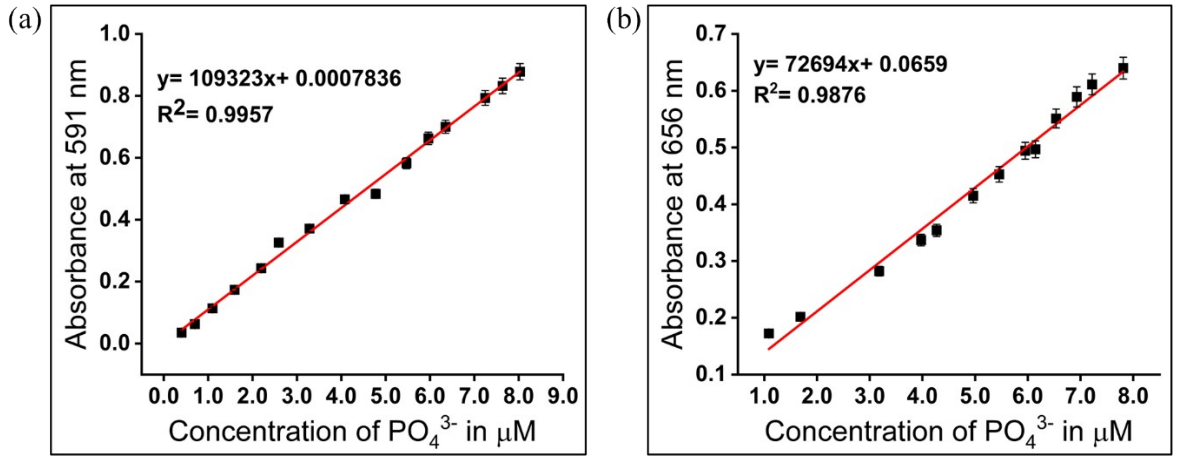

Fig. S80 A linear calibration plot of (a) N4R1–PO_4^{3-} vs. the amount of PO_4^{3-} ions and (b) N4R2– PO_4^{3-} vs. the amount of PO_4^{3-} ions for the quantitative analysis of food and water samples

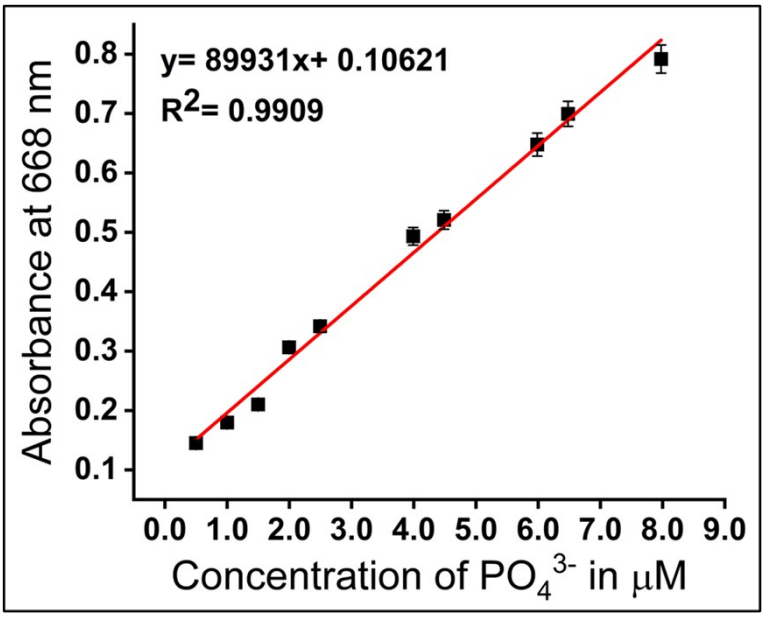

Fig. S81 A linear calibration plot of N4R3 $–PO_4^{3–}$ vs. the amount of $PO_4^{3–}$ ions for the quantitative analysis of food and water samples

Table S1 Absorption maximum difference ($\Delta\lambda_{max}$) of N4R1-N4R3 (2×10^{-5} M) in the presence of AsO_2^-, AsO_4^{3-} , PO_4^{3-} ions (2 equiv.)

Receptor	Solvent system	λ_{max} (nm)	$\Delta\lambda_{max}$ (nm)
N4R1+ AsO_2^-	30% aq. MeCN	595	177
N4R1+ AsO_4^{3-}	30% aq. MeCN	601	183
N4R1+ PO_4^{3-}	30% aq. MeCN	592	174
N4R1+ AsO_2^-	30% aq. Me_2SO	618	178
N4R1+ AsO_4^{3-}	30% aq. Me_2SO	619	179
N4R1+ AsO_2^-	50% aq. Me_2SO	618	178
N4R1+ PO_4^{3-}	30% aq. Me_2SO	591	151
N4R2+ AsO_2^-	30% aq. Me_2SO	675	227
N4R2+ AsO_4^{3-}	30% aq. Me_2SO	674	226
N4R2+ AsO_2^-	50% aq. Me_2SO	675	227
N4R2+ PO_4^{3-}	30% aq. Me_2SO	656	208
N4R3+ AsO_2^-	30% aq. Me_2SO	668	222
N4R3+ AsO_4^{3-}	30% aq. Me_2SO	668	222
N4R3+ AsO_2^-	50% aq. Me_2SO	673	227
N4R3+ PO_4^{3-}	30% aq. Me_2SO	668	222

Table S2 Binding ratio, binding constant, and detection limit of receptors N4R2 and N4R3 in the presence of arsenite, arsenate and phosphate ions

Receptor + Anion	Solvent System	Binding ratio	Binding Constant (M^{-1})	Detection Limit (ppb)
N4R2+ $NaAsO_2$	30% aq. Me_2SO	1:1	9.686×10^5	82.48
N4R2+ $NaAsO_2$	50% aq. Me_2SO	1:1	3.348×10^6	36.38
N4R2+ Na_3AsO_4	30% aq. Me_2SO	1:1	1.791×10^6	68.02
N4R2+ Na_3PO_4	30% aq. Me_2SO	1:1	4.446×10^5	304.12
N4R3+ $NaAsO_2$	30% aq. Me_2SO	1:1	2.514×10^6	44.24
N4R3+ $NaAsO_2$	50% aq. Me_2SO	1:1	1.927×10^6	37.01
N4R3+ Na_3AsO_4	30% aq. Me_2SO	1:1	2.520×10^6	69.81
N4R3+ Na_3PO_4	30% aq. Me_2SO	1:1	9.358×10^4	203.57

Table S3 Oscillator strength of Receptor- arsenite complexes

Receptor	Frequency (nm)	Oscillator strength
N4R1+ AsO_2^-	470.20911627	0.01673332
	486.62519979	0.08977062
	507.04500791	0.04606335
	634.22674976	0.02802549
	827.65296604	0.00240035
N4R2+ AsO_2^-	462.51567701	0.01430886
	492.02523177	0.0661842
	514.15578255	0.1736253
	661.56117412	0.05790929
	788.82093965	0.00074214
N4R3+ AsO_2^-	471.82908791	0.00092362
	494.98773793	0.07022809
	531.31456273	0.03769263
	689.02871961	0.07068465

	799.00266924	0.00695228

Table S4 λ_{max} of N4R1- N4R3 and complexes calculated from the theoretical DFT method and experimental UV- Vis spectroscopy

Receptor	Theoretical λ_{max}	Experimental λ_{max} from UV- Vis
N4R1	462 nm	440 nm
N4R1+ AsO_2^-	635 nm	618 nm
N4R2	496 nm	448 nm
N4R2+ AsO_2^-	663 nm	675 nm
N4R3	510 nm	446 nm
N4R3+ AsO_2^-	689 nm	673 nm

Table S5 Determination of AsO_2^- spiked into different food and water samples using N4R2 and N4R3

Receptor	Samples	AsO_2^- spiked (µM)	AsO_2^- found (µM) (n=3)	% Recovery (n= 3)	% RSD
N4R2	Potato juice	3.0	2.98	99.33	0.08
	Cucumber juice	3.0	2.97	99.00	0.15
	Tomato juice	3.0	2.99	99.67	0.20
	Apple juice	3.0	2.96	98.67	0.26
N4R2	Tap water	4.0	3.99	99.75	0.16
	River water	4.0	3.97	99.25	0.24
	Sea water	4.0	3.96	99.00	0.11
N4R3	Potato juice	4.0	3.95	98.75	0.09
	Cucumber juice	4.0	3.98	99.50	0.16
	Tomato juice	4.0	3.98	99.50	0.13
	Apple juice	4.0	3.97	99.25	0.26
N4R3	Tap water	4.5	4.48	99.55	0.07
	River water	4.5	4.49	99.77	0.18
	Seawater	4.5	4.43	98.44	0.23

Table S6 Determination of PO_4^{3-} spiked into different food and water samples using N4R2 and N4R3

Receptor	Samples	PO_4^{3-} spiked (µM)	PO_4^{3-} found (µM) (n=3)	% Recovery (n= 3)	% RSD
N4R2	Potato juice	3.0	2.99	99.66	0.13
	Cucumber juice	3.0	2.96	98.66	0.17
	Tomato juice	3.0	2.95	98.33	0.21
	Apple juice	3.0	2.98	99.33	0.05
N4R2	Tap water	4.0	3.98	99.50	0.12
	River water	4.0	3.99	99.75	0.21
	Seawater	4.0	4.08	102.00	0.26
N4R3	Potato juice	4.0	3.97	99.25	0.08
	Cucumber juice	4.0	3.95	98.75	0.13
	Tomato juice	4.0	3.99	99.75	0.17
	Apple juice	4.0	3.96	99.00	0.20
N4R3	Tap water	4.5	4.43	98.44	0.16
	River water	4.5	4.49	99.77	0.15
	Seawater	4.5	4.55	101.11	0.19

Table S7: Determination of arsenite spiked into different food and water samples with one equivalent of various anions spiked (F^-+ AcO^-+ $H_2PO_4^-$+ NO_3^-)

Receptor	samples	Arsenite spiked (µM)	Arsenite found (µM) (n= 3)	% Recovery (n= 3)	% RSD
N4R1+ Anions	Potato juice	3.0	2.99	99.67	0.17
	Cucumber juice	3.0	2.97	99.00	0.06
	Tomato juice	3.0	2.97	99.00	0.28
	Apple juice	3.0	2.95	98.33	0.27

N4R1+ Anions	Tap water	3.0	2.98	99.33	0.15
	River water	3.0	2.99	99.66	0.18
	Seawater	3.0	2.97	99.00	0.22
N4R2+ Anions	Potato juice	2.5	2.48	99.20	0.34
	Cucumber juice	2.5	2.47	98.80	0.24
	Tomato juice	2.5	2.48	99.20	0.11
	Apple juice	2.5	2.49	99.60	0.29
N4R2+ Anions	Tap water	2.5	2.49	99.60	0.16
	River water	2.5	2.47	98.80	0.26
	Seawater	2.5	2.45	98.00	0.21
N4R3+ Anions	Potato juice	4.0	3.96	99.00	0.28
	Cucumber juice	4.0	3.98	99.50	0.06
	Tomato juice	4.0	3.97	99.25	0.24
	Apple juice	4.0	3.97	99.25	0.22
N4R3+ Anions	Tap water	4.0	3.99	99.75	0.06
	River water	4.0	3.96	99.00	0.16
	Seawater	4.0	3.97	99.25	0.24

RSD: Relative standard deviation

Table S8: Determination of phosphate spiked into different food and water samples with one equivalent of various anions spiked (F^-+ AcO^-+ $H_2PO_4^-$+ NO_3^-)

Receptor	**samples**	**Phosphate spiked (µM)**	**Phosphate found (µM) (n= 3)**	**% Recovery (n= 3)**	**% RSD**
N4R1+ Anions	Potato juice	3.0	2.96	98.66	0.16
	Cucumber juice	3.0	2.99	99.66	0.11
	Tomato juice	3.0	2.97	99.00	0.16
	Apple juice	3.0	2.98	99.33	0.21
	Tap water	3.0	2.99	99.66	0.07

N4R1+ Anions	River water	3.0	3.01	100.33	0.28
	Sea water	3.0	3.03	101.00	0.22
N4R2+ Anions	Potato juice	4.0	3.97	99.25	0.18
	Cucumber juice	4.0	3.97	99.25	0.14
	Tomato juice	4.0	3.99	99.75	0.17
	Apple juice	4.0	3.96	99.00	0.10
N4R2+ Anions	Tap water	4.0	3.97	99.25	0.22
	River water	4.0	4.02	100.50	0.23
	Sea water	4.0	4.07	101.75	0.09
N4R3+ Anions	Potato juice	5.0	4.98	99.60	0.11
	Cucumber juice	5.0	4.96	99.20	0.15
	Tomato juice	5.0	4.99	99.80	0.16
	Apple juice	5.0	4.97	99.40	0.23
N4R3+ Anions	Tap water	5.0	4.99	99.80	0.17
	River water	5.0	5.01	100.20	0.21
	Seawater	5.0	5.08	101.60	0.27

RSD: Relative standard deviation